Boson localization and correlated pinning of superconducting vortex arrays

David R. Nelson
Lyman Laboratory of Physics, Harvard University, Cambridge, Massachusetts 02138

V. M. Vinokur
Materials Science Division, Argonne National Laboratory, Argonne, Illinois 60439
(Received 28 May 1993)

A theory of vortex pinning in high-temperature superconductors by correlated disorder in the form of twin boundaries, grain boundaries, and columnar defects is described. Mapping vortex trajectories onto boson world lines leads to a "superfluid" flux liquid at high temperatures, as well as low-temperature "Bose-glass" and "Mott-insulator" phases, in which the flux lines are localized. Currents perpendicular to the average vortex direction act like an electric field applied to charged bosons, while currents parallel to the field act like an imaginary magnetic field in this approach. We discuss the equilibrium and dynamic properties of these phases, and propose a scaling theory for the flux-liquid to Bose-glass transition, at which the linear resistivity vanishes. Although the Bose-glass predictions share some features with vortex-glass behavior predicted for point disorder, the response to tilting the magnetic field in the two cases differs dramatically, thus allowing the two theories to be distinguished experimentally.

I. INTRODUCTION AND SUMMARY

A. Overview

The static and dynamic response of the flux lines in the cuprate high-temperature superconductors has been the subject of numerous recent experimental and theoretical investigations.[1,2] Interest in this problem is motivated in part by important technological questions, but also by the intellectual challenge of dealing with large assemblies of flexible lines subject to *both* thermal fluctuations and pinning by point, line, and planar disorder. A complete understanding requires new ideas and phases, including entangled flux liquids,[3] with a linear resistivity, and if point-like disorder is important, a possible vortex-glass phase, with zero linear resistivity and nonlinear current-voltage characteristics.[4] Although the original theory described the vortex glass in terms of undetermined critical exponents,[4] the nonlinear resistive properties may be estimated more quantitatively in certain intermediate regimes via a collective pinning theory.[5]

On the theoretical side, the question of whether a distinct vortex-glass phase, dominated by point disorder, actually exists in three dimensions is still not completely settled. It is clear that a single vortex line, subject to random point pinning and pulled through the sample by a current-induced Lorentz force, exhibits glassy behavior.[5] The behavior of *interacting* fluxon assemblies is more subtle, however. In dense flux liquids, for example, collisions and close encounters between vortices screen out a weak random potential, whose effect on the equilibrium properties may then be calculated with ordinary perturbation theory.[6] Similar conclusions apply to the dynamical response of dense flux liquids.[7,8]

Explicit glassy behavior, in the form of nonlinear current-voltage characteristics, does emerge for dense lines in the low-temperature limit from a collective pinning approach,[5] which assumes local crystalline order and then treats phonon distortions caused by the random pinning potential.[9] The nonlinear resistivity which results from such theories would be correct at all current and length scales if the "topology" of nearest neighbors surrounding every line in the moving flux assembly subjected to a Lorentz force remained fixed. It is unclear, however, how topology-changing defects such as dislocations, vacancies, and interstitials alter the quantitative theoretical predictions at the very lowest currents and longest length scales.

Computer simulations of a simplified random gauge-field model on a lattice *have* found evidence for a genuine vortex-glass phase in three dimensions.[10] There is as yet no biasing of the magnetic-field direction in these simulations, however: The average magnetic field is zero. The London penetration depth in the gauge glass, moreover, is infinite, so that vortices interact logarithmically at all length scales. It is possible that the vortex-glass phase exists in the case of long-range interactions, but disappears when the London penetration depth is finite.[11]

To counter such theoretical uncertainties, we can of course appeal to striking experiments on vortex transport in yittrium barium copper oxide (YBCO),[12,13] which provide impressive evidence of a genuine phase transition. One might question, however, whether these transitions are really caused by uncorrelated "point" disorder in the form of, say, oxygen vacancies, as assumed in the original vortex-glass phenomenology.[4] The films studied by Koch *et al.*[12] are heavily microtwinned, and such twins usually extend completely through the sample along the c axis. One also expects grain boundaries, as well as forests of screw dislocations parallel to the growth direction,[14] providing another source of *correlated* disorder along the c axis. Although dislocations are probably absent in significant concentrations in the large single crystals of Ref. 13, these samples still contain twins, with spacings

ranging from micrometers down to several hundred angstroms. Most twins lie in planes spanned by the c axis and in one of two perpendicular directions inclined at $\pm 45°$ to the principal axes of the local ab plane. The resistivity measurements of Refs. 12 and 13 were all taken with the field aligned with the c axis, a direction which *maximizes* effects of the correlated pinning centers discussed above.

Experimental observation of a sharp downward dip in the resistivity as the field orientation is rotated through the $\hat{c}$ direction[15] provided early evidence of twin-boundary pinning. One would expect the resistivity to be a *slowly* varying function of orientation angle near the $\hat{c}$ direction if point disorder dominated. Additional support for this view appears in recent low-temperature neutron-diffraction measurements of heavily twinned YBCO.[16] A square pattern of Bragg peaks strongly suggestive of pinning by two orthogonal families of twin planes appeared for fields parallel to the c axis. Only when the field was tilted appreciably away from this direction did the expected triangular pattern of peaks appear.

There are now new experiments which confirm the importance of twins. Charalambous *et al.*[17] have found an abrupt shoulder in the temperature-dependent resistivity of twinned YBCO crystals, provided the field is oriented perpendicular to the c axis. The behavior is quite nonlinear near the shoulder, which becomes sharper at low currents. This resistivity drop, which is distinctly different from the vortex-glass-like behavior observed for fields *parallel* to c, was interpreted as evidence for first-order freezing transition into an Abrikosov flux lattice. The field is inclined at $\pm 45°$ to the twin boundaries in this geometry, significantly reducing their influence as pinning centers. Extensive investigations of twin-boundary pinning by Kwok and co-workers[18] as a function of angle also reveal a shoulder, but only when the field is tipped appreciably away from alignment with the twin planes. In completely *twin-free* samples, a sudden shoulder is observed even for fields along the c axis. Earlier torsional oscillator experiments by Farrell and co-workers[19] on twin-free YBCO also found a sharp feature whose dependence of the tipping angle agreed with that expected for a freezing transition.

Perhaps the best evidence for first-order freezing in the absence of twins comes from recent work by Safar *et al.*, who have studied untwinned, single-crystal YBCO with picovolt voltage sensitivity and millikelvin temperature resolution.[20] These authors find hysteresis loops, strongly suggesting that the melting transition of the Abrikosov flux lattice is first order in the clean limit. We should stress that point disorder, in the form of oxygen vacancies, is undoubtedly present in all the above experiments. This pinning is, however, evidently quite weak at the elevated temperatures of the melting transition expected in pure systems. The theoretical arguments predicting a *first-order* transition[21] in clean limit are reviewed in Appendix A.

The above experiments do not mean that point disorder can be neglected entirely. It is well known that any amount of point disorder, however small, will break up crystalline translational order on sufficiently long length scales.[9] Worthington *et al.*[22] present evidence for separate vortex melting and vortex-glass transitions in the same sample. Observation of vortex-glass-like effects required irradiation to enhance the point disorder and occurred at a lower temperature than melting. Freezing was argued to lead initially to a "vortex slush" phase with large but finite regions of translational order and a small but nonzero resistivity. The hysteresis loops observed in twin-free YBCO by Safar *et al.* eventually disappear at sufficiently high magnetic fields.[23] One explanation is that disorder increases in importance at high fields, because the resistivity drop now occurs at slightly lower temperatures. Thus first-order melting at moderate fields could be replaced by a continuous vortex-glass transition when the field is high. Other explanations are possible, however.[24]

B. Correlated vs point disorder

To understand experiments such as those of Refs. 12 and 13, it may be critical to determine how *correlated* disorder affects the configurations and dynamics of vortex assemblies at both high and low temperatures. One significant source of correlated disorder is surely twin boundaries. Potentially even more important for applications are *columnar* pins, produced by bombardment of crystals with energetic heavy ions of tin, iodine, or lead.[25–28] In $YBa_2Cu_3O_7$, for example, Civale *et al.*[26] have reported greatly enhanced pinning due to long aligned columns of damaged material, 15 μm or more in length and ~ 60 Å in diameter. Even more striking results on thallium-based compounds have been reported by Budhani, Suenaga, and Liou.[26] The concentration of columnar pins is easy to control experimentally (unlike the density of twin boundaries) and may lead to a significant upward shift in the apparent irreversibility line.[26] These two kinds of correlated disorder are illustrated schematically in Fig. 1.

The main focus of this paper is correlated disorder as embodied in columnar pins.[29] The behavior induced by a *mosaic* of grain boundaries [see Fig. 1(c)], running randomly at $\pm 45°$ angles within the local (a,b) plane, should be similar, however, at least at scales large compared to the mosaic size. Related behavior might also be expected due to random arrays of grain boundaries aligned with the c axis. We shall discuss as well flux motion transverse to single family of parallel twin boundaries, which is relevant to the physics at scales smaller than the mosaic size.

Our emphasis on correlated pinning allows us to map the physics of flux lines onto the problem of localization of quantum-mechanical bosons in two dimensions,[30] similar to an analogy proposed earlier for vortices in pure systems.[3] This mapping exploits methods developed to understand the behavior of ^{4}He films on disordered substrates.[31] At low temperatures we find a "Bose-glass" phase, with flux lines localized on columnar pins, separated by a sharp phase transition from an entangled liquid of delocalized lines. This Bose glass has an infinite tilt modulus c_{44} and is in fact stable over a finite range of tip-

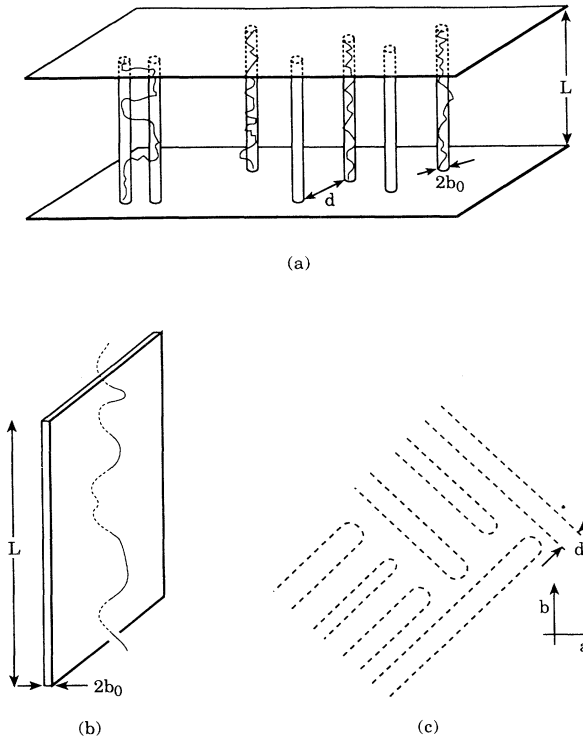

FIG. 1. Varieties of correlated disorder. In (a), columnar pins of diameter $2b_0$ and average separation d pierce a sample of thickness L. A single twin plane of thickness $2b_0$ is shown in (b). In (c), an edge-on view of twin boundaries inclined at $\pm 45°$ angles within the ab plane is shown.

ping angles away from the direction parallel to the correlated disorder. The resistivity vanishes, in the sense that current-voltage characteristics are highly nonlinear. Specifically, we find that the electric field $\mathcal{E}$ induced by a small current J in the limit $J \to 0$ scales in the thermodynamic limit like

$$\mathcal{E} \sim \exp[-(E_k/T)(J_0/J)^{1/3}] . \tag{1.1}$$

Here E_k and J_0 are characteristic energy and current scales calculated (up to constants of order unity) in Sec. IV. Transport in this regime bears a remarkable resemblance to variable range hopping of electrons in disordered semiconductors.[32] The most important excitations in this regime are "double kinks," which allow vortex lines to "tunnel" to distant unoccupied defects with nearly the same energy. At intermediate current scales, $J_0 < J < J_1$, the behavior is also nonlinear, with $\mathcal{E} \sim \exp[-(E_k/T)J_1/J]$. The relevant excitations are now "half loops," which allow pinned vortices to escape into interstitial regions. Depending on the field strength, temperature, sample thickness, and pin density, a number of other interesting regimes are possible. See Sec. IV for details.

The theory also predicts a "Mott-insulator" phase at low temperatures when the fluxon density exactly matches the density of columnar pins. See Fig. 2. *Both* the tilt modulus and compressional modulus c_{11} are

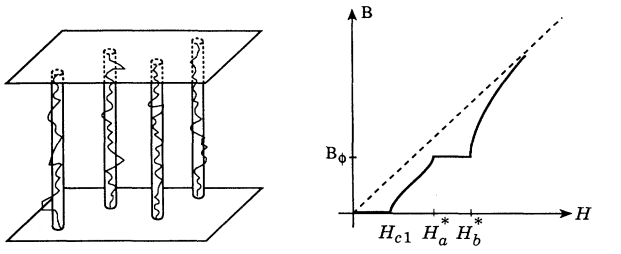

FIG. 2. Mott insulator phase. (a) At low temperatures, every columnar pin is occupied with a flux line, (b) B vs H constitutive relation showing the lock in to the matching field $B_\phi = \phi_0/d^2$ over a finite range of external fields H.

infinite in the Mott insulator. The magnetic field is locked at the "matching field" $B = B_\phi \equiv n_{\text{pin}}\phi_0$ over a range of external magnetic inductions H within in this phase, as shown in Fig. 2. Here, n_{pin} is the areal density of columnar pins (which are assumed for simplicity to pass completely through the sample) and $\phi_0 = \hbar c/2e$ is the flux quantum. Flux motion in this regime is also highly nonlinear and resembles transport in the Meissner phase. As illustrated in Fig. 3, the Mott insulator is buried deep within the Bose glass phase, where relaxation times are very long. Equilibration time problems may thus make the Mott insulator difficult to access experimentally.

As is the case for point disorder, the effect of correlated pinning on an entangled flux liquid is rather benign and can be calculated using perturbation theory.[6,7] Although we expect the usual linear resistivity in this phase, correlated disorder does show up as a ridge of scattering which might be observable in neutron-diffraction experiments.[16]

Figure 3 shows a schematic phase diagram, indicating the three phases discussed above. Also shown is a dashed curve $B^*(T)$, above which interactions play an important role in determining vortex configurations and dynamics

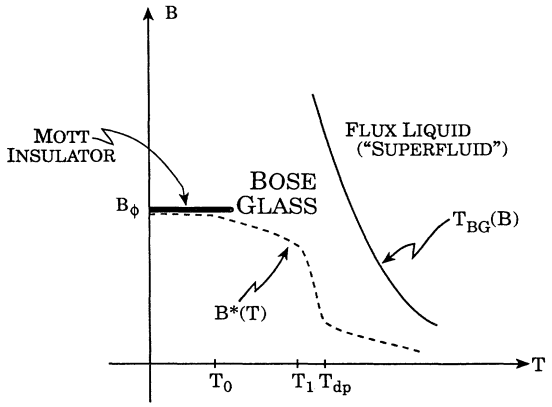

FIG. 3. Phase diagram in limit of strong correlated disorder. Mott insulator appears as a line phase at $B = B_\phi$. Interactions are important in determining the localization length and transport at intermediate current scales above the dashed crossover line $B^*(T)$. A sharp phase transition line $T_{\text{BG}}(B)$ separates the flux liquid from the Bose glass.

in the low-temperature phases. Of particular interest is the transition at T_{BG} from the Bose-glass to the entangled-flux-liquid or "superfluid" phase, which we identify with the experimentally observed "irreversibility line." Although an exact theory of this transition is not available, its critical behavior can be parametrized in terms of a scaling theory with just two undetermined critical exponents, as in the vortex-glass phenomenology.[4] The root-mean-squared transverse wandering $l_\perp(T)$ of a localized vortex line transverse to the field direction is expected to diverge as $T \to T_{BG}$ from below,[31]

$$l_\perp(T) \sim \frac{1}{(T_{BG}-T)^{\nu'}} . \tag{1.2}$$

The time scale τ for relaxation of a fluctuation with this size is assumed to diverge with a new critical exponent z',

$$\tau \sim l_\perp^{z'} . \tag{1.3}$$

We then find that the resistivity $\rho(T)$ should vanish as $T \to T_{BG}$ from above,

$$\rho \sim (T-T_{BG})^{\nu'(z'-2)} . \tag{1.4}$$

Precisely at T_{BG}, scaling predicts a power-law relation between the electric field $\mathcal{E}$ and current,

$$\mathcal{E} \sim J^{(1+z')/3} . \tag{1.5}$$

These critical-exponent relations are remarkably similar to those predicted by the vortex-glass theory.[4] Indeed, the analogous vortex-glass predictions near a transition temperature T_{VG} are that $\rho \sim (T-T_{VG})^{\nu(z-1)}$ and $\mathcal{E} \sim J^{(1+z)/2}$, where ν and z are yet another pair of undetermined exponents. How can one easily decide whether vortex-glass or Bose-glass physics dominates in a given experimental situation? In this paper we use "vortex glass" to mean a distinct thermodynamic phase, with zero linear resistivity, dominated by point disorder. By "Bose glass" we mean an alternative thermodynamic phase, again with zero linear resistivity, but now dominated by *correlated* disorder, in the form of lines or planes which extend across an appreciable fraction of the sample thickness. These phases have similar "glassy" properties, but very different underlying microscopic physics. In contrast to point disorder, which *promotes* flux-line wandering and entanglement,[3] correlated disorder *inhibits* wandering and promotes localization.

Fortunately, these two disorder-induced "glasses" have dramatically different responses to tipping the external magnetic field away from the c axis. Suppose for simplicity that the disorder is strong enough to suppress first-order freezing into an Abrikosov flux crystal for $\mathbf{H} \| \hat{\mathbf{c}}$. If point disorder causes a vortex-glass transition, then the resulting irreversibility line $T_{VG}(H_\perp)$ should be an analytic function of the transverse magnetic field as $H_\perp$ is varied through $H_\perp = 0$. Except for the usual Ginzburg-Landau anisotropies associated with the copper-oxide planes,[33] point disorder should act on a tilted vortex array just as it does for $H_\perp = 0$. The vortex-glass temperature should thus be a simple parabolic function of $H_\perp$ for small perpendicular fields, $T_{VG}(H_\perp) \approx T_{VG}(0)[1+\alpha H_\perp^2]$. If the vortex-glass transition tracks the equilibrium melting temperature,[4] T_{VG} should actually *increase* with increasing tilt,[33] i.e., $\alpha > 0$.

Correlated disorder, on the other hand, is turned off as the tilt is increased: Vortices will eventually "tunnel" through columnar and twin disorder at some average tipping angle for large enough $H_\perp$. Indeed, the scaling theory predicts a sharply decreasing *cusp* in the phase boundary $T_{BG}(H_\perp)$ as the field is tilted away from the c axis—see Fig. 4. The perpendicular critical field $H_\perp^c(T)$ marking this transition out of the Bose glass to a flux liquid is predicted to vary as

$$H_\perp^c(T) \sim \pm[T_{BG}(0)-T]^{3\nu'} . \tag{1.6}$$

For $H_\perp < H_\perp^c$, we have a transverse Meissner effect, i.e., $\mathbf{B}_\perp = 0$. If we approach $T_{BG}(0)$ by letting $|H_\perp|$ tend to zero (i.e., on path A in Fig. 4), scaling implies that the resistivity must vanish according to

$$\rho \sim |H_\perp|^{(z'-2)/3} . \tag{1.7}$$

Indications of a cusp in the irreversibility line for field orientations near the c axis in twinned single-crystal YBCO were noted years ago by Worthington *et al.*[34] More generally, the theory predicts an asymptotic scaling form for the linear resistivity,

$$\rho(t,\theta) = |t|^{\nu'(z'-2)} f(\theta |t|^{-3\nu'}) , \tag{1.8}$$

where $t = (T-T_{BG})/T_{BG}$ and $\theta \approx H_\perp/H_z$ is the tilt angle. Note that Eqs. (1.4)–(1.7) represent four distinct predictions depending on only two critical exponents. Recent simulations of a simplified model of lattice bosons in imaginary time[35] yield the estimates $\nu' = 1 \pm 0.01$ and $z' = 6 \pm 0.5$. A fit of the data in Refs. 12 and 13 to the *Bose*-glass scaling hypothesis yields $\nu' \approx 1.3 \pm 0.5$ and $z' \approx 7 \pm 2$. The cusp will be rounded off in thin samples due to finite-size effects, which are particularly pronounced in the direction parallel to the correlated disorder.

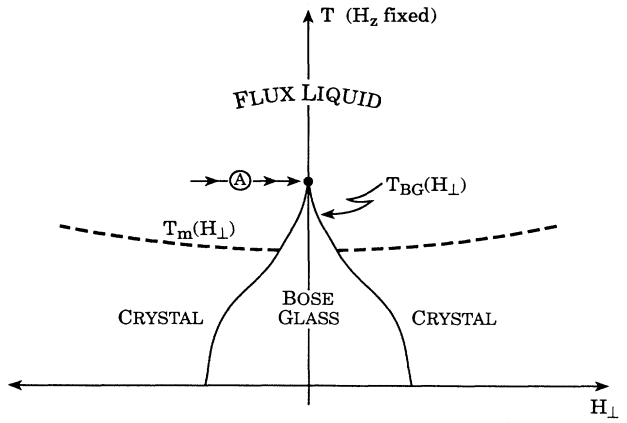

FIG. 4. Phase diagram in the $(T, H_\perp)$ plane with the field H_z along direction of the correlated disorder fixed. Note the sharp cusp in $T_{BG}(H_\perp)$ for small $H_\perp$. The crystalline phase is an Abrikosov lattice for fields tipped away from a single family of parallel twins. The "crystal" is a smecticlike phase for columnar pins or a mosaic of twin boundaries.

The transition curves leading to the tip of the cusp in Fig. 4 are in a different universality class than the Bose-glass transition which occurs for perfect alignment with the correlated disorder. The physics here is reflected in a kind of commensurate-incommensurate transition:[36] Vortices initially running parallel to extended defects in the Bose glass develop a series of solitonlike kinks upon crossing this phase boundary. These kinks allow jumps between neighboring twin planes, grain boundaries, and/or line defects, and cause the vortex arrays to tilt and entangle in a flux-liquid phase (see Ref. 37 and Sec. IV). At low temperatures the transition may instead proceed from a Bose glass into a tilted (and anisotropic) Abrikosov flux lattice, broken up by point disorder[9] only at the very largest length scales. If the tilt is away from a single family of parallel twins, crystalline order will extend quite far in both directions perpendicular to the average flux-line orientation. A first-order transition line $T_m(H_\perp)$ then presumably separates the flux liquid from this crystal. For *columnar* pins the low-temperature crystalline phase is a series of smecticlike vortex sheets, periodic along the direction of the columns. As discussed in Appendix A, this smectic phase can arise via a *continuous* freezing transition (dashed line in Fig. 4) from the flux liquid. The resistivity near the tilted flux-liquid–to–Bose-glass transition line is determined by the density of kinks.[37] We have not tried to analyze the Bose-glass–to–flux-crystal transition which is presumably induced by tilting at low temperatures. There may in fact be a small sliver of flux liquid interposed between the Bose-glass and crystalline phases at *all* nonzero temperatures, in analogy to what happens near H_{c1} in the absence of correlated disorder.[3]

Most realistic samples are, of course, subject to *both* point and correlated disorder, and the analysis of this paper only applies to field, temperature, and current ranges where point disorder can be neglected. The experimental evidence for first-order melting in the absence of correlated pinning[17–20] suggests that point disorder in single crystals may *not* be important near the irreversibility line, unless artificially enhanced by neutron or proton bombardment.[22] Calculations on flux lines in 1+1 dimensions with both columnar and point disorder included show that *correlated* disorder dominates at the transition if the point disorder is weak.[37] We expect that similar conclusions apply in 2+1 dimensions. Point disorder may affect the asymptotic dynamics of the low-temperature *phase,* however.[38] One possibility is that anisotropic excitations—influenced by both correlated and point pinning—control the asymptotic dynamics at very small currents. Another is that point disorder ultimately dominates in the low-temperature phase as the current vanishes. The relevant length scale for this behavior can be of order kilometers, however (see Sec. IV E), i.e., so large as to be experimentally unobservable.

C. Critical currents and instabilities for J‖B

The analogy with the quantum mechanics of two-dimensional particles also allows simple estimates of the temperature dependence of critical currents $J_c(T)$ below T_{BG} in the presence of correlated disorder. $J_c(T)$ is the current (perpendicular to the average field direction) which produces a Lorentz force $f_c = J_c\phi_0/c$ strong enough so that significant thermal activation is no longer needed for an isolated vortex to break away from its pinning site. For $J > J_c(T)$, one is in a flux-flow transport regime, only mildly perturbed by pinning. As illustrated in Fig. 5, the critical currents for high-T_c superconductors are often much larger than the current scales $\tilde{J}$ which control the behavior as $J \to 0$.[39] The results summarized below are restricted to the regime $B < B^*(T)$ in Fig. 3, so that interactions between vortices are relatively unimportant. See Sec. IV G for critical currents due to moving vortex bundles when $B > B^*(T)$.

The renormalization of critical currents by thermal fluctuations is illustrated in Fig. 6. We model a columnar pin by a cylindrical well with vortex binding energy per unit length U_0 and radius c_0. The solution of the London and Ginzburg-Landau equations for the vortex line near the cylindrical cavity with radius c_0 gives, for the binding energy,[2,40]

$$U_0 \approx \varepsilon_0 \ln\left[\frac{c_0}{\sqrt{2}\xi_{ab}}\right], \quad c_0 \gg \sqrt{2}\xi_{ab}\ ,$$
$$U_0 \approx \varepsilon_0 \left[\frac{c_0}{2\xi_{ab}}\right]^2, \quad c_0 \ll \sqrt{2}\xi_{ab}\ , \tag{1.9a}$$

with $\varepsilon_0 = (\phi_0/4\pi\lambda_{ab})^2$ and where ξ_{ab} is the superconducting coherence length. A useful formula which interpolates between these limits is

$$U_0 \approx \tfrac{1}{2}\varepsilon_0 \ln[1 + (c_0/\sqrt{2}\xi_{ab})^2]\ .$$

The critical current is determined by the maximal pinning force the vortex line experiences near a linear defect. Neglecting interaction effects, one finds, at zero temperature,

$$J_c = \frac{3\sqrt{3}}{4\sqrt{2}} J_{pb}, \quad c_0 > \sqrt{2}\xi_{ab}\ ,$$
$$J_c = \frac{27\sqrt{2}}{64}\left[\frac{c_0}{\sqrt{2}\xi_{ab}}\right]^2 J_{pb}, \quad c_0 < \sqrt{2}\xi_{ab}\ , \tag{1.9b}$$

where $J_{pb} = c\phi_0/12\sqrt{3}\pi^2\lambda_{ab}^2\xi_{ab}$ is the pair-breaking current. This critical current, up to numerical constants

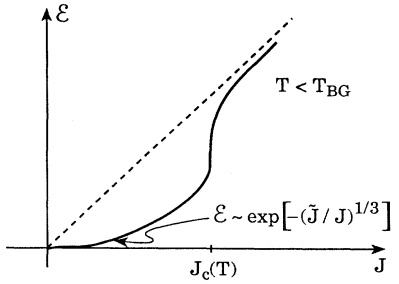

FIG. 5. Schematic current-voltage characteristic in the Bose-glass phase. Conventional flux-flow behavior is recovered for $J > J_c$. A distinct current scale $\tilde{J}$ controls the variable-range hopping behavior near the origin.

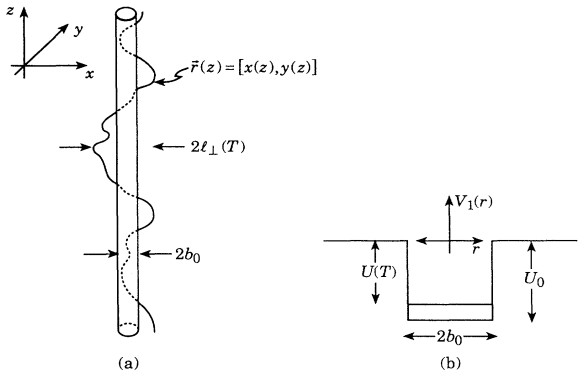

FIG. 6. Schematic of a flux line interacting with a columnar pin. (a) The line is confined to a tube of radius $l_\perp(T)$. (b) Cylindrical square well potential which models the binding of the line to the pin. The binding potential is reduced from U_0 to $U(T)$ by thermal fluctuations.

and logarithmic corrections, is also given by equating the Lorentz force with U_0/ξ_{ab}, i.e.,

$$J_c(0)\approx cU_0/\phi_0\xi_{ab} \ . \tag{1.9c}$$

In the presence of thermal fluctuations, however, U_0 should be replaced by a smaller binding *free* energy $U(T)$ per unit length, to account for the entropy lost by confining the flux line to the vicinity of the pin. This entropy is determined by the zero-point energy in the ground state of a fictitious two-dimensional quantum-mechanical particle confined to the cylindrical well.[41] As illustrated in Fig. 6, ξ_{ab} should now be replaced by $l_\perp(T)$, which is the spatial extent of the corresponding ground-state wave function. For $T\gtrsim T_1$, where T_1 is a characteristic pinning temperature estimated in Appendix D, we find a strong thermal renormalization of $J_c(T)$,

$$J_c(T)\approx J_c(0)e^{-3(T/T^*)^2}$$

$$\text{(line disorder, } T_1<T<T_{dp}) \ . \tag{1.10a}$$

Here $T^*=\sqrt{\tilde{\epsilon}_1 U_0}b_0$, with $b_0=\max\{c_0,\sqrt{2}\xi_{ab}\}$, is the energy scale of the pin.

For $T>T_{dp}$, where T_{dp} is a temperature such that $l_\perp(T_{dp})=d$, the spacing between pins, the critical current falls off more slowly,

$$J_c(T)\simeq J_c(0)\left[\frac{b_0}{d}\right]^3\left[\frac{T^*}{T}\right]^4$$

$$\text{(line disorder, } T>T_{dp}) \ , \tag{1.10b}$$

reflecting the collective pinning of one line by many pins.

The discussion of critical currents for planar pins such as twin boundaries is similar, except that now one needs to solve a problem in one-dimensional quantum mechanics.[41] We show here that, for Lorentz forces perpendicular to the twins, the renormalized critical current is approximately

$$J_c(T)\approx\tfrac{1}{2}J_c(0)(T^*/T)^4$$

$$\text{(planar disorder, } T_1<T<T_{dp}) \ , \tag{1.11a}$$

again for T greater than a characteristic temperature scale T_1. For a single family of parallel twins with average spacing d, a depinning temperature can again be defined by the condition $l_\perp(T_{dp})=d$, where $l_\perp$ is the localization length perpendicular to the planes. When $T>T_{dp}$, the collective pinning result for the critical current is

$$J_c(T)\approx J_c(0)\left[\frac{b_0}{d}\right](T^*/T)^2$$

$$\text{(planar disorder, } T>T_{dp}) \ . \tag{1.11b}$$

It is interesting to contrast Eqs. (1.10) and (1.11) with the analogous result for *point* disorder, namely,[42]

$$J_c(T)\approx J_c(0)e^{-(T/\tilde{T})^3} \quad \text{(point disorder)} \ , \tag{1.12}$$

where $\tilde{T}$ is a characteristic energy scale for point disorder. The relative importance of pinning by points, lines, and planes in a given context depends crucially of course on the characteristic energies T^* or $\tilde{T}$ for each type of defect. We stress again that interactions are not included in the above estimates. Nevertheless, the different temperature dependences embodied in Eqs. (1.10)–(1.12) show clearly that point disorder is particularly susceptible to being thermally neutralized, while planar and columnar disorder are much more robust.

We have also considered the stability of pinned vortex lines to currents J *parallel* to B. There is extensive work on this problem by Clem,[43] Brandt,[44] and others during the classic (pre-high-T_c) era of superconductivity research. A nonzero J_z tends to produce helical instabilities in vortex arrays. In an entangled flux liquid, one would expect this instability to lead to a linear resistivity, just as for currents perpendicular to the lines. As shown by Brandt,[44] a nonzero shear modulus in a weakly pinned Abrikosov flux lattice resists this instability, suggesting that $\mathbf{J}\|\mathbf{B}$ is an excellent geometry in which to study melting or a possible entanglement-induced shear modulus.[3,8]

A detailed study of the response of interacting vortices in the Bose-glass or Mott-insulator phase to $\mathbf{J}\|\mathbf{B}$ in the presence of thermal fluctuations is beyond the scope of this paper. We do show, however, that J_z acts on flux lines like an *imaginary* magnetic field applied to quantum-mechanical bosons. We then use this analogy to calculate the probability per unit length of the thermally activated escape of a single vortex trapped on a columnar pin to form an unboundedly growing helix. Because the magnetic field is imaginary, it adds a destabilizing parabolic contribution to the binding potential. The pitch of the unstable helical eigenmode plays the role of the cyclotron frequency. For small currents J_z, the escape over this barrier can be calculated via the WKB approximation of elementary quantum mechanics. The physics is similar to nuclear β decay.

D. Outline

In Sec. II we first review a simple model of interacting flux lines subjected to correlated disorder. The analogy with quantum mechanics is illustrated by estimating critical currents for columnar and planar pins. Having established the basic energy and length scales, we then discuss a tight-binding model which assumes that the vortices spend most of the time in the vicinity of a random array of columnar pins. The instability of a bound flux line to a current $\mathbf{J}\|\mathbf{B}$ is described as well.

In Sec. III we describe the phases and phase diagrams expected for the tight-binding model developed in Sec. II.[31] The responses to compression and tilt are discussed, as well as density correlations in the flux liquid. We determine the range of translational correlations in the presence of correlated disorder and describe what is known about the transition from the Mott insulator to the Bose glass.

Section IV treats the dynamics of pinned flux lines at low temperatures. Bose-glass dynamics mediated by half-loop and double-kink configurations is described. We point out that half-loop configurations may be particularly important in the Mott insulator and discuss various percolationlike transport regimes which occur over immediate length scales in the Bose glass. We argue that variable-range hopping via "superkinks" dominates the asymptotic dynamics at the lowest currents and largest length scales in the Bose glass. We also review the stability of this picture of the dynamics to both tilting the field and the introduction of point disorder.[37] We discuss as well the dynamics of vortex bundles at high fields where short-range crystalline order is important.

In Sec. V we describe the scaling theory of the Bose-glass–to–flux-liquid transition, with an emphasis on its predictions about the response of flux lines to tilt, and discuss the stability of the transition to weak point disorder.

Section VI describes the changes needed to adapt the theory to pinning by mosaics and single families of twin boundaries.

II. FREE ENERGIES, PATH INTEGRALS, AND QUANTUM MECHANICS

In this section we introduce and analyze statistical systems of vortices in the presence of correlated disorder. The models considered are the simplest ones which capture both the physics of flux-line localization and of interactions. Understanding the relevant free energies requires evaluation of path integrals over the trajectories by which vortex lines cross the sample in the direction of the applied field. These path integrals can be evaluated by exploiting an analogy with the quantum mechanics of two-dimensional particles in imaginary time. We illustrate the use of this technique both for isolated vortices and interacting assemblies of lines.

A. Model free energy

We start with a model free energy F_N for N flux lines in a sample of thickness L, defined by their trajectories $\{\mathbf{r}_j(z)\}$ as they traverse a sample with both columnar pins and external magnetic field aligned with the z axis, i.e., in the direction perpendicular to the CuO_2 planes,

$$F_N=\frac{1}{2}\tilde{\varepsilon}_1\sum_{j=1}^{N}\int_0^L\left|\frac{d\mathbf{r}_j(z)}{dz}\right|^2dz + \frac{1}{2}\sum_{i\neq j}\int_0^L V[|\mathbf{r}_i(z)-\mathbf{r}_j(z)|]dz + \sum_{j=1}^{N}\int_0^L V_D(\mathbf{r}_j(z))dz\ , \tag{2.1a}$$

with

$$V_D(\mathbf{r})=\sum_{k=1}^{M}V_1(\mathbf{r}-\mathbf{R}_k)\ . \tag{2.1b}$$

Here $V(|\mathbf{r}_i-\mathbf{r}_j|)=2\varepsilon_0K_0(r/\lambda_{ab})$ is the interaction potential between lines with in-plane London penetration depth λ_{ab} and the random potential $V_D(\mathbf{r})$ arises from a z-independent set of M disorder-induced columnar pinning potentials $V_1(\mathbf{r})$ centered on sites $\{\mathbf{R}_k\}$. The tilt modulus $\tilde{\varepsilon}_1\approx(M_\perp/M_z)\varepsilon_0\ln(\lambda_{ab}/\xi_{ab})$, where the material anisotropy is embodied in the effective-mass ratio $M_\perp/M_z\ll1$, and $\varepsilon_0\approx(\phi_0/4\pi\lambda_{ab})^2$ is the energy scale for the interactions. A slightly better approximation which takes interactions into account when $B\gg\phi_0/\lambda_{ab}^2$ is $\tilde{\varepsilon}_1\approx(M_\perp/M_z)\varepsilon_0\ln(a_0/\xi_{ab})$, where $a_0=(\phi_0/B)^{1/2}$ is the vortex-lattice constant. For $B\lesssim\phi_0/\lambda_{ab}^2$, we have $\tilde{\varepsilon}_1\approx\varepsilon_0$ because of magnetic couplings between the CuO_2 planes.[4] The elastic contribution $\frac{1}{2}\tilde{\varepsilon}_1|d\mathbf{r}_j/dz|^2$ is the first nontrivial term in a small tipping angle expansion of the line energy of nearly straight vortex lines.[3] The stretching energy evaluated in this approximation should be *quantitatively* correct provided

$$\left|\frac{d\mathbf{r}_j}{dz}\right|^2\ll M_z/M_\perp \tag{2.2}$$

for the most important vortex configurations.[45] The interactions can extend to arbitrarily distant flux lines, but have been taken to be local in z. Locality in z is a good approximation for describing fluctuations in the "nonrelativistic" limit of nearly straight lines, which for anisotropic systems again translates into the condition Eq. (2.2)—see Appendix B. Correlated disorder only pushes the system further into this "nonrelativistic" regime. Equation (2.2) is well satisfied in a high-temperature flux liquid except close to the upper critical field as discussed in Appendix B.

We model $V_D(\mathbf{r})$ for simplicity by a random array of identical cylindrical traps of average spacing d passing completely through the sample with well depth per unit length U_0 and effective radius b_0. Here

$$b_0=\max\{c_0,\sqrt{2}\xi_{ab}\}\ , \tag{2.3}$$

in accordance with the calculations of Mkrtchyan and Schmidt.[40] Here $c_0\approx25$–40 Å is the radius of the columnar pins and ξ_{ab} is the superconducting coherence length in the ab plane. The characteristic temperature T_0 such

that $\sqrt{2}\xi_{ab}(T_0)=c_0$ and above which b_0 is proportional to the coherence length is estimated in Appendix D. Upon assuming the pins are parallel and randomly distributed with $b_0 \ll d$, we find that $\bar{V}_D \approx (b_0/d)^2 U_0$, while the random potential fluctuations $\delta V_D(\mathbf{r})=V_D(\mathbf{r})-\bar{V}_D$ satisfy

$$\overline{\delta V_D(\mathbf{r})\delta V_D(\mathbf{r}')}=\Delta_1\delta^{(2)}(\mathbf{r}-\mathbf{r}') , \tag{2.4a}$$

with

$$\Delta_1 \approx (U_0^2 b_0^4/d^2)[1+\mathcal{O}(b_0^2/d^2)] . \tag{2.4b}$$

The overbars represent a quenched random average over the disorder. A more realistic model might use a potential which vanishes linearly as $r\to 0$ instead of the simple square well used here.[40,46] Such modifications will change coefficients of order unity, which we suppress in these and most subsequent estimates of physical quantities.

Although we consider here explicitly only fields nearly parallel to the c axis, qualitatively similar models and results should apply for fields in, say, the ab plane. The interactions will now be anisotropic, and the tilt modulus $\tilde{\varepsilon}_1$ will be replaced by an anisotropic 2×2 matrix whose largest component reflects the confining effect of the CuO_2 planes on flux-line wandering away from the ab plane in the c direction.

A complete statistical treatment of the free energy (2.1) requires integration of $e^{-F_N/T}$ over all vortex trajectories $\{\mathbf{r}_j(z)\}$. The grand canonical partition function, for example, is[3]

$$\mathcal{Z}_{\rm gr}=\sum_{N=0}^{\infty} e^{\mu NL/T}\int \mathcal{D}\mathbf{r}_1(z)\cdots\int \mathcal{D}\mathbf{r}_N(z) e^{-F_N/T} , \tag{2.5}$$

where the chemical potential

$$\mu=\varepsilon_1-H\phi_0/4\pi \tag{2.6}$$

changes sign at H_{c1}. Expressions for equilibrium correlation functions are similar. To average over a quenched random distribution of columnar pins, we must also evaluate quantities such as

$$\overline{\ln\mathcal{Z}_{\rm gr}}=\frac{\int \mathcal{D}V_D(\mathbf{r})\ln\mathcal{Z}_{\rm gr}\exp[(-1/2\Delta_1)\int d^2r\, V_D^2(r)]}{\int \mathcal{D}V_D(\mathbf{r})\exp[(-1/2\Delta_1)\int d^2r\, V_D^2(r)]} . \tag{2.7}$$

Related averages for a few flux lines and a few columnar pins are evaluated in the next section.

B. Critical currents from elementary quantum mechanics

Consider a vortex line trapped near a single columnar pin parallel to z in an otherwise defect-free sample of thickness L, as shown in Fig. 6. As discussed in the Introduction, we require the binding *free* energy per unit length

$$U(T)=U_0-TS , \tag{2.8}$$

where S is the entropy reduction due to confinement. This free energy is given by a path integral,

$$e^{U(T)L/T}=\frac{\int \mathcal{D}\mathbf{r}(z)\exp[(-\tilde{\varepsilon}_1/2T)\int_0^L(d\mathbf{r}/dz)^2dz-(1/T)\int_0^L V_1[\mathbf{r}(z)]dz]}{\int \mathcal{D}r(z)\exp[(-\tilde{\varepsilon}_1/2T)\int_0^L(d\mathbf{r}/dz)^2dz]} , \tag{2.9}$$

where the denominator is required to subtract off the entropy of an unconfined line far from the pin. The cylindrically symmetric confining potential $V_1(r)$, indicated in Fig. 6(b), tends to zero as $|\mathbf{r}|\to\infty$ and need not be a square well in general. The path integrals in (2.9) follow from standard statistical methods which express them in terms of the eigenvalues of a transfer matrix.[47] In the limit $L\to\infty$, the smallest eigenvalue dominates, and $U(T)=-E_0(T)$, where $E_0(T)$ is the ground-state energy of a two-dimensional "Schrödinger equation"[41]

$$\left[-\frac{T^2}{2\tilde{\varepsilon}_1}\nabla_\perp^2+V_1(r)\right]\psi_0(\mathbf{r})=E_0\psi_0(\mathbf{r}) . \tag{2.10}$$

Here and henceforth, all vectors $\mathbf{r}$ will refer to positions in the plane perpendicular to $\hat{\mathbf{z}}$. Note that T plays the role of the Planck parameter $\hbar$ and $\tilde{\varepsilon}_1$ plays the role of mass m in this quantum-mechanical analogy.

The ground-state wave function $\psi_0(\mathbf{r})$ determines the localization length $l_\perp(T)$ displayed in Fig. 6(a). As shown in Appendix C, the probability $P(\mathbf{r})$ of finding a point on the vortex at transverse displacement $\mathbf{r}$ relative to the center of the pin is independent of z and given by the square of $\psi_0(\mathbf{r})$, just as in elementary quantum mechanics,

$$\mathcal{P}(\mathbf{r})=\psi_0^2(\mathbf{r})\Big/\int d^2r\,\psi_0^2(\mathbf{r}) . \tag{2.11}$$

We then define the localization length as

$$l_\perp^2=\int d^2r\, r^2\psi_0^2(r)\Big/\int d^2r\,\psi_0^2(r) . \tag{2.12}$$

The properties of a vortex near a columnar pin now follow from standard results for a quantum particle in a cylindrical potential.[48] We write Eq. (2.10) in radial coordinates as

$$\frac{1}{r}\frac{d}{dr}\left[r\frac{d}{dr}\psi_0(r)\right]+k^2(r)\psi_0(r)=0, \quad r<b_0 , \tag{2.13a}$$

and

$$\frac{1}{r}\frac{d}{dr}\left[r\frac{d}{dr}\psi_0(r)\right]-\kappa^2\psi_0(r)=0, \quad r>b_0 , \tag{2.13b}$$

with

$$\frac{T^2k^2(r)}{2\tilde{\varepsilon}_1}\equiv E_0-V_1(r) \tag{2.14a}$$

and

$$\frac{T^2\kappa^2}{2\tilde{\varepsilon}_1}\equiv -E_0 , \tag{2.14b}$$

and where we assume a binding potential $V_1(r)$ which vanishes for $r>b_0$.

For the special case of a cylindrical square well [$V_1(r)\equiv -U_0$, $r<b_0$, and $V_1(r)=0$, $r>b_0$], the binding free energy $U(T)=-E_0$ takes the form[41]

$$U(T)=U_0 f(T/T^*) , \tag{2.15}$$

where T^* is an important characteristic energy scale defined by

$$T^*=\sqrt{\tilde{\varepsilon}_1 U_0}\,b_0 . \tag{2.16}$$

When $T\ll T^*(T)$, the well is effectively infinite, and we find the usual particle-in-a-box result

$$U(T)\approx U_0-c_1\frac{T^2}{2\tilde{\varepsilon}_1 b_0^2} , \tag{2.17}$$

where c_1 is a constant related to the first zero of the Bessel function $J_0(x)$ which solves Eq. (2.13a) in this limit. The localization length is then

$$l_\perp(T)\approx b_0[1+\mathcal{O}(1/\kappa b_0)] . \tag{2.18}$$

The low-temperature correction in Eq. (2.17) represents the entropy lost each time a wandering flux line is reflected off the confining walls of the binding potential.[49] At a crossover temperature T_1, defined by $T^*(T_1)=T_1$, this "zero-point energy" of confinement becomes comparable to the well depth.

When $T>T_1$, the flux line is only weakly bound [$|E_0|\ll(-1/b_0)\int_0^{b_0}V_1(r)dr\equiv U_0$], although strictly localized states *always* exist in this effectively two-dimensional (2D) problem. Equation (2.13a) may now be approximated by

$$\frac{1}{r}\frac{d}{dr}\left[r\frac{d}{dr}\psi_0(r)\right]\approx\frac{2\tilde{\varepsilon}_1}{T^2}V_1(r)\psi_0(r) . \tag{2.19}$$

Upon using a normalization such that $\psi_0(r)\approx 1$ for $r<b_0$, Eq. (2.19) can be integrated to yield

$$\left.\frac{d\psi_0}{dr}\right|_{r=b_0}=\frac{2\tilde{\varepsilon}_1}{b_0T^2}\int_0^{b_0}V_1(r)r\,dr . \tag{2.20}$$

Outside the well, Eq. (2.13b) is solved by

$$\psi_0(r)=\text{const}\times K_0(\kappa r) \propto \ln(\kappa r) , \tag{2.21}$$

where we have approximated the zero-order Bessel function $K_0(x)$ by a form appropriate to the limit $b_0\ll\kappa^{-1}$. Equating logarithmic derivatives of $\psi_0(r)$ at $r=b_0$ leads immediately to the usual result for a weakly bound quantum particle in two dimensions, namely,[48]

$$E_0(T)\equiv -U(T) \approx -\frac{1}{2}U_0\left[\frac{T}{T^*}\right]^2 e^{-2(T/T^*)^2} , \tag{2.22}$$

where we have specialized to the case of a square well. In this limit we have $l_\perp(T)\approx\kappa^{-1}=T/\sqrt{2\tilde{\varepsilon}_1 U(T)}$, so that

$$l_\perp(T)\approx b_0 e^{(T/T^*)^2} . \tag{2.23a}$$

The flux line now "diffuses" within a confining radius of order $l_\perp(T)$ as it crosses the sample. The length along $\hat{z}$ required to diffuse across this tube is $l_z\approx l_\perp^2/(T/\tilde{\varepsilon}_1)$, i.e.,

$$l_z=(b_0^2\tilde{\varepsilon}_1/T)e^{2(T/T^*)^2} . \tag{2.23b}$$

The qualitative behavior of the binding free energy as a function of temperature is shown in Fig. 7. The critical current renormalized by thermal fluctuations is of order

$$J_c(T)\approx cU(T)/\phi_0 l_\perp(T) , \tag{2.24a}$$

which replaces the zero-temperature estimate (1.9c). Upon combining Eqs. (2.22) and (2.23a) and ignoring preexponential factors, we find that $J_c(T)$ takes the form (1.10a) for $T>T_1$, as discussed in the Introduction.

A more precise expression using (1.9b) results from a simple quantum-mechanical derivation analogous to derivation of the Frantz-Keldysh effect:

$$J_c=J_{pb}\frac{3\sqrt{2}}{8}\left[\frac{c_0}{\sqrt{2}\xi}\right]^2\left[\frac{T}{T^*}\right]^2 e^{-3(T/T^*)^2} . \tag{2.24b}$$

This derivation exploits the equivalence between a supercurrent and a fictitious electric field acting on fluxons viewed as quantum-mechanical particles—see Sec. IV.

A key experimental parameter is the crossover temperature T_1, which must in general be determined self-consistently from $T^*(T_1)=T_1$, since $\tilde{\varepsilon}_1$, U_0, and b_0 are

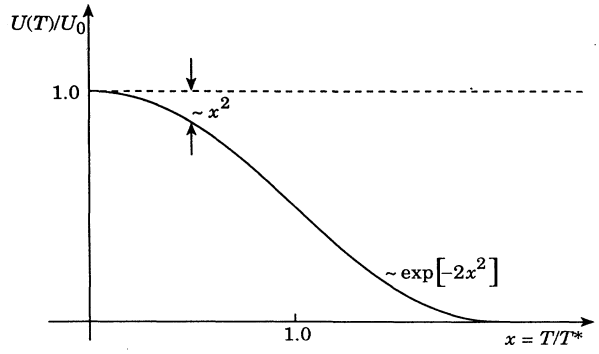

FIG. 7. Renormalized binding free energy $U(T)$ for the pin in Fig. 6.

themselves temperature dependent. We estimate T_1 for the layered cuprates in Appendix D.

Critical currents for *planar* pins with well depth U_0 and overall width $2b_0$ [see Fig. 1(b)] can be calculated in a similar fashion. We again find the scaling form (2.15) with $f(x)=1-(\pi^2/4)x^2$ for $x \ll 1$, i.e., $T \ll T_1$. For $T \gg T_1$, the results are[41]

$$U(T) \approx \tfrac{1}{2} U_0 (T^*/T)^2 \tag{2.25}$$

and

$$l_\perp(T) \approx b_0 (T/T^*)^2 \ . \tag{2.26}$$

Equation (1.11a) for the critical current associated with planar pins now follows immediately from Eq. (2.24a). [Equation (1.11b) is derived in Sec. VI B.)

C. Tunneling between pinning sites

Section II B describes the "atomic physics" of flux lines and columnar pins. The localization length is like the Bohr radius of an isolated "atom" consisting of one columnar pin and one vortex line. Now consider a vortex line which is able to hop between *two* nearby identical columnar pinning sites at $\mathbf{r}_1$ and $\mathbf{r}_2$ (analogous to a H_2^+ molecule) as it traverses the sample—see Fig. 8. The binding potential in Eq. (2.10) in this case is

$$V_2(\mathbf{r}) = V_1(\mathbf{r}-\mathbf{R}_1) + V_1(\mathbf{r}-\mathbf{R}_2) \ , \tag{2.27}$$

where identical wells of depth U_0 and radius b_0 are assumed. As in a quantum double well,[48] the dominant configurations are those in which the particle delocalizes further by "tunneling" from one well to another. In the subspace spanned by the isolated pin ground-state wave functions $\psi_0(\mathbf{r}-\mathbf{R}_1)$ and $\psi_0(\mathbf{r}-\mathbf{R}_2)$, the effective Hamiltonian (generalized to allow for *many* columnar pins in the next subsection) takes the form

$$\mathcal{H}_2 = \begin{bmatrix} E_0 & t \\ t & E_0 \end{bmatrix} , \tag{2.28}$$

where E_0 is the ground-state energy determined in the previous subsection and $t>0$ is a tunneling matrix element. The two lowest-energy eigenvalues for the double well are then

$$E_\pm = E_0 \pm t \ . \tag{2.29}$$

To determine t we use the method of Baz', Zel'dovich, and Perelomov[50] to find the ground-state energy E_- in a regime such that

$$b_0 \ll l_0 \ll d_{12} \ , \tag{2.30}$$

where $l_0 = \sqrt{T^2/2\tilde{\varepsilon}_1 |E_0|}$ is the localization length for one pin and $d_{12}=|\mathbf{R}_1-\mathbf{R}_2|$ is the pin separation. Away from the cylindrical wells, we take

$$\psi_{\rm out}(\mathbf{r}) = K_0(\kappa_- |\mathbf{r}-\mathbf{R}_1|) + K_0(\kappa_- |\mathbf{r}-\mathbf{R}_2|) \ , \tag{2.31}$$

where

$$\frac{T^2\kappa_-^2}{2\tilde{\varepsilon}_1} \equiv E_- \ . \tag{2.32}$$

Just outside the pin at $\mathbf{R}_1 \equiv \mathbf{0}$, we can approximate,

$$\psi_0(\mathbf{r}) \approx -\ln(\kappa_- r) + \left[\frac{2}{\pi\kappa_- d_{12}}\right]^{1/2} e^{-\kappa_- d_{12}} \ . \tag{2.33}$$

Inside this pin we can use the estimate (2.20) described above. Upon equating logarithmic derivatives on the boundary of pin 1, we find an implicit equation for κ_-,

$$-\ln(\kappa_- b_0) + \left[\frac{2}{\pi\kappa_- d_{12}}\right]^{1/2} e^{-\kappa_- d_{12}} = (T/T^*)^2 \ . \tag{2.34}$$

A straightforward iterative solution in the regime (2.30) gives

$$E_-(T) \approx E_0(T)\left[1+2\left[\frac{2T}{\pi E_{12}}\right]^{1/2} e^{-E_{12}/T}\right] , \tag{2.35}$$

where

$$E_{12} = \sqrt{2\tilde{\varepsilon}_1 U(T)}\, d_{12} \tag{2.36}$$

and $U(T)$ is given by Eq. (2.22). Upon comparing with Eq. (2.29), we find that the tunneling matrix element is

$$t = 2\left[\frac{2}{\pi}\right]^{1/2} \frac{U(T)}{\sqrt{E_{12}/T}} e^{-E_{12}/T} \ . \tag{2.37}$$

The flux line has now delocalized a distance $\sim d_{12}$ in the transverse direction. Delocalization proceeds via wandering in a tube of radius $l_\perp(T)$, given by Eq. (2.23a), and occasional tunneling across to a neighboring tube, as indicated in Fig. 8. The spacing between such tunneling events along the z axis is of order

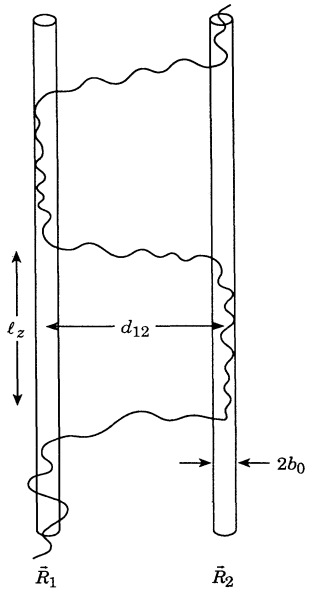

FIG. 8. "Tunneling" of a flux line between two neighboring columnar pins. The analogous quantum-mechanical system is a H_2^+ molecule.

$$l_z(T)\approx\left[\frac{b_0^2\tilde{\varepsilon}_1}{T}e^{2(T/T^*)^2}\right]e^{E_{12}/T}, \tag{2.38}$$

where the prefactor (an inverse "attempt frequency" in imaginary time) comes from the isolated pin result Eq. (2.23b). Note the close analogy between Fig. 8 and the configurations of a classical one-dimensional Ising model with exchange constant $J=E_{12}$ disrupted by kinks along the z axis.

D. Tight-binding model

When many columnar pins are present, we can generalize the effective Hamiltonian (2.28) to a tight-binding model which allows vortex lines to hop between a randomly distributed array of defect sites. "Tight binding" means that each vortex spends most of its time near one of these sites. The grand canonical partition function Eq. (2.5) is then $\mathcal{Z}_{\rm gr}\propto\exp(-E_0L/T)$, where E_0 is the ground-state energy of the tight-binding model,

$$\mathcal{H}_{\rm TB}=-\mu\sum_j a_j^\dagger a_j+\sum_{i\neq j}t_{ij}(a_i^\dagger a_j+a_j^\dagger a_i)+V_{\rm int}\sum_j a_j^\dagger a_j a_j^\dagger a_j\ . \tag{2.39}$$

Here $a_j^\dagger$ and a_j are boson creation and annihilation operators which create and destroy flux lines on a columnar pin at site $\mathbf{R}_j$ and $V_{\rm int}$ is a typical interaction energy for two vortices on the same site. The tight-binding model (2.39) approximates the low-lying states of the full Hamiltonian entering the transfer-matrix representation of Eq. (2.5), i.e.,

$$\mathcal{Z}_{\rm gr}=\sum_{N=0}^{\infty}e^{\mu NL/T}\mathrm{Tr}\{e^{-\mathcal{H}_N L/T}\}\ , \tag{2.40a}$$

where

$$\mathcal{H}_N=-\frac{T^2}{2\tilde{\varepsilon}_1}\sum_{j=1}^{N}\nabla_\perp^2+\varepsilon_0\sum_{i\neq j}K_0(|\mathbf{r}_i-\mathbf{r}_j|/\lambda_{ab})+\sum_{j=1}^{N}V_D(\mathbf{r}_j)\ . \tag{2.40b}$$

The hopping-matrix element between sites separated by a distance d_{ij} is a direct generalization of Eq. (2.37),

$$t(d_{ij})\approx 2\left[\frac{2}{\pi}\right]^{1/2}\frac{U(T)}{\sqrt{E_{ij}/T}}e^{-E_{ij}/T}, \tag{2.41}$$

with $E_{ij}=\sqrt{2\tilde{\varepsilon}_1U(T)}d_{ij}$.

We shall assume the cost of double occupancy of a pinning site is prohibitively large. A reasonable estimate of $V_{\rm int}$ is

$$V_{\rm int}\approx\varepsilon_0\ln(H_{c2}/H)\ , \tag{2.42}$$

reflecting the energetic cost of one doubly quantized vortex as opposed to two singly quantized ones. The logarithmic term is included to correct for interactions with distant vortices.[51] We use a simple on-site repulsion (as in the Hubbard model of correlated electrons) because the physics at very low currents and near the Bose-glass transition is dominated by length scales much larger than the interaction range λ_{ab} of the vortices. If desired, the on-site term in Eq. (2.39) could be generalized to explicitly reflect the longer-ranged potential in Eq. (2.40b). The effect of a longer-range interaction on transport is discussed in Sec. IV.

The "particles" described by this Hamiltonian are bosons[3] because the ground-state wave function of any permutation symmetric Hamiltonian is bosonic.[47] The particle statistics only matter at high temperatures, in any case, when there is a significant probability for fluxons to exchange positions. In the strongly localized regime, identical results would emerge for fermions. The tight-binding approximation Eq. (2.39) allows us to conveniently extract results from a phenomenological theory of boson localization,[31] which also used a tight-binding formulation. For many applications, however, it is more convenient to use the classical expression (2.1) for the flux-line free energy.

The first two terms of Eq. (2.39) determine a noninteracting density of states $g(\varepsilon)$, such that

$$\mathcal{N}(\varepsilon)=\int_{-\infty}^{\varepsilon}g(\varepsilon')d\varepsilon' \tag{2.43}$$

is the number of eigenvalues per unit area with energy less than ε and $g(\varepsilon)$ is normalized such that $\mathcal{N}(+\infty)=1/d^2$. Note that $g(\varepsilon)$ has units of $(\text{energy}\times\text{length})^{-1}$. For an extensive discussion of the density of states for this "Lifshitz model" (in the context of hopping transport in amorphous semiconductors), see Ref. 32. Dispersion arises, even if all pinning sites have identical sizes and well depths, because vortices can resonantly tunnel between nearly columnar pins. The fluxon on the extreme left of Fig. 1(a), for example, is more tightly bound than the others because of this tunneling. In this model the bandwidth γ should be of order $\gamma\approx t$, where t is given by Eq. (2.41), evaluated at a typical columnar pin spacing d. Interactions generate an additional contribution to the bandwidth, of order $V_{\rm int}$.[32] In order-of-magnitude estimates, we shall take

$$\gamma\approx\max\{t(d),V_{\rm int}\}\ . \tag{2.44}$$

Suppose that these states are filled up to a chemical potential such that approximately half the columnar pins is filled. The density of states corresponding to the most weakly bound flux lines is then $g(\mu)\approx 1/d^2\gamma$, i.e.,

$$d^2g(\mu)\approx\min\left\{\left[\frac{\tilde{\varepsilon}_1d^2}{U^3(T)T^2}\right]^{1/4}\times\exp[\sqrt{2\tilde{\varepsilon}_1U(T)}d/T],V_{\rm int}^{-1}\right\}. \tag{2.45}$$

Note that this characteristic density of states is temperature independent and determined by $V_{\rm int}$ for $T\lesssim(d/b_0)T^*(T)$.

E. J||B and quantum mechanics in an imaginary magnetic field

We discuss finally a mapping onto quantum mechanics in an imaginary magnetic field possible when **J**||**B**. When **J**⊥**B** the mapping is onto quantum mechanics of particles in a *real* electric field—see Sec. IV. For **J**||**B** a general analysis is complicated because currents are then typically confined to a penetration depth of the sample surface in the Bose-glass and Mott-insulator phases; this penetration length presumably diverges as one approaches the high-temperature flux liquid. Even the response of individual vortices and of the Abrikosov flux lattice are subtle in this geometry.[42,43] We shall restrict our attention to a few comments, showing how vortices in an approximately *uniform* current **J**||**B** are destabilized from their columnar pinning sites. The analysis would pertain to vortices trapped by columnar pins in samples with transverse dimensions smaller than this penetration length, which diverges like $l_\perp(T)$ as $T \to T_{\rm BG}$.

If we add an external current $\mathbf{J}=J_z\hat{\mathbf{z}}$ to a system of vortex lines with average direction along $\hat{\mathbf{z}}$, the free energy of Eq. (2.1) is modified,

$$F_N \to F_N - \frac{1}{4\pi}\int d^2r \int dz\, \mathbf{H}_{\rm ext}\cdot\mathbf{B}(\mathbf{r},z) , \tag{2.46}$$

where

$$\nabla\times\mathbf{H}_{\rm ext}=\frac{4\pi}{c}J_z\hat{\mathbf{z}} ,$$

i.e.,

$$\mathbf{H}_{\rm ext}=\frac{4\pi J_z}{c}\frac{1}{2}(\hat{\mathbf{z}}\times\mathbf{r}) , \tag{2.47}$$

for a cylindrical sample with axis along $\hat{\mathbf{z}}$.

To evaluate the extra term, we need an expression the perpendicular magnetic field $\mathbf{B}_\perp(\mathbf{r},z)$, which for *isotropic* superconductors satisfies

$$[1-\lambda^2\nabla^2]\mathbf{B}_\perp=\phi_0\sum_{j=1}^{N}\frac{d\mathbf{r}_j}{dz}\delta[\mathbf{r}-\mathbf{r}_j(z)] . \tag{2.48}$$

Results for anisotropic systems can be obtained via the methods of Ref. 33. The columnar pinning potentials are independent of z, and the helical vortex distortions induced by J_z have a wave vector q_z^* which vanishes as $J_z \to 0$.[42,43] We can thus, to a first approximation, neglect the z derivative in the Laplacian appearing in Eq. (2.48).[52] Equation (2.48) is then easily inverted to give

$$\mathbf{B}_\perp(\mathbf{r},z)=\frac{\phi_0}{\lambda^2}\sum_{j=1}^{N}K_0\left[\frac{|\mathbf{r}-\mathbf{r}_j|,z}{\lambda}\right]\frac{d\mathbf{r}_j}{dz} . \tag{2.49}$$

The additional contribution to the free energy (2.46) becomes

$$\delta F_N=-\frac{\phi_0}{c}\sum_{j=1}^{N}\int_0^L dz\,\mathbf{a}[\mathbf{r}_j(z)]\cdot\frac{d\mathbf{r}_j}{dz} , \tag{2.50}$$

with

$$\mathbf{a}(\mathbf{r})=\frac{J_z}{2\lambda^2}\int d^2r' K_0\left[\frac{|\mathbf{r}-\mathbf{r}'|}{\lambda}\right](\hat{\mathbf{z}}\times\mathbf{r}') . \tag{2.51}$$

Upon adding the extra term to Eq. (2.1a), we find an expression which is formally identical to the Lagrangian for quantum-mechanical particles in imaginary time subjected to a fictitious "vector potential" $\mathbf{a}(\mathbf{r})$.[47] This vector potential is a nonlocal average weighted by $K_0(r/\lambda)$ over a region of size λ of a "microscopic" vector potential

$$\mathbf{a}_{\rm mic}(\mathbf{r})=\frac{J_z}{2}(\hat{\mathbf{z}}\times\mathbf{r}) . \tag{2.52}$$

Consider the consequences of this mapping for one vortex $\mathbf{r}(z)$ initially confined to one columnar pin at the origin of a cylindrical sample and let us approximate $\mathbf{a}(\mathbf{r}_\perp)\approx\mathbf{a}_{\rm mic}(\mathbf{r}_\perp)$. The statistical mechanics is now controlled by a partition function of the form

$$\mathcal{Z}=\int\mathcal{D}\mathbf{r}(z)\exp\left[-\frac{\tilde{\varepsilon}_1}{T}\int_0^L\left[\frac{d\mathbf{r}}{dz}\right]^2 dz + \frac{\phi_0}{cT}\int_0^L\mathbf{a}_{\rm mic}(\mathbf{r})\cdot\frac{d\mathbf{r}}{dz}dz - \frac{1}{T}\int_0^L V_1[r(z)]dz\right] . \tag{2.53}$$

Instead of Eq. (2.10), the "Schrödinger equation" for the smallest eigenvalue of the transfer matrix now reads

$$\frac{1}{2\tilde{\varepsilon}_1}\left[\frac{T}{i}\nabla_\perp+\frac{i\phi_0}{c}\mathbf{a}_{\rm mic}(\mathbf{r})\right]^2\psi_0(r) + V_1(r)\psi_0(r)=E_0\psi_0(r) . \tag{2.54}$$

Note that the "magnetic field" $\sim i(\nabla\times\mathbf{a}_{\rm mic})$ is purely imaginary. The cross term in the "kinetic energy" vanishes for radially symmetric eigenfunctions, and so Eq. (2.54) leads to a Schrödinger equation with an unstable effective potential,

$$V_{\rm eff}(r)=V_1(r)-\frac{\phi_0^2J_z^2r^2}{8\tilde{\varepsilon}_1c^2} , \tag{2.55}$$

indicated schematically in Fig. 9.

The potential in Fig. 9 reflects at instability in the underlying path integral (2.53) for large $\mathbf{r}(z)$. Once the vortex escapes from its columnar pin, it presumably forms a growing helix and generates voltage by expanding toward $r=\infty$.[42,43] The pitch of the initial helix corresponds to a wave vector

$$q_z^*=J_z\phi_0/\tilde{\varepsilon}_1c , \tag{2.56}$$

which represents the "Lamour precession frequency" of the fictitious quantum particle.

Vortices will escape from columnar pins when **J**||**B** with a probability determined by the WKB tunneling rate out of the unstable potential (2.55), in analogy to quantum-mechanical β decay. A fluxon bound with free energy $U(T)$ before the current is turned on must penetrate the barrier shown in Fig. 9. To escape completely it must tunnel a distance of order

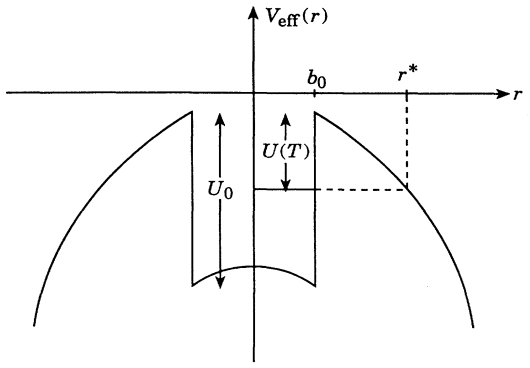

FIG. 9. Effective flux-line potential near a columnar pin with a current $\mathbf{J}\|\mathbf{B}$. The vortex bound state is unstable; the equivalent quantum problem is β decay.

$$r^* \approx \sqrt{8U\tilde{\varepsilon}_1}c/\phi_0 J_z \ . \tag{2.57}$$

The probability for this event is proportional to[48]

$$\exp\left[-\frac{2}{T}\int_{b_0}^{r^*}\{2\tilde{\varepsilon}_1[V_{\rm eff}(r)-U]\}^{1/2}dr\right] . \tag{2.58}$$

Upon approximating the exponential in the limit $r^* \gg l_\perp \geq b_0$ and neglecting factors of order unity, we find that the probability per unit length of escape is

$$P \approx \frac{[U_0-U(T)]^{1/2}}{\tilde{\varepsilon}_1^{1/2} l_\perp} e^{-(J_c^*/J_z)} , \tag{2.59}$$

where the critical current for this process is

$$J_c^* \approx \frac{c\tilde{\varepsilon}_1 U(T)}{T\phi_0} \ . \tag{2.60}$$

Note from (2.22) that this critical current has a different temperature dependence for $T > T^*$ than that predicted by Eq. (1.10a) for $\mathbf{J}\perp\mathbf{B}$.

F. "Uncertainty principle" for vortex lines

Now we describe briefly one last illustration of the analogy with quantum mechanics. Upon viewing Eq. (2.9) as a quantum-mechanical amplitude, we see that $\tilde{\varepsilon}_1(d\mathbf{r}/dt)$ is the "momentum" $\mathbf{p}$ for a fictitious 2D particle. The momentum and position operators in the corresponding Schrödinger equation then satisfy the commutation relations

$$[\hat{p}_\alpha, \hat{r}_\beta] = T\delta_{\alpha\beta} , \tag{2.61}$$

where α,β are the coordinate indices in the plane perpendicular to the vortex. Equation (2.61) leads in turn to an "uncertainty principle"

$$\Delta p \, \Delta r = T \ . \tag{2.62}$$

Upon estimating the uncertainty in the momentum as $\Delta p \simeq \tilde{\varepsilon}_1(u/z)$, where u is the mean characteristic thermal transverse displacement of the vortex line and z is the corresponding length of the fluctuating vortex segments, we arrive at (with $\Delta r \simeq u$)

$$\frac{u^2}{z} \sim \frac{T}{\tilde{\varepsilon}_1} \ . \tag{2.63}$$

Equation (2.63) describes the uncertainty in the vortex position due to thermal fluctuations and mimics the quantum-mechanical uncertainty principle. This basic result, already used to derive Eq. (2.23b), is equivalent to "diffusion" of vortex lines along the z axis with diffusion constant $D = T/\tilde{\varepsilon}_1$.[3]

III. FLUX-LIQUID, BOSE-GLASS, AND MOTT-INSULATOR PHASES

The physics of the right-binding model Eq. (2.39) was discussed by Fisher *et al.*[31] in the context of real bosons—helium films on disordered substrates at $T=0$. The temperature translates into an inverse sample thickness in the boson analogy, and so "$T=0$" in flux arrays simply means thick samples.[53] Varying the physical temperature in superconducting vortex arrays means changing "Planck's constant" in this quantum-mechanical analogy.[3]

The three phases described in Ref. 31 are all relevant to fluxon arrays with correlated disorder. The "superfluid" maps onto the high-temperature flux liquid in Fig. 3. In this entangled vortex liquid, flux lines are delocalized and hop freely from one columnar pin to another as they traverse the sample. All vortex trajectories $\mathbf{r}_j(z)$ "diffuse" as they wander across the sample, in the sense that

$$\lim_{z\to\infty} \overline{\langle |\mathbf{r}_j(z)-\mathbf{r}_j(0)|^2 \rangle} \approx 2D_R|z| \ , \tag{3.1}$$

where the brackets and overbar denote thermal and disorder averages, respectively.[54] The renormalized "diffusion constant" in Eq. (3.1) is expected to be $D_R \approx T/\tilde{\varepsilon}_1$ when the disorder is weak,[3] but should become much smaller near the Bose-glass transition, i.e., for $T \gtrsim T_{\rm BG}(B)$.

Each flux line is localized to the vicinity of one or more columnar pins in the low-temperature Bose glass and is described by an exponentially decaying eigenfunction such as those discussed in Sec. II. We can formally define a localization length via

$$\lim_{z\to\infty} \overline{\langle |\mathbf{r}_j(z)-\mathbf{r}_j(0)|^2 \rangle} = l_\perp^2(T) \ . \tag{3.2}$$

Delocalization occurs for vortex densities and temperatures such that the localization tubes surrounding neighboring flux lines overlap.[41] When this happens the localization length diverges at $T_{\rm BG}$,

$$l_\perp(T) \sim \frac{1}{|T-T_{\rm BG}|^{\nu_\perp}} \ , \tag{3.3}$$

where $\nu_\perp$ is an important critical exponent, determined from simulations of disordered bosons to be[35]

$$\nu_\perp \approx 1.0 \ . \tag{3.4}$$

There is also a correlation length along the z axis,

$$l_{\parallel}(T)=l_{\perp}^2/D_0 \ , \tag{3.5}$$

which is the distance along z it takes a flux line to "diffuse" across a tube of diameter the localization length. (See Fig. 10.) Here D_0 is a short-distance parameter which describes diffusion via tunneling between neighboring pins on scales less than $l_{\perp}$. The macroscopic large-scale diffusion constant D_R *vanishes* in the Bose glass. The simplest scaling hypothesis, which seems to be confirmed by computer simulations,[35] is that D_0 remains finite at $T_{\rm BG}$, so that $l_z(T)$ diverges according to[31]

$$l_{\parallel}(T)\sim \frac{1}{(T-T_{\rm BG})^{\nu_{\parallel}}} \ , \tag{3.6}$$

with $\nu_{\parallel}=2\nu_{\perp}$.

The Mott insulator arises when the vortex density matches the density of columnar pins at low temperatures (see Fig. 2). The fluxons are again localized, not only by the pinning sites themselves, but also by interactions with neighboring lines. It is again possible to define a localization length via Eq. (3.2). Unlike the Bose glass, however, the Mott insulator is *incompressible*—the vortex density will remain locked to the density of pins over a finite range of external fields, as in Fig. 2(b). As indicated in Fig. 2, the Mott insulator behaves in many respects like a Meissner phase with $B=B^*$ instead of $B=0$. We shall assume, following Ref. 31, that the Mott-insulator line phase in Fig. 3 terminates below $T_{\rm BG}(B)$, although there is evidence contradicting this assumption in the simulations of Krauth, Trivedi, and Ceperley.[35]

In the remainder of this section, we describe the equilibrium properties of each of the above phases. Real-time dynamics in response to a Lorentz force requires special treatment which we reserve to Secs. IV and V.

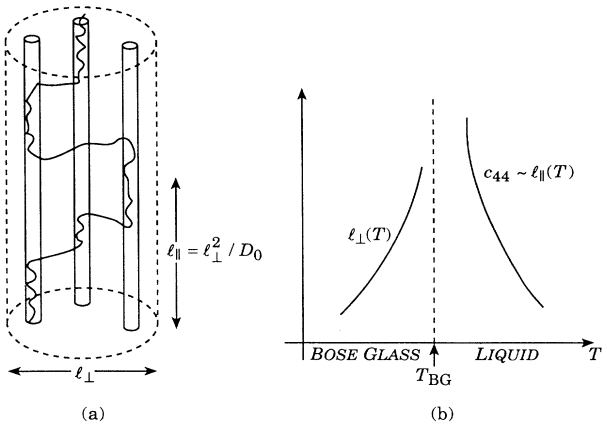

FIG. 10. (a) Flux-line wandering in a tube of size $l_{\perp}(T)$ which contains several columnar pins. $l_{\parallel}(T)$ is the distance along z needed for the line to wander across the tube diameter. (b) Divergence of $l_{\perp}(T)$ at the Bose-glass transition. The tilt modulus c_{44} diverges like $l_{\parallel}(T)$ as $T_{\rm BG}$ is approached from above.

A. Flux liquids with weak correlated disorder

At high temperatures, flux liquids are stable to correlated disorder, just as they are when the disorder is uncorrelated.[6] The properties of this "superfluid" can be extracted from a coherent-state path-integral treatment of Eq. (2.5) or, equivalently, of its representation via Eq. (2.40) as a quantum partition function. We also use a more general hydrodynamic theory approach which allows for nonlocal elastic constants.[6,8] Both methods lead to the important conclusion that the tilt modulus of the flux liquid is proportional to the inverse superfluid density of the fictitious "superfluid." We shall also compute the characteristic signature of correlated disorder in density-correlation functions of flux liquids, which may be measurable via neutron diffraction.[16]

Standard methods[55,56] allow the quantum partition function (2.40) to be expressed via a coherent-state path integral

$$\mathcal{Z}_{gr}=\int \mathcal{D}\psi(\mathbf{r}_{\perp},z)\int \mathcal{D}\psi^*(\mathbf{r}_{\perp},z)e^{-S(\psi,\psi^*)/T} \ , \tag{3.7}$$

where the "action" is

$$S=\int_0^L dz\int d^2r_{\perp}\left[T\psi^*\partial_z\psi+\frac{T^2}{2\tilde{\epsilon}_1}|\nabla_{\perp}\psi|^2-\mu|\psi|^2+\frac{1}{2}v_0|\psi|^4+\delta V_D(\mathbf{r}_{\perp})|\psi|^2\right] . \tag{3.8}$$

We have absorbed $\bar{V}_D\approx(b_0/d)^2U_0$ into the chemical potential and, for simplicity, replaced the pair potential by $V(\mathbf{r}_{\perp})=v_0\delta(\mathbf{r}_{\perp})$. Arbitrary in-plane potentials are easily treated,[6] but will have the same long-wavelength behavior, provided they have a finite range, of order λ_{ab} for flux lines. The amplitude of the complex field $\psi(\mathbf{r}_{\perp},z)$ is related to the fluctuating local flux-line density $n(\mathbf{r}_{\perp},z)$ by

$$n(\mathbf{r}_{\perp},z)=|\psi(\mathbf{r}_{\perp},z)|^2 \ . \tag{3.9}$$

As discussed in Ref. 41, entanglement of the flux lines is equivalent to phase coherence in ψ, and so we shall set

$$\psi(\mathbf{r}_{\perp},z)=|\psi(\mathbf{r}_{\perp},z)|e^{i\theta(\mathbf{r}_{\perp},z)} \tag{3.10}$$

and expand about the minimum of the action in Eq. (3.8),

$$\psi(\mathbf{r}_{\perp},z)=\sqrt{n_0+\pi(\mathbf{r}_{\perp},z)}\,e^{i\theta(\mathbf{r}_{\perp},z)} \approx\sqrt{n_0}\left[1+\frac{\pi(\mathbf{r}_{\perp},z)}{2n_0}\right]e^{i\theta(\mathbf{r}_{\perp},z)} \ , \tag{3.11}$$

where the average vortex density $n_0=B/\phi_0$ of this model is

$$n_0=\mu/v_0 \ . \tag{3.12}$$

Upon keeping only terms quadratic in $\theta(\mathbf{r}_{\perp},z)$ and $\pi(r_{\perp},z)$ and integrating out the amplitude fluctuation $\pi(\mathbf{r}_{\perp},z)$, we find an effective action which depends on the phase only,

$$S_{\rm eff}=\int_0^L dz\int d^2r_\perp\left\{\frac{(Tn_0)^2}{2}\left[\frac{1}{c_{44}}(\nabla_\perp\theta)^2+\frac{1}{c_{11}}(\partial_z\theta)^2+i\frac{T}{v_0}\delta V_D(\mathbf{r}_\perp)\partial_z\theta\right]\right\}, \tag{3.13}$$

where[41]

$$c_{44}=n_0\tilde{\varepsilon}_1 \tag{3.14a}$$

and

$$c_{11}=n_0^2 v_0 \tag{3.14b}$$

are the tilt and bulk modulus, respectively, for this simplified model of interacting flux lines.

The crucial point is that the disorder potential multiplying $\partial_z\theta(\mathbf{r}_\perp,z)$ in Eq. (3.13) is independent of z, so that it shows up only as a surface term at this level of description.[57] We conclude that weak correlated disorder has little effect on the properties of the "superfluid" flux liquid. Upon dropping this surface term and comparing Eq. (3.13) to the "phase only" representation of disordered bosons,[31] we find that c_{11}^{-1} is proportional to the compressibility of the "superfluid" and that, more importantly, c_{44}^{-1} is proportional to the superfluid density. Since the superfluid density vanishes at the localization transition,[31] we conclude that the tilt modulus of the flux lines *diverges* at $T_{\rm BG}$.

An infinite tilt modulus is to be expected in the Bose glass, since the correlated disorder keeps localized vortices from following a tilt in the external field. "Superfluidity" of the flux liquid means precisely that c_{44} is *finite*—there is a nonzero linear response to tipping the field, even in the presence of correlated disorder. Note that once the vortex liquid has been tipped relative to the correlated pins, we have the equivalent of a "supercurrent in imaginary time" as the fluxons " flow" through and around the columnar defects with increasing timelike variable z. Real superfluid films of ^{4}He are able to flow in a similar fashion without resistance across disordered substrates.

Correlations in the boson order parameter (3.10) are measured by

$$G(\mathbf{r}_\perp,z)=\langle\psi^*(\mathbf{r}_\perp,z)\psi(\mathbf{0},0)\rangle\ , \tag{3.15}$$

where we have dropped in disorder average since $\delta V_D(\mathbf{r}_\perp)$ is irrelevant at this level of approximation. The approach of $G(r_\perp,z)$ to its asymptotic value for large arguments allows us to extract correlation lengths in the flux-liquid "superfluid" phase.[58,31] Upon using Eq. (3.13) to evaluate the average, we find that

$$\lim_{r_\perp\to\infty} G(r_\perp,z)\approx|\langle\psi\rangle|^2\left[1+\left[\frac{l_\perp}{r_\perp}\right]\right] \tag{3.16a}$$

and

$$\lim_{z\to\infty} G(r_\perp,z)\approx|\langle\psi\rangle|^2\left[1+\left[\frac{l_\parallel}{z}\right]\right], \tag{3.16b}$$

where

$$l_\perp(T)=\frac{\sqrt{c_{11}c_{44}}}{Tn_0^2} \tag{3.17a}$$

and

$$l_\parallel(T)=\frac{c_{44}}{Tn_0^2}\ . \tag{3.17b}$$

For simplicity, we have assumed wave-vector-independent elastic constants. Nonlocal elastic parameters[52] would lead to crossovers at intermediate length scales, but should not affect the asymptotic analysis as $l_\perp$ and $l_\parallel$ diverge at $T_{\rm BG}$. Following the classic treatment by Josephson of the finite-temperature λ transition in bulk superfluid helium,[59] we assume that these lengths diverge at $T_{\rm BG}$ in the same way as their low-temperature counterparts in Eqs. (3.3) and (3.6).[31] Note that Eqs. (3.17) can be combined to give

$$l_\parallel(T)=\frac{Tn_0^2}{c_{11}}l_\perp^2(T)\ . \tag{3.18}$$

The bulk modulus c_{11} is expected to be finite in both the Bose-glass and flux-liquid phases. The exponent relation

$$\nu_\parallel=2\nu_\perp\ , \tag{3.19}$$

assumed for $T<T_{\rm BG}$, is thus consistent with Eq. (3.18) provided c_{11} is *also* finite at $T_{\rm BG}$ as well.[31] Equation (3.17b) predicts the way in which $c_{44}(T)$ diverges as $T\to T_{\rm BG}^+$,

$$c_{44}(T)\sim\frac{1}{|T-T_{\rm BG}|^{2\nu_\perp}}\ . \tag{3.20}$$

The physical reason for this divergence is the stiffening effect of pinning by columnar defects as $T\to T_{\rm BG}^+$. The tilt modulus is strictly infinite in the Bose-glass phase because the flux lines become locked to the columnar pin direction—see Sec. IV D. The behaviors of the localization length $l_\perp(T)$ below $T_{\rm BG}$ and the tilt modulus $c_{44}(T)$ above $T_{\rm BG}$ are summarized in Fig. 10(b).

We can also describe the flux liquid via a more general Landau expansion which expresses the free energy as a functional of two coarse-grained hydrodynamic fields: the vortex density

$$n(\mathbf{r}_\perp,z)=\sum_{j=1}^N\delta[\mathbf{r}_\perp-\mathbf{r}_j(z)] \tag{3.21a}$$

and a tangent field in the plane perpendicular to z,

$$\mathbf{t}(\mathbf{r}_\perp,z)=\sum_{j=1}^N\frac{d\mathbf{r}_j}{dz}\delta[\mathbf{r}_\perp-\mathbf{r}_j(z)]\ . \tag{3.21b}$$

To quadratic order in $\delta n(\mathbf{r}_\perp,z)=n(\mathbf{r}_\perp,z)-n_0$ and $\mathbf{t}(\mathbf{r}_\perp,z)$, we have[6,8]

$$F=\frac{1}{2n_0^2}\int d^2r_\perp dz\int d^2r'_\perp\int dz'[c_{44}(\mathbf{r}_\perp-\mathbf{r}'_\perp,z-z')\mathbf{t}(\mathbf{r}_\perp,z)\cdot\mathbf{t}(\mathbf{r}'_\perp,z')+c_{11}(\mathbf{r}_\perp-\mathbf{r}'_\perp,z-z')\delta n(\mathbf{r}_\perp,z)\delta n(\mathbf{r}'_\perp,z')]$$
$$+\int d^2r_\perp\int dz\,\delta V_D(\mathbf{r}_\perp)\delta n(\mathbf{r}_\perp,z)\ , \tag{3.22}$$

where $\delta V_D(\mathbf{r}_\perp)$ is the correlated disorder potential with correlations given by Eq. (2.4) and the conservation of vortex lines imposes the constraint

$$\partial_z\delta n+\nabla_\perp\cdot\mathbf{t}=0\ . \tag{3.23}$$

Here $c_{11}(\mathbf{r}_\perp,z)$ and $c_{44}(\mathbf{r}_\perp,z)$ are nonlocal generalizations of the constant moduli given in Eq. (3.14), which can be estimated rather accurately from their values in an unperturbed Abrikosov flux lattice.[6,60]

Straightforward computations, similar to those for point disorder in Ref. 6, now lead to the Fourier-transformed density-density correlation function

$$S(\mathbf{q}_\perp,q_z)=\overline{\langle|\delta\hat{\mathbf{n}}(\mathbf{q}_\perp,q_z)|^2\rangle}$$
$$=\frac{Tn_0^2q_\perp^2}{\hat{c}_{44}(q_\perp,q_z)q_z^2+\hat{c}_{11}(q_\perp,q_z)q_\perp^2}$$
$$+\Delta_1\frac{n_0^4}{\hat{c}_{11}^2(q_\perp,0)}\delta(q_z)\ , \tag{3.24}$$

where $\hat{c}_{44}(q_\perp,q_z)$ and $\hat{c}_{11}(q_\perp,q_z)$ are transforms of the nonlocal functions $c_{44}(\mathbf{r}_\perp,z)$ and $c_{11}(r_\perp,z)$. In addition to the contours of constant scattering expected for neutron diffraction off flux liquids in clean systems,[3] there is a sharp ridge of intensity running down the $q_\perp$ axis due to the columnar pins. See Fig. 11. This spike would show up as a "central peak" in a q_z scan at fixed nonzero $\mathbf{q}_\perp$ and should be a characteristic signature of the presence of correlated disorder. *Below* T_{BG}, essentially all the scattering will be confined to a ridge along the $q_\perp$ axis with maximum width in the q_z direction of order $l_\parallel^{-1}$.

A natural scaling hypothesis for the wave-vector-dependent tilt modulus just above T_{BG} reads

$$\hat{c}_{44}(T,q_\perp,q_z)=l_\parallel\Phi(q_\perp l_\perp,q_z l_\parallel)\ , \tag{3.25}$$

with $\Phi(0,0)$ finite and where

$$\lim_{y\to\infty}\Phi(0,y)\sim 1/y\ , \tag{3.26}$$

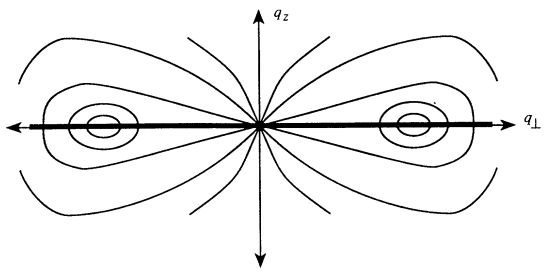

FIG. 11. Contours of constant scattering intensity in a flux liquid with weak correlated disorder. The disorder shows up as a δ-function ridge of intensity along the $q_\perp$ axis.

so that c_{44} remains finite for $q_z\neq 0$ precisely at T_{BG}. When this scaling ansatz is inserted into Eq. (3.24), one finds that the contours of constant scattering near the origin in Fig. 11 are "pinched down": Although $q_z\propto q_\perp$ on these contours away from T_{BG}, one has $q_z\propto q_\perp^2$ as $T\to T_{BG}^+$, signaling the onset of localization.

We discuss finally the stability of this description of a weakly perturbed flux liquid. A complete treatment for all magnetic fields would require a detailed theory of the Bose-glass transition itself, which is unavailable. At very low vortex densities ($B\lesssim\phi_0/\lambda_{ab}^2$), however, we can study the stability of the model flux liquid described by Eq. (2.1) to weak disorder via a renormalizable-group method applied previously to point disorder.[6] Identical conclusions emerge from adapting treatments of flux-liquid *dynamics*[7] to the case of correlated disorder. Because we reach a similar result via a concise "quantum-mechanical" argument in Sec. III C, we only quote the main conclusion: Flux liquids are stable to weak correlated disorder provided $T>T_{BG}(B)$, where

$$T_{BG}(B)=\text{const}\times T^*\left[\frac{\phi_0}{d^2B}\right]^{1/4}\ , \tag{3.27}$$

with $T^*=(d^2\tilde{\varepsilon}_1^2\Delta_1)^{1/4}=\sqrt{U_0\tilde{\varepsilon}_1}b_0$.

The instability of the theory for $T<T_{BG}(B)$ presumably signals the onset of flux-line localization and a disentangled phase with $\langle\psi(\mathbf{r}_\perp,z)\rangle=0$.

B. Bose glass: Interaction field and depinning temperature

It is natural to discuss the Bose-glass phase accordingly to whether vortex lines can be pinned individually by columnar defects or whether *collective* effects of vortex-vortex interactions are important for pinning. The characteristic "interaction field" $B^*(T)$ which separates the region of single vortex pinning from the region where the properties of Bose glass are governed by interactions and the pinning of vortex bundles can easily be estimated. First, consider the situation $a_0>d$ and let us take $T<T_1$, so that energetic rather than entropic considerations control B^*. Then, in order to adjust itself to the random array of columnar defects, the vortex line should be shifted over the distance d. This shift costs interaction energy $c_{66}d^2$, where $c_{66}=\varepsilon_0/4a_0^2$ is the local elastic modulus, while the energy gain is U_0. Upon comparing these energies, one arrives at the characteristic field $B^*(T)\approx(U_0/\varepsilon_0)\phi_0/d^2$. In the regime $c_0<\sqrt{2}\xi_{ab}$, we have [see Eq. (1.9a)]

$$B^*(T)\approx(\phi_0/d^2)(c_0/\xi_{ab})^2$$
$$\approx B_\phi(c_0/\xi_0)^2(1-T/T_c)\quad(T<T_1)\ , \tag{3.28a}$$

where $\xi_0 \equiv \xi_{ab}(T=0)$ and $B_\phi = \phi_0/d^2$ is the matching field which appears in Fig. 3. At low temperatures $T < T_0$, where $c_0 \gtrsim \sqrt{2}\xi$, $B^* \approx B_\phi$. For $T_1 < T < T_{dp}$, where T_{dp} is given by Eq. (3.29) above, we determine $B^*(T)$ by setting $(\varepsilon_0/a_0^2)d^2 \equiv U(T)$, with $U(T)$ given by (2.22), and find

$$B^*(T) \approx \frac{U_0}{\varepsilon_0} B_\phi \left[\frac{T}{T^*}\right]^2 e^{-2(T/T^*)^2} \quad (T_1 < T < T_{dp}) . \tag{3.28b}$$

At high magnetic fields $a_0 \ll d$, methods of 2D collective pinning have to be used: See Secs. III D and IV G.

We now assume $B < B^*(T)$ and allow $T > T_1$. For $T \lesssim T_1$, each flux line is localized on one or two columnar pins as in Fig. 1(a). The binding energies and wave functions for vortices bound to one or two isolated pins were discussed in Sec. II. A new regime arises, however, when $T > T_{dp}$, where the depinning temperature $T_{dp} > T_1$ is defined by

$$l_\perp(T_{dp}) = d . \tag{3.29}$$

We estimate T_{dp} in Appendix D. The localization length of one vortex line is now determined by the interplay of *many* columnar pins. Multiple rods in a transverse region of size $l_\perp(T) \gg d$ will now be incorporated into the ground state. Energies should now be measured relative to $\bar{V}_D \approx (-b_0^2/d^2)U_0$, and we need to solve a Schrödinger equation such as Eq. (2.10) with the random potential $\delta V_D(\mathbf{r})$ replacing $V_1(\mathbf{r})$.

We proceed variationally by minimizing

$$E_0(\psi) = \frac{T^2}{2\tilde{\varepsilon}_1} \int d^2r (\nabla\psi)^2 + \int d^2r\, \psi^2 \delta V_D(\mathbf{r}) , \tag{3.30a}$$

with a wave function $\psi_0(r)$ of spatial extent $l_\perp$ with $\psi_0(r) \sim 1/l_\perp$ for $r < l_\perp$, so that

$$\int d^2r \psi_0^2(r) = 1 . \tag{3.30b}$$

The localized state is produced by a favorable *fluctuation* in the local density of pins. To estimate the second term, we compute its mean-square fluctuation using Eq. (2.4),

$$\overline{\left[\int d^2r\, \delta V_D(\mathbf{r}) \psi_0^2(r)\right]^2} \approx \Delta_1/l_\perp^2 \approx U_0^2 b_0^4/l_\perp^2 d^2 . \tag{3.31}$$

A typical contribution from the random potential in a favorable region is thus of order $-U_0 b_0^2/l_\perp d$. A straightforward estimate of the first term in (3.30a) then gives

$$E_0 \approx \frac{T^2}{\tilde{\varepsilon}_1 l_\perp^2} - \frac{U_0 b_0^2}{l_\perp d} . \tag{3.32a}$$

Minimizing over $l_\perp$ now leads to our basic result,

$$l_\perp(T) \approx d(T/T^*)^2 \quad (T > T_{dp}) , \tag{3.32b}$$

and a binding energy $U(T) = -E_0$ which is approximately

$$U(T) \approx U_0 \left[\frac{b_0}{d}\right]^2 \left[\frac{T^*}{T}\right]^2 \quad (T > T_{dp}) . \tag{3.33a}$$

The distance along z required for the vortex line to sample this localization tube is $l_z(T) = \tilde{\varepsilon}_1 l_\perp^2/T$. We see that the localization length now grows much more slowly with temperature than the isolated pin result (2.23a). This slow growth arises because the spreading of the ground-state wave function is restrained by the multiple pinning centers away from the central one. Upon substituting for $l_\perp(T)$ and $U(T)$ in Eq. (2.24a), we derive the estimate Eq. (1.10b) for the critical current when $T > T_{dp}$.

We can use Eq. (3.33a) to estimate the interaction field $B^*(T)$ in the regions where $T > T_{dp}$; vortices must now move a distance of order $l_\perp(T)$ to adjust to the random pinning potential. Upon setting $(\varepsilon_0/a_0^2)l_\perp^2(T) = U(T)$, we obtain

$$B^*(T) = \frac{U_0}{\varepsilon_0} B_\phi \left[\frac{b_0}{d}\right]^2 (T^*/T)^6 \quad (T > T_{dp}) . \tag{3.33b}$$

The crossover line obtained by combining Eqs. (3.28a), (3.28b), and (3.33b) is shown as the dashed curve in Fig. 3. As $T \to T_c$, $B^*(T) \propto (T_c - T)^6$—see Appendix D.

C. Bose glass: Estimation of the transition temperature

In the limit of very low fields, $B \lesssim \phi/\lambda_{ab}^2$, flux lines interact via a short-range potential, $V(r) \propto \exp(-r/\lambda_{ab})$. The localization length then grows according to Eq. (3.32b) until it becomes comparable to the intervortex spacing a_0. The transition from the Bose glass to the vortex liquid occurs when $l_\perp(T) \gtrsim a_0$, which leads immediately to Eq. (3.27). In Appendix D we show that this result may be reexpressed in terms of a critical Bose-glass transition field $B_{BG}(T)$, which vanishes as $T \to T_c$ according to

$$B_{BG}(T) \propto (T_c - T)^4 . \tag{3.34}$$

In the limit $B > \phi_0/\lambda_{ab}^2$, interactions restrict the growth of the localization length *well before* the transition to a flux liquid ever occurs. We first treat the case $B \lesssim B_\phi$, so that essentially every vortex is able to find one or more columnar pins to localize on for $T < T_{BG}$. To estimate T_{BG} and determine how interactions delay localization we examine the fluctuations of one representative flux line in the confining potential provided by, say, six neighboring vortices. See Fig. 12(a). Delocalization occurs when there is an appreciable probability for this flux line to escape over one of the six saddle points. There is also one columnar pin near the center of this potential, which makes the escape more difficult and delays the transition to the flux liquid. In a strongly pinned Bose glass, more irregular confining cages of five, six, or seven vortices are likely. Figure 12(b) shows the combined potential seen by the flux line in a schematic cross section cutting through two of the saddle points. The intervortex pair potential is $V(r) = 2\varepsilon_0 \ln(r/\lambda_{ab})$ in this regime; the characteristic height of the saddle point relative

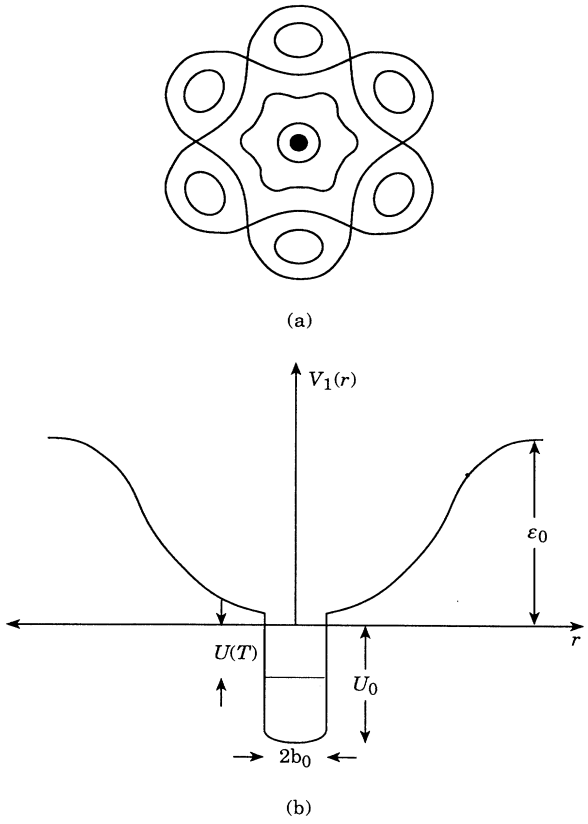

FIG. 12. Flux line confined both by a columnar pin and interactions with six near neighbors. (a) Contours of constant potential. The black dot at the center represents the columnar pin. (b) Cross section of the potential in (a) containing the pin and two saddle points.

to the minimum is then of order ε_0.

When the columnar pins are *absent,* delocalization proceeds via *melting* at a temperature which we now estimate via a simple harmonic-oscillator argument. The confining potential near the minimum is parabolic, and vortex-line fluctuations are controlled by a "Schrödinger equation," which reads

$$\left[-\frac{T^2}{2\tilde{\varepsilon}_1}\nabla_\perp^2+\frac{1}{2}kr^2\right]\psi_0(r)=E_0\psi_0(r)\ , \tag{3.35}$$

where

$$k\approx\left.\frac{d^2V(r)}{dr^2}\right|_{r=a_0}\approx\varepsilon_0/a_0^2$$

to give the correct barrier height at $r=a_0$. The natural "frequency" of this two-dimensional oscillator is $\omega_0=\sqrt{k/\tilde{\varepsilon}_1}$ or

$$\omega_0=\frac{1}{a_0}\left[\frac{\varepsilon_0}{\tilde{\varepsilon}_1}\right]^{1/2}\ , \tag{3.36}$$

and its ground-state energy is

$$E_0=T\omega_0\ , \tag{3.37}$$

with corresponding eigenfunction

$$\psi_0(r)=\frac{1}{\sqrt{2\pi}r_\perp}\exp[-(r/2r_*)^2]\ . \tag{3.38}$$

Here $T\omega_0\equiv\varepsilon_0(r^*/a_0)^2$ defines a typical length scale for transverse vortex fluctuations, namely,

$$r^*(T)=\left[\frac{T^2a_0^2}{\varepsilon_0\tilde{\varepsilon}_1}\right]^{1/4}\ . \tag{3.39}$$

Melting occurs when $r^*=c_La_0$, where c_L is the Lindemann constant. Alternatively, we can say that melting arises when the zero-point energy of the equivalent quantum oscillator becomes a fixed fraction of the saddle-point barrier energy,

$$T\omega_0=c_L'\varepsilon_0\ , \tag{3.40}$$

which leads to a melting temperature

$$T_m=c_L'\sqrt{\varepsilon_0\tilde{\varepsilon}_1}a_0\ , \tag{3.41}$$

with $c_L'=c_L^2$ in agreement with more elaborate estimates with nonlocal elastic constants using the traditional Lindemann criterion.[61]

Consider now the effect of the square well near the center of the harmonic potential in Fig. 12(b). Provided $T<T_{dp}$, the localization length will be $l_\perp=l_0(T)$, with [see Eq. (2.23a)]

$$l_0(T)\approx b_0e^{(T/T^*)^2}\ . \tag{3.42}$$

In this regime the wave function's extent is determined by tunneling through a barrier of order $U(T)$. At higher fields or temperatures, however, the wave function must tunnel as well through the harmonic interaction potential.[62] The range of the wave function will be determined by interactions when $U=T^2/2\tilde{\varepsilon}_1l_0^2<\frac{1}{2}\varepsilon_1(l_0^2/a_0^2)$, i.e., for $l_0>r^*$, in which case we have $l_\perp(T)=r^*$. The crossover temperature at which this transition takes place is given by

$$T_\times\approx\frac{\sqrt{2}}{2}T^*\ln^{1/2}\left[\frac{\sqrt{2}}{2}\frac{d}{b_0}\left[\frac{U_0}{\varepsilon_0}\right]^{1/2}\right]\ , \tag{3.43}$$

where we have set $a_0=d$ since $B\approx B_\phi$.

The overall qualitative behavior of $l_\perp(T)$ together with the Lindemann criterion is depicted in Fig. 13. Note that the Bose-glass transition always occurs at a higher temperature than T_m, as one might expect.

A more quantitative estimate of T_{BG} could be obtained by computing the wave function in the various tunneling regimes and using $l_\perp(T_m)=c_La_0$. An equivalent and more convenient procedure, however, is to calculate the shift in the harmonic-oscillator ground state due to the square well. To leading order in U_0, we have

$$E_0=T\omega_0+\int d^2r\ V_1(r)\psi_0^2(r)$$
$$\approx T\omega_0-\frac{b_0^2}{r^{*2}}U_0\ , \tag{3.44}$$

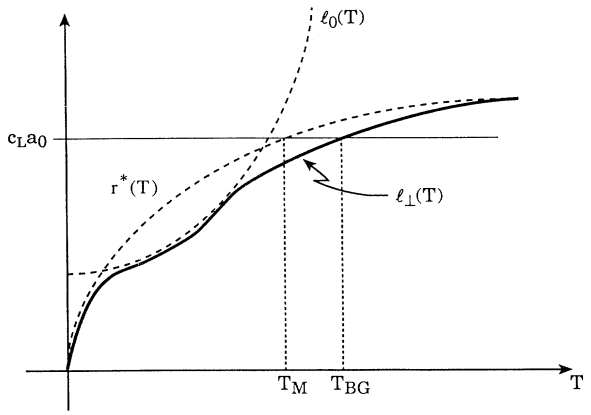

FIG. 13. The localization length $l_\perp(T)$ as determined by the columnar pin and the interaction potential in Fig. 12. The columnar pin delays the delocalization predicted by the Lindemann criterion.

where we have, as usual, neglected factors of order unity. The precise position of the square well is immaterial provided it is within r^* of the center. Upon using the Lindemann criterion (3.40), we obtain

$$T_{BG} \approx T_m \left[1 + \left[\frac{T^*}{T_m} \right]^2 \right] , \tag{3.45}$$

i.e., a significant increase in T_{BG} relative to T_m. Although the melting and Bose-glass temperatures are related, the detailed nature of these transitions is of course different. Melting is typically a first-order transformation by which a regular array of vortices loses its translational periodicity. The Bose-glass transition is expected to be continuous[31] and occurs when a translationally disordered array of pinned vortices delocalizes.

We can also estimate T_{BG} in the limit $\phi_0/\lambda_{ab}^2 < B \ll B_\phi$, when many columnar pins occupy a single harmonic well. Provided $T > T_{dp}$, the localization length will now increase according to Eq. (3.32b) until interactions cause it to behave like $r^*(T)$ beyond a crossover temperature,

$$T_x' = \left[\frac{a_0}{d} \right]^{2/3} \left[\frac{T^*}{\sqrt{\varepsilon_0 \tilde{\varepsilon}_1} a_0} \right]^{1/3} T^* . \tag{3.46}$$

Upon inverting this relation we recover the crossover field $B^*(T)$ for $T > T_{dp}$ displayed in Eq. (3.33b). To lowest order in the fluctuating potential $\delta V_D(r)$, the shift in the harmonic-oscillator ground-state energy is

$$E_0 = T\omega_0 + \frac{1}{2\pi (r^*)^2} \int d^2 r \, \delta V_D(r) e^{-r^2/2(r^*)^2} . \tag{3.47}$$

We assume that a favorable fluctuation in this potential has positioned the average vortex position near the well center. We find from Eq. (2.4) that the root-mean-squared value of the integral in (3.47) is of order $(-U_0 b_0^2/d) r^*$, which leads via (3.40) to a Bose-glass transition temperature

$$T_{BG} \approx T_m \left[1 + \frac{a_0}{d} \left[\frac{T^*}{T_m} \right]^2 \right] . \tag{3.48}$$

Note that the correction agrees with (3.45) when $d = a_0$, but is much larger when $d \ll a_0$, i.e., when there are many pins per vortex. Of course, this enhancement cannot continue indefinitely, since the sample T_c will eventually degrade. Qualitatively similar behavior has been observed by Budhani, Suenaga, and Liou upon irradiating thallium-based cuprates.[26]

If $B \gtrsim B_\phi$, every pin is occupied and the excess vortices go into the interstitial spaces between the random columnar pins. These vortices will still be localized at low temperatures by interactions with vortices trapped on the pinning sites. Most flux lines are still bound to columnar pins in this regime and the estimate (3.45) should remain approximately correct.

When $B \gg B_\phi$, vortex configurations will be dominated by patches of crystalline order broken up by the correlated pinning potential, and we expect that $T_{BG} \approx T_m$. The translational correlation length will be estimated in the next section.

D. Range of translational order in the Bose glass for $B > B_\phi$

For $B < B^*(T)$ the range of translational order R_a in the Bose glass is at most of order a_0. When $B \gg B_\phi$ the translational order is much more extended, and it is of some interest to know, for example, the translational correlation length R_0 when $T \approx T_{BG} \approx T_m$. We shall not attempt to analyze correlations in the interesting intermediate regime $B^*(T) < B < B_\phi$. To determine the range of translational order when $B \gg B_\phi$, we use the collective pinning approach.[9] The free energy for displacements $\mathbf{u}(\mathbf{r}_\perp, z)$ describing local crystallinity in the presence of disorder is

$$F = \frac{1}{2} \int d^2 r_\perp dz [c_{66} u_{ij}^2 + c_{11} u_{kk}^2 + c_{44} (\partial_z \mathbf{u})^2 - V_{pin}(\mathbf{u}, \mathbf{r}_\perp)] , \tag{3.49}$$

where $u_{ij} = \frac{1}{2}(\partial_i u_j + \partial_j u_i)$, $i,j = x,y$, and the shear modulus is $c_{66} \approx \varepsilon_0/4a_0^2$.[63] Note that pinning potential depends on z only through $\mathbf{u}(\mathbf{r}_\perp, z)$. As long as the mean-square relative displacement $|\mathbf{u}(\mathbf{r}_\perp, z) - \mathbf{u}(\mathbf{0}, z)|^2$ does not exceed b_0^2, the scale of the microscopic columnar pinning potential, one can treat random field perturbatively and write V_{pin} in a form $V_{pin} = \mathbf{f}_{pin}(\mathbf{r}_\perp) \cdot \mathbf{u}(\mathbf{r}_\perp, z)$.[9] The statistical properties of $\mathbf{f}_{pin}$ are given by the correlator

$$\overline{f_{pin}(\mathbf{r}_\perp) f_{pin}(\mathbf{r}_\perp')} \approx \tilde{\Delta} \delta^{(2)}(\mathbf{r}_\perp - \mathbf{r}_\perp') , \tag{3.50a}$$

with

$$\tilde{\Delta} \approx \left[\frac{b_0}{a_0} \right]^2 \frac{1}{d^2} \left[\frac{U_0}{b_0} \right]^2 . \tag{3.50b}$$

Here $(b_0/a_0)^2 (1/d^2)$ is the effective concentration of defects which are within b_0 of a vortex in the relatively stiff

local lattice. The correlation function $C(\mathbf{r}_\perp) = [\mathbf{u}(\mathbf{r}_\perp) - \mathbf{u}(0)]^2$ can now easily be found,

$$C(\mathbf{r}_\perp) \approx 4 \left[\frac{U_0}{\varepsilon_0} \right]^2 \frac{a_0^2 r_\perp^2}{d^2} \left| \ln \frac{s}{r_\perp} \right| , \tag{3.51}$$

where $s = d$ for $r_\perp < d$, and $s = a_0$ for $r_\perp > d$. The *pinning* correlation length R_c is defined by the condition $C(r_\perp = R_c) = b_0^2$,[2,9] which leads to a self-consistent equation for R_c,

$$R_c = \frac{1}{2} d \frac{b_0}{a_0} \frac{\varepsilon_0}{U_0} \frac{1}{\sqrt{|\ln(s/R_c)|}} . \tag{3.52}$$

When $T_0 < T$ (see Appendix D), $U_0 \approx \varepsilon_0 c_0^2 / \xi_{ab}^2$, $b_0 \approx \sqrt{2} \xi_{ab}$, and (neglecting logarithms and constants of order unity)

$$R_c \approx d \frac{\xi_{ab}^3}{a_0 c_0^2} . \tag{3.53}$$

Note that since the pinning potential does not depend on z, the dispersion of c_{44} is irrelevant for pinning at spatial scales $r_\perp \lesssim R_c$ (but becomes important for creep processes at small currents $J \ll J_c$—see Sec. IV G).

At larger distances $r_\perp > R_c$, $C(r_\perp) > b_0^2$ and the perturbative approach is inapplicable, since the behavior of $C(\mathbf{r}_\perp)$ is governed by the low-lying metastable states of a vortex lattice in a random field. The scaling behavior of $C(\mathbf{r}_\perp)$ is governed now by the 2D wandering exponent $\zeta \approx \frac{2}{5}$,[2,5]

$$C(\mathbf{r}_\perp) = b_0^2 \left[\frac{r_\perp}{R_c} \right]^{2\zeta} = b_0^2 \left[\frac{r_\perp}{R_c} \right]^{4/5} . \tag{3.54}$$

The critical radius R_a for the breakup of translational order is given by condition $C(R_a) = a_0^2$. One then finds (again with logarithmic accuracy and neglecting constants of order unity)

$$R_a = R_c \left[\frac{a_0}{b_0} \right]^{5/2} \approx a_0 \frac{d (a_0 \xi_{ab})^{1/2}}{c_0^2} \quad (T_0 < T < T') , \tag{3.55}$$

where the last line assumes $T > T_0$ and T' is defined below.

The above analysis assumes that the root-mean-square thermal fluctuation u_T of a vortex position is small, so that energetic considerations alone control the breakup of translational order. The quantity u_T is just the size $r^*(T)$ of the harmonic-oscillator wave function discussed in the previous section. When u_T exceeds the pin size b_0, there is a significant thermal enhancement of the translational correlation length R_a. Upon using Eq. (3.39) for $r^*(T)$, we find that this new regime arises whenever $T > T'$, where T' is a relatively low temperature given by the solution of

$$T' = \sqrt{\varepsilon_0 \tilde{\varepsilon}_1} b_0^2 / a_0 , \tag{3.56}$$

where the temperature-dependent quantities on the right-hand side are evaluated at $T = T'$. More precise numerical estimates of T' can be found by the method used to determine T^* in Appendix D.

When $T > T'$, Eq. (3.50b) for the correlator of the random potential is modified in a number of ways. First, the well depth U_0 is modified as in Eq. (3.44), $U_0 \to (b_0/u_T)^2 U_0$, and its corresponding range is changed, $b_0 \to u_T$. In addition, the effective density of pins which interact with a vortex becomes

$$\left[\frac{b_0}{a_0} \right]^2 \frac{1}{d^2} \to \left[\frac{u_T}{a_0} \right]^2 \frac{1}{d^2} .$$

Collecting together these changes, we find that the variance of the disorder is now

$$\tilde{\Delta} \to \left[\frac{b_0}{u_T} \right]^4 \frac{U_0^2}{a_0^2 d^2} . \tag{3.57}$$

Because the length R_a is now determined by $C(R_a) = u_T^2$, we find

$$R_c \approx d \left[\frac{\varepsilon_0}{U_0} \right] \frac{u_T^3}{a_0 b_0^2} \quad (T > T') , \tag{3.58}$$

which becomes

$$R_c \approx d \frac{u_T^3}{a_0 c_0^2} \tag{3.59}$$

for $T > T_0$. Proceeding as before to calculate R_a, we find that

$$R_a = a_0 \frac{d (u_T a_0)^{1/2}}{c_0^2} . \tag{3.60}$$

Note that these formulas differ from those relevant to $T < T'$ by the substitution of u_T for ξ_{ab}.

We can now determine the range of translational correlations at T_{BG}, assuming that $T_{\mathrm{BG}} \approx T_m$ for $B \gg B_\phi$. The Lindemann substitution $u_T = c_L a_0$ leads to

$$R_a(T_m^-) \approx a_0 c_L^{1/2} \left[\frac{a_0}{c_0} \right] \left[\frac{d}{c_0} \right] . \tag{3.61}$$

With $c_L = 0.15$, $d = 350$ Å ($B_\phi = 1T$), $a_0 = 225$ Å ($B = 4T$), and $c_0 = 35$ Å, we find $R_a = 33 a_0$. True Bose-glass behavior will only become evident on scales large compared to R_a.

The nature of the delocalization transition depends on the relation between R_a and the translational correlation length ξ_T just above T_m in clean materials. If $\xi_T \lesssim R_a(T_m^-)$, the system should melt via a first-order transition similar to the clean limit. If $\xi_T > R_a(T_m^-)$, the first-order transition is replaced by the second-order Bose-glass transition whose scaling properties are described in Sec. V.

E. Mott insulator

The Mott-insulator phase[31] should arise at low temperatures over a range of external fields H such that $B = B_\phi$,

provided the vortices can achieve thermal equilibrium given the sluggish dynamics in this temperature range. See Figs. 2 and 3. To a first approximation, every flux line occupies exactly one columnar pin, although occasionally two lines will tunnel cooperatively between two closely spacing columnar pinning sites, as in the H_2 molecule. With its infinite bulk and tilt moduli, the Mott insulator resembles the Meissner phase. Its transport properties will be discussed in Sec. IV.

The transitions out of the Mott insulator at the fields H_a^* and H_b^* in Fig. 2(b) are similar to the transition at H_{c1}. For $H > H_b^*$ a few extra flux lines occupy the interstices between the completely occupied pinning sites. Interactions are presumably sufficient to localize these lines. When $H < H_a^*$ one has instead a few wandering vacancies. Vacancies wander whenever a vortex line "tunnels" from an occupied to an unoccupied pin. Again, we expect that these vacancies will localize at low temperatures to produce a Bose glass. Upon adapting the renormalization-group treatment of point disorder near $H_{c1}(T)$ of Ref. 6, we find that correlated disorder changes the character of the transition expected in pure systems. The precise nature of the transitions out of the Mott insulator (and the transition at H_{c1} when correlated disorder is present) is unknown.

IV. VORTEX DYNAMICS AT LOW TEMPERATURES

We treat vortex transport in the Bose-glass and Mott-insulator phases by adapting the equilibrium analysis presented in Secs. II and III. When $\mathbf{J}\perp\mathbf{B}$ a Lorentz force per unit length perpendicular to $\mathbf{J}$ acts on all vortices,[64]

$$\mathbf{f}_L = \frac{\phi_0}{c}\hat{\mathbf{z}}\times\mathbf{J} , \tag{4.1}$$

which leads to an additional term

$$\delta F_N = -\mathbf{f}_L \cdot \sum_{j=1}^{N} \int_0^L \mathbf{r}_j(z)dz \tag{4.2}$$

in the vortex-free energy Eq. (2.1a). We exploit the analogy with boson quantum mechanics by noting that this term represents a fictitious "electric field" $\mathbf{E}=(1/c)\hat{\mathbf{z}}\times\mathbf{J}$ acting on particles with charge ϕ_0.[65]

The dynamics of the Bose glass is determined by the competition between the 2D array of columnar pinning centers and the 3D thermal fluctuations of vortex lines. A detailed picture can be obtained in the regime $T \lesssim T_1$ and $B < B^*(T)$, where each vortex is localized on one or two columnar defects and the pins outnumber the vortices. The boson mapping then reduces single vortex dynamics to a problem of hopping conductivity of 2D localized particles with the hopping-matrix elements t_{ij} displayed in Eqs. (2.39) and (2.41). See Table I. The boson electric field $\mathbf{E}$ maps onto the superconducting current, as mentioned above. The boson current density and conductivity map onto the vortex velocity (i.e., the true electric field $\mathcal{E}$) and superconducting resistivity, respectively. Note that we indicate the true electric field and the fictitious boson "electric field" by the symbols $\mathcal{E}$ and $\mathbf{E}$, respectively. As discussed in Sec. II E, a current $\mathbf{J}\|\mathbf{B}$ acts like an imaginary "magnetic field" on the bosons. Note that the inverse sample thickness plays the role of boson "temperature."

We can now reproduce for Bose-glass dynamics the rich variety of hopping conductivity phenomena in semiconductors[32] by transcribing the proper quantities. For example, the famous low-temperature Mott variable-range hopping conductivity in two dimensions, $\sigma \sim \exp[-(T_0/T)^{1/3}]$, becomes a superconducting *resistivity* which vanishes with thickness according to $\rho \sim \exp[-(L/L_0)^{1/3}]$, where L_0 is a characteristic sample dimension calculated below. We shall also find it convenient to view the vortices as charged directed "polymers" in a perpendicular electric field, since this gives insight into the physics in the imaginary-time direction.

In the thermally assisted flux-flow (TAFF) model of vortex transport, the resistivity $\rho = \mathcal{E}/J$ behaves according to[66]

$$\rho(T) \approx \rho_0 e^{-U_B(J)/T} , \tag{4.3}$$

where ρ_0 is a characteristic flux-flow resistivity and $U_B(J)$ is a barrier height. In the remainder of this section, we determine this barrier height under various circumstances. In contrast to the original TAFF models, this barrier diverges as $J \to 0$. Similar diverging barriers for vortex transport have been hypothesized for vortex glasses dominated by point disorder.[4,5]

Although most of our explicit results apply to the regime $T \lesssim T_1$, $B < B^*$, we believe the behavior as $J \to 0$ is the same throughout the Bose-glass phase. We expect, for example, that the asymptotic law (1.1) applies everywhere for $T < T_{BG}$ outside of the Mott-insulator phase.

A. Tunneling via half loops

The critical current $J_c \approx cU/\phi_0 l_\perp$ in the strongly pinned Bose glass was discussed in Sec. II B. Note that $U(T)$ and $l_\perp(T)$ are of order U_0 and b_0, respectively, if $T \lesssim T_1$. We now consider the regime of moderate currents, $J_1 < J < J_c$, where

$$J_1 = cU_0/\phi_0 d , \tag{4.4}$$

and d is now the average spacing between *unoccupied*

TABLE I. Boson analogy applied to vortex transport.

Charged bosons	Mass	$\hbar$	$\beta\hbar$	Pair potential	Charge	Electric field	Current
Superconducting Vortices	$\tilde{\varepsilon}_1$	T	L	$2\varepsilon_0 K_0(r/\lambda_{ab})$	ϕ_0	$\frac{\hat{\mathbf{z}}\times\mathbf{J}}{c}$	$\mathcal{E}$

pins. In the above current range, we can ignore these nearby pins and use the one flux-line free energy

$$F_1=\int_0^L dz\left[\frac{1}{2}\tilde{\varepsilon}_1\left[\frac{d\mathbf{r}}{dz}\right]^2+V_1[\mathbf{r}(z)]-\mathbf{f}_L\cdot\mathbf{r}(z)\right]dz\ , \tag{4.5}$$

with $f_L=J\phi_0/c$.

Consider a vortex line trapped on a columnar pin, as shown in Fig. 14. Escape from this metastable state proceeds via the "half-loop" saddle-point configuration illustrated in the figure. Although an explicit variational analysis based on Eq. (4.5) is possible, it is easier to simply estimate the magnitudes of the various terms. If the half loop extends for a distance z along the pin and has perpendicular extent r, the energy relative to the case $\mathbf{f}_L=0$ is

$$\delta F_1(r,z)\approx\frac{\tilde{\varepsilon}_1 r^2}{z}+U_0 z-f_L rz\ . \tag{4.6}$$

Optimization with respect to r and z and yields the saddle-point parameters

$$r^*=\left[\frac{U_0}{\tilde{\varepsilon}_1}\right]^{1/2} z^*=U_0 c/\phi_0 J \tag{4.7}$$

and saddle-point energy

$$\delta F_1^*=\frac{c\tilde{\varepsilon}_1^{1/2}U_0^{3/2}}{\phi_0 J}\ . \tag{4.8}$$

Upon identifying this saddle-point energy with the barrier $U_B(J)$ in Eq. (4.3), we find that the electric field $\mathcal{E}$ generated by half-loop tunneling is

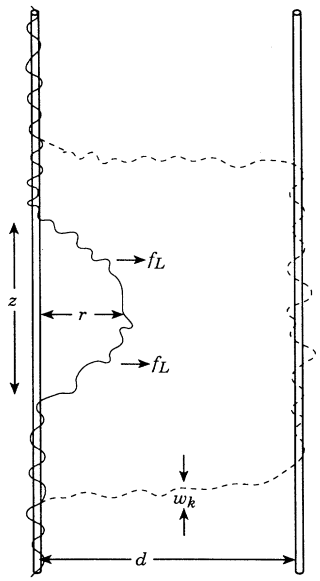

FIG. 14. Half-loop and double-kink transport processes for flux lines. The Lorentz force f_L attempts to push the line to the right.

$$\mathcal{E}\approx\rho_0 J\exp[-(E_k/T)(J_1/J)]\ , \tag{4.9a}$$

with $E_k=\sqrt{\tilde{\varepsilon}_1 U_0}d$. A similar result was obtained recently by Brandt.[45] A more quantitative calculation of the exponential factor valid for $T<T_{dp}$ using the quantum-mechanical analogy to the ionization of an atom in an electric field[48] leads to

$$\mathcal{E}\sim\exp\left[-\frac{4\sqrt{2}}{3}[E_k(T)/T](J_1/J)\right]\ , \tag{4.9b}$$

with $E_k(T)\equiv\sqrt{\tilde{\varepsilon}_1 U(T)}d$. The preexponential factor can be calculated in a similar fashion. When $J\le J_1$ we have $z^*\ge d$ and neighboring occupied pins must be taken into account. If $\sqrt{\tilde{\varepsilon}_1/U_0}d<c_0$, where c_0 is the CuO_2 plane spacing (as may happen for the highly anisotropic bismuth- or thallium-based compounds), our continuum description should be replaced by a more microscopic one in terms of "pancake vortices."[45] We shall see, however, that even in this case the continuum description becomes valid for currents $J\ll J_1$: The "double-kink" excitations which dominate the variable-range hopping (VRH) regime (see Sec. IV C) are always larger than c_0 as $J\to 0$.

B. Tunneling via double kinks

When $J<J_1$ the transverse displacement of the liberated vortex segment exceeds the mean distance between occupied pinning sites. The transition of a vortex line from one rod to another can then in principle take place via a thermally activated double-kink configuration which throws a vortex segment onto an adjacent columnar defect. A double kink is shown as a dashed line in Fig. 14. If the two wells are exactly identical, the double-kink energy is approximately $2E_k$, where the kink has width

$$w_k=\left[\frac{\tilde{\varepsilon}_1}{U_0}\right]^{1/2} d \tag{4.10a}$$

and energy

$$E_k=\sqrt{\tilde{\varepsilon}_1 U_0}d\ . \tag{4.10b}$$

Once this excitation has nucleated, the kinks will separate to $z=\pm\infty$ as the vortex spreads from one rod to the next.

The above scenario bears a strong resemblance to dislocation motion over a Peierls potential.[67] A crucial distinction, however, is the *dispersion* which characterizes the energies of the different pinning sites. As discussed in Sec. II D, dispersion arises due to interactions, and because vortices are sensitive via thermal fluctuations to the different random environments which surround pinning sites. The bandwidth γ due to tunneling and interactions was estimated in Eq. (2.44). Suppose that the density of states $g(\varepsilon)$ is filled by vortices up to a chemical potential μ well away from the band edges. Double-kink tunneling must in general then lead to a state with a higher energy per unit length. *Any* such energy difference, however, will produce an infinite barrier in an infinitely thick sample. This barrier shows up as linear potential binding the two kinks together.

Dispersion of energy levels can only be neglected in samples thin enough so that $L < L_1$, where

$$L_1 = E_k/\gamma \ . \tag{4.11}$$

In this regime, samples will exhibit a nearest-neighbor hopping conductivity with

$$\mathcal{E} \approx \rho_0 J e^{-c_1 E_k/T} , \tag{4.12}$$

where the constant c_1 can be determined from percolation theory.[32]

C. Variable-range hopping

The dispersion of flux-binding energies is essential for $J < J_1$ and $L > L_1$. The most important excitation in this regime is illustrated in Fig. 15: Fluxons move by sending out a tonguelike pair of "superkinks" connecting the vortex to a state which optimizes the tunneling probability. Once the tongue is established, the superkinks move outward, and the vortex spreads to the new site. Spreading is not possible on the intervening higher-energy pins, because the barrier is proportional to the sample thickness. Tunneling via superkinks is the analogue of Mott variable-range hopping of electrons between localized states in semiconductors.[32]

Consider two superkinks with separation Z along the pins and extending a transverse distance R, as in Fig. 15. The free energy, relative to the energy without kinks, consists of three terms

$$\delta F_{\rm SK}(R,Z) = 2E_k \left[\frac{R}{d} \right] + \frac{Z}{g(\mu)R^2} - f_L RZ \ , \tag{4.13}$$

with E_k given by Eq. (4.10b). The first term is the energy of the kinks themselves, while the last comes from the Lorentz force. To understand the middle term, consider the states available to a weakly bound flux line about to hop. All states up to a chemical potential μ are filled. The density of nearly compatible states with energies just above μ is $g(\mu)$. The total number of states with energy within $\Delta\varepsilon$ of this flux line at distances less than or equal to R is $g(\mu)\Delta\varepsilon R^2$. By setting $g(\mu)\Delta\varepsilon R^2 = 1$, we determine the expected energy difference (per unit length) for a hop of size R,

$$\Delta\varepsilon = 1/g(\mu)R^2 \ . \tag{4.14}$$

There is a linear potential $\Delta\varepsilon Z$ binding the two kinks together, which leads to Eq. (4.13).

If $f_L = 0$, we optimize (4.13) to find the *shape* of the optimal low-temperature thermal fluctuation,

$$Z^* \approx \frac{E_k g(\mu)}{d} (R^*)^3 \ . \tag{4.15}$$

Optimizing with $f_L \neq 0$ leads to

$$R^* \approx \left[\frac{Z^* d}{E_k g(\mu)} \right]^{1/3} \approx \left[\frac{c}{g(\mu)\phi_0 J} \right]^{1/3} . \tag{4.16}$$

Since the width of this superkink is of order $W_k^* \approx (\sqrt{\tilde{\varepsilon}_1}/U_0)R^*$, we have $Z^* \gg W_k^*$ and are justified in neglecting weak additional attractive interactions (logarithmic for $Z^* < \lambda_{ab}$, exponential as $J \to 0$) between superkinks. The slope of the vortex-line segment within a superkink is approximately $\sqrt{\tilde{\varepsilon}_1}/U_0$. In view of Eq. (2.2), the continuum, small-tilt description of vortex fluctuations will be correct provided $\varepsilon_0/U_0 \ll (M_z/M_\perp)^2$, which is easily satisfied for anisotropic high-T_c materials. The energy of the saddle-point configuration (4.16) is

$$\delta F_{\rm SK}^* = \frac{E_k}{d} \left[\frac{c}{g(\mu)\phi_0 J} \right]^{1/3} . \tag{4.17}$$

Upon identifying $\delta F_{\rm SK}^*$ with the barrier height in Eq. (4.3), we find non-Ohmic variable-range hopping behavior[68]

$$\mathcal{E} \approx \rho_0 J \exp[-(E_k/T)(J_0/J)^{1/3}] , \tag{4.18}$$

where

$$J_0 = \frac{c}{\phi_0 g(\mu) d^3} \ . \tag{4.19}$$

When $L = \infty$ the intermediate percolation regime of the previous subsection never occurs. We then return to the "half-loop" description of vortex transport for $J > J_2$, where

$$J_2 = J_1 [U_0 g(\mu)]^{1/2} d \ . \tag{4.20}$$

When the sample thickness is finite, the behavior is ultimately Ohmic at the very lowest currents. The crossover to a linear resistivity occurs when $Z^* = L$, i.e., for $J < J_L \ll J_0$, where

$$J_L \approx cE_k/\phi_0 dL \tag{4.21}$$

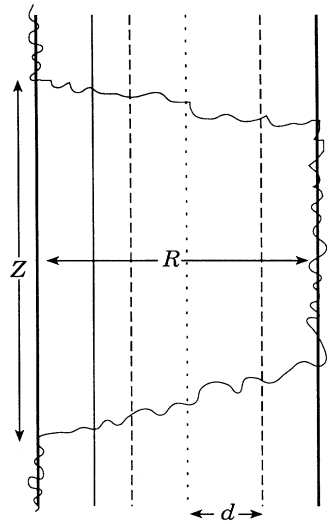

FIG. 15. Double-superkink configuration required for variable-range hopping. The "tongue" of vortex line seeks out a compatible low-energy pin so that the line can spread.

and the asymptotic resistivity then has a very unusual dependence on sample thickness,

$$\rho \approx \rho_0 \exp[-(L/L_0)^{1/3}] , \tag{4.22}$$

where

$$L_0 \approx T^3 g(\mu)/\tilde{\epsilon}_1 U_0 . \tag{4.23}$$

The non-Ohmic Bose-glass current-voltage characteristics will thus disappear in thin superconducting films when $J \to 0$ or $L < L_0$. Up to logarithmic corrections, $g(\mu) \approx 1/d^2 \epsilon_0$ in the low-temperature regime [see Eq. (2.45)], and so

$$L_0(T) \approx d(b_0/d)^3 (M_\perp U_0/M_z \epsilon_0)^{1/2} (T/T^*)^3 .$$

Particularly unusual behavior can arise when $B \ll B_\phi$, i.e., when the band of localized states is nearly empty. Vortex motion in this case is determined by rare fluctuations in the spatial distribution of rods: The vortex line can be captured by the dead ends of the percolation network and/or can reach a position where no favorable rods are available at the distance of the optimal jump. Therefore the vortex remains trapped in such a position for a long time, which determines the characteristic rate of jumps and, therefore, the mean vortex velocity. We consider a relevant trap formed by a rod which has no neighbors within a hemispherical cavity (centered about the direction of the Lorentz force) of radius R. Then the vortex can easily enter such trap, but cannot return back or jump fast enough against $\mathbf{f}_L$. The time the vortex spends at this trap is $t \sim \exp(R/r_T)$, where $r_T = T/\sqrt{2\tilde{\epsilon}_1 U(T)}$. The vortex can jump to another rod over the distance R if the energy difference per unit length between the final and initial positions is $\Delta\epsilon \sim f_L R$ [see Eq. (4.13)]. Then the relevant trap can be viewed as the volume in configurational $(\mathbf{R},\epsilon)$ space free from the localized states within the band $\Delta\epsilon$ above the initial vortex state. The probability to find such a volume is

$$P[R] \sim R \exp\left[-A g(\mu) \frac{\pi R^2}{2} f_L R \right] ,$$

where A is a numerical factor of order of unity. The mean jump time is then

$$\bar{t} \simeq \int dR\, P[R] e^{R/r_T} \simeq \exp\left[A_1 \left[\frac{E_k}{T} \right]^{3/2} \left[\frac{J_0}{J} \right]^{1/2} \right] ,$$

and the electric field corresponding to this hopping rate is

$$\mathcal{E} \sim \exp[-A_1 (E_k/T)^{3/2} (J_0/J)^{1/2}] . \tag{4.18'}$$

Note that this version of variable-range hopping vortex dynamics can only be realized at very small fields where the concentration of relevant hemispherical traps exceeds the concentration of vortex lines, namely, for

$$B < B_\phi \exp[-A_1 (E_k/T)^{3/2} (J_0/J)^{1/2}] .$$

Note that as $J \to 0$ the regime of B to which this theory applies vanishes exponentially fast. For fixed B, we expect eventually to return to the prediction (4.18) in an infinite sample when $J \to 0$.

There is a rich variety of additional effects associated with the rare fluctuations in the concentration of columnar pins. For example, a nonmonotonic resistivity arises in the regime $L < L_0$ [see Eq. (4.22)], analogous to the nonmonotomic *conductivity* discussed in Ref. 69. We leave the detailed discussion of these phenomena for another publication.

D. Response to tilt

The stability of the Bose glass to a perpendicular magnetic field can now be studied. For a more extensive treatment, which exploits insights from soluble model in 1+1 dimensions, see Ref. 37.

A perpendicular field $\mathbf{H}_\perp$ changes Eq. (2.1a) according to

$$F_N \to F_N - \frac{\phi_0 \mathbf{H}_\perp}{4\pi} \cdot \sum_{j=1}^{N} \int_0^L dz \frac{d\mathbf{r}_j}{dz} . \tag{4.24}$$

Since the tilt modulus is finite for $T > T_{BG}$, there will be a finite linear response to $H_\perp$ in the flux liquid,

$$\mathbf{B}_\perp = (\phi_0^2 n_0^2/4\pi c_{44}) \mathbf{H}_\perp . \tag{4.25}$$

The behavior in the Bose glass is more subtle. The linear response vanishes ($c_{44} = \infty$), and $H_\perp$ must actually exceed a threshold $H_\perp^c(T)$ before $B_\perp$ becomes nonzero: There is a transverse Meissner effect. When the flux lines finally do begin to tip over, they exhibit "variable-range tilting," similar to the variable-range hopping discussed in the previous section.

Vortex lines tilt at small angles by proliferating superkinks of the same sign, as illustrated in Fig. 16. These kinks are similar to those induced by CuO_2 planes for flux lines directed close to the *ab* plane.[36] The kinks in our case have variable size, however, so that the vortices can avoid unfavorable intermediate pinning sites. The free energy of one such kink when $H_\perp = 0$ can be calculated as

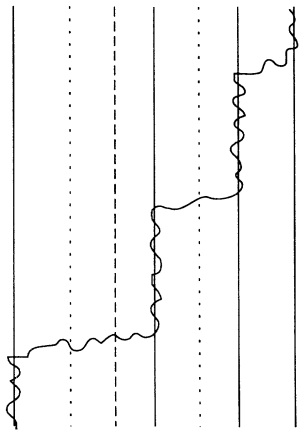

FIG. 16. Variable-range tilting. The response to a perpendicular field for $H_\perp > H_\perp^c(T)$ is to produce a set of widely spaced superkinks connecting compatible sites.

in the variable-range hopping problem. We suppose that the average superkink size is R and that spacing between kinks is Z. The energy per superkink in Fig. 16 is then

$$\mathcal{F}_1 = E_k \left[\frac{R}{d} \right] + \frac{Z}{g(\mu)R^2} - \frac{H_\perp \phi_0}{4\pi} R \ , \tag{4.26}$$

where the last term arises from the extra contribution to Eq. (4.24). Unlike the imposition of a Lorentz force, tilting does not destabilize a localized vortex line. Indeed, $H_\perp$ can be incorporated into a renormalized single-kink energy

$$\tilde{E}_k(H_\perp) = E_k - \frac{H_\perp \phi_0 d}{4\pi} \ . \tag{4.27}$$

Optimizing Z for a fixed kink width $W = W^*$ leads to (4.15) with $\tilde{E}_k$ replacing E_k and the superkink energy

$$\mathcal{F}_1^* \approx \tilde{E}_k(H_\perp) \frac{W^*}{d} \ . \tag{4.28}$$

Tilting a flux line by a small angle θ would require a macroscopic number of superkinks proportional to $L\theta$ and hence an infinite energy cost in the thermodynamic limit whenever $\mathcal{F}_1^* > 0$.

For $H < H_\perp^c(T)$, where

$$H_\perp^c(T) \approx 4\pi E_k / \phi_0 d \approx 4\pi \sqrt{\tilde{\varepsilon}_1 U_0}/\phi_0 \ , \tag{4.29}$$

$c_{44} \propto (dB_\perp/dH_\perp)^{-1}$ remains infinite and the Bose glass will exhibit a transverse Meissner effect. For $H > H_\perp^c$ the conductivity is mediated by kink propagation. As discussed in Ref. 37, these kinks tend to form chains along the direction of tilt, with areal density $n_{\rm chain}$ which vanishes like

$$n_{\rm chain} \propto (H_\perp - H_\perp^c)^{3/2} \ . \tag{4.30a}$$

The resistivity in this regime is proportional to $n_{\rm chain}$ and so[37]

$$\mathcal{E} \propto (H_\perp - H_\perp^c)^{3/2} J \tag{4.30b}$$

as $H \to H_\perp^c$ from above.

Formula (4.29) describes the lock-in transition, analogous to that discussed in Ref. 36. The critical angle for this transition is $\theta_c \approx H_\perp^c / B$, which we may write as

$$\theta_c \approx \frac{1}{4\pi} \frac{\sqrt{\tilde{\varepsilon}_1 U_0}}{\varepsilon_0} \left[\frac{a_0}{\lambda_{ab}} \right]^2 \ . \tag{4.31a}$$

Above a still larger "accommodation angle" θ_a,

$$\theta_a \approx \left[\frac{U_0}{\tilde{\varepsilon}_1} \right]^{1/2} \ , \tag{4.31b}$$

there is crossover to a regime where kinks disappear completely. Just below the accommodation angle, tilted vortices begin to organize themselves into kinks in order to adjust to the columnar pinning tracks.

E. Response to point disorder

Weak point disorder ultimately destabilizes the Bose glass, but only at rather large length scales. To see this we add a new random potential to Eq. (2.1a),

$$F_N \to F_N - \sum_{j=1}^{n} \int_0^L dz \, \delta V_D'[r_j(z), z] \ , \tag{4.32}$$

where the new point-disorder potential has variance

$$\overline{\delta V_D'(\mathbf{r}_1, z_1) \delta V_D'(\mathbf{r}_2, z_2)} = \Delta_0 \delta^2(\mathbf{r}_1 - \mathbf{r}_2) \delta(z_1 - z_2) \ , \tag{4.33}$$

where Δ_0 can be expressed through experimentally accessible parameters as[2]

$$\Delta_0 \simeq \left[\frac{M_\perp}{M_z} \right]^{1/2} \varepsilon_0^2 \xi_{ab}^3 (J_{cp}/J_{pb})^{3/2} \ , \tag{4.34}$$

with J_{pb} the pair-breaking current defined under Eq. (1.9b) and J_{cp} the critical current due to point defects. Usually, for high-temperature superconductors, $J_{cp}/J_{pb} \simeq 0.01$.

It is easily shown that this disorder potential does not significantly affect the energy barriers which lead to Eq. (4.9) in the "half-loop" regime. Consider, however, the superkink pair shown in Fig. 15. As the vortex tries to spread, the line segment joining the pair is subjected to the random point potential over a volume of order $Zl_\perp^2$. This potential leads to an additional contribution to the energy[38]

$$\delta F_{\rm SK} = 2E_k \left[\frac{R}{d} \right] + \frac{Z}{g(\mu)R^2} - \frac{\Delta_0^{1/2} Z^{1/2}}{l_\perp} \ . \tag{4.35}$$

The energy of a superkink pair of size Z from optimizing the first two terms is $(E_k^2 Z / d^2 g(\mu))^{1/3}$. The last term dominates this energy (and will trap the spreading superkink pair) for $Z > L_\times$, where

$$L_\times \approx \frac{E_k^4}{d^4 g^2(\mu)} \frac{l_\perp^6(T)}{\Delta_0^3} \ . \tag{4.36}$$

Upon taking $d^2 g(\mu) \sim 1/\varepsilon_0$, $U_0 \sim \varepsilon_0$, and $l_\perp \approx b_0$ as is appropriate when $T < T_1$, we find, for reasonable parameter values ($M_\perp/M_z = 10^2$, $d = 240$ Å, $b_0 = 24$ Å)

$$L_\times \approx \left[\frac{M_\perp}{M_z} \right]^{1/2} d \left[\frac{d}{b_0} \right]^3 \left[\frac{J_{pb}}{J_{cp}} \right]^{9/2} \approx 2 \text{ km} \ .$$

The regime where point disorder disrupts the predictions of the Bose-glass theory is thus likely to be of only academic interest, unless this disorder is greatly enhanced by, say, proton or neutron irradiation. The crossover length $L_\times$ is even larger for $T > T_1$.

Although point disorder disrupts the Bose glass at low temperatures and currents, the behavior on scales larger than $L_\times$ is unknown. The behavior could be that of an isotropic point-disorder-dominated vortex glass. An alternative asymptotic state is an anisotropic glass involving both columnar and point disorder in an essential way. We note in any case that weak point disorder is unlikely to change the Bose-glass transition itself—see Sec. V and Ref. 37.

F. Effect of interactions

Interactions between vortices are already partially included in our variable-range hopping analysis, because we exclude multiple occupancy of pinning sites (d is the spacing between *unoccupied* sites in the above sections) and allow for the interaction contribution to the bandwidth in Eq. (2.44). Interactions have the additional effect of lowering the density of states at the chemical potential $g(\mu)$. However, $g(\mu)$ will not be lowered to zero, provided the range of interactions (here of order λ_{ab}) is finite—see Ref. 32. It is nevertheless interesting to consider the case $\lambda_{ab} \gg a_0$, where the long-range logarithmic interaction between vortices dominates over intermediate current and length scales.

It is well known from the theory of variable-range hopping[32] that the long-range Coulomb interactions between particles drive the density of states $g(\mu)$ to zero at the Fermi level, giving rise to so-called Coulomb gap. This, in turn, changes the variable-range hopping exponent μ in the relation $\mathcal{E} \sim \exp[-(\tilde{J}/J)^{\mu}]$. One can easily repeat the consideration by Shklovskii and Efros[32] for vortices subject to logarithmic vortex-vortex interactions at *all* length scales. One finds that interactions change μ from $\mu = \frac{1}{3}$ to the value $\mu = 1$ (with logarithmic accuracy).

If $B > B^*(T)$, however, the Coulomb-gap effect relevant in the physics of semiconductors is masked by the collective effects due to the existence of a local vortex solid with a finite shear modulus. A similar situation in the semiconductors would correspond to the formation of the two-dimensional Wigner crystal. Indeed, the gap in the density of states becomes important if the distance of the hop, i.e., the transverse size of the superkink, exceeds the vortex spacing. The collective effects in the vortex lattice come into play, however, when the change in interaction energy due to superkink formation exceeds the superkink energy $E_{\rm SK} = E_k (J_1/J)^{1/3}$. One can easily find comparing these two energies that collective effects become relevant at transverse displacements $u \ll a_0$. Therefore, to account for the interactions in a locally crystalline array, one has to consider collective pinning and creep through the system of columnar pins.

The effects of the "Coulomb" gap can possibly be observed in the motion of the vortex liquid and will be discussed elsewhere. In the next section, we concentrate on the critical currents and vortex dynamics in the collective creep regime $B > B^*(T)$.

G. Dynamics of vortex bundles

1. *Pinning and critical currents of vortex bundles*

Now we find critical currents in the field range $B^*(T) < B < B_m(T)$, where B_m is the melting field at temperature T. The temperature dependence of the interaction field $B^*(T)$ is summarized in Appendix D. We consider sufficiently high temperatures $T > T_0$, so that $\sqrt{2}\xi_{ab} > c_0$; i.e., the coherence length plays a role of the defect radius and $U_0 \approx \varepsilon_0 (c_0/2\xi_{ab})^2$. In the low-temperature regime $T < T'$, with T' given by Eq. (3.56), only a small fraction of vortices of order $(b_0/d)^2$ are within b_0 of a columnar defects and hence pinned directly. The others are kept at their positions by the elastic interactions with these strongly pinned vortices. Two mechanisms of the formation of the critical current are possible in this regime. One of them is related to the pinning of the vortex bundles of the transverse size R_c from (3.53): The critical current is defined by the balance between the Lorentz force exerted on this bundle and the shear deformation energy necessary to shift this bundle to the next metastable state. Another mechanism becomes relevant, however, when $R_c \ll d$. In this case vortices which are locked *between* these pinned islands of the size of R_c will move under the sufficient current before the depinning of the vortices trapped by rods take place. The corresponding critical current is given by the balance between elastic and the Lorentz forces in the area d^2: $(1/c) J_c^{pl} B d^2 a_0 \sim c_{66} a_0^2$ and

$$J_c^{pl} \approx J_{pb} \frac{B_\phi}{B} \frac{\xi_{ab}}{a_0}, \quad B_\phi \ll B, \quad T_0 < T < T_1 , \tag{4.37}$$

where J_{pb} is the pair-breaking current defined below Eq. (1.9b).

The critical current due to pinning of vortex bundles can be found from the condition $(1/c) J_c^{\rm col} B R_c^2 \xi_{ab} \sim c_{66} \xi_{ab}^2$. Using (3.53) for the correlation radius, one immediately finds

$$J_c^{\rm col} \approx \frac{c U_0}{\phi_0 \xi_{ab}} \frac{B^*}{B} \sim J_{pb} \left[\frac{c_0}{\xi_{ab}} \right]^2 \frac{B^*}{B} ,$$
$$B^* < B < B_\phi, \quad T_0 < T < T_1 . \tag{4.38a}$$

Note that this expression matches (up to the numerical factor) the critical current (1.9b) for the single vortex pinning in the Bose-glass state. The plastic pinning mechanism holds in the region where R_c is sufficiently small:

$$R_c < d \left[\frac{c_0}{\xi_{ab}} \right]^2 .$$

When $T > T_1$ the thermal renormalization of the collective pinning potential becomes essential, and we must use Eq. (3.59) for R_c. It is easy to check that for $B > B^*$ and $T > T_1$ the pinning correlation length $R_c > d$, and so the conventional collective pinning picture applies. The critical current is then found straightforwardly:

$$J_c^{\rm col} \approx \frac{c U_0}{\phi_0 \xi_{ab}} \left[\frac{\xi_{ab}}{u_T} \right]^5 \frac{B^*}{B}$$
$$= J_{pb} \left[\frac{c_0}{\xi_{ab}} \right]^2 \left[\frac{\xi_{ab}}{u_T} \right]^5 \frac{B^*}{B} ,$$
$$B^* < B < B_m, \quad T > T_1 . \tag{4.38b}$$

Upon writing u_T as $u_T^2 = (1/2\sqrt{\pi}) \gamma T a_0 / \varepsilon_0$, we obtain $J_c^{\rm col} \propto B^{1/4}/T^{5/2}$.

We have seen that two main regimes of the pinning can exist in the region $B > B^*$: (i) the plastic pinning (at $T < T_1$) with critical current given by Eq. (4.37) and (ii) collective pinning with critical currents from Eqs. (4.38).

Note that the condition for plastic pinning to exist can be rewritten as

$$B^* < B < B^* \left[\frac{\xi_{ab}}{c_0} \right]^2 \left[\frac{d}{\xi_{ab}} \right]^2 ,$$

which means that the condition $(\xi_{ab}/c_0)^3 > d/\xi_{ab}$ should be satisfied. Accordingly, we consider two creep mechanisms: plastic creep and collective creep of vortex bundles. Recall that the current at which the transition from the single vortex creep to the creep of the vortex bundles occurs is defined by the condition[2,9]

$$L_z(J) = a_0 , \tag{4.39}$$

where $L_z(J)$ is the characteristic length of the fluctuating segment appearing in the single vortex creep process.

We emphasize that these results apply to transport at *intermediate* current and length scales. As $J \to 0$, the relevant length scale for transport eventually exceeds R_a. On scales large compared to R_a, we expect that variable-range hopping of flux *bundles* leads to a result of the form (4.18) in the asymptotic limit $J \to 0$.

2. Creep through plastic barriers

The thermally activated motion of the vortex bundles over the plastic barriers occurs via jumps over a distance a_0 separating different metastable states *between* the tracks. Therefore this "plastic" creep corresponds to the so-called charge-density-wave (CDW) limit of vortex motion. The characteristic size of the bundle and the dependence of creep activation energy on the applied current J are obtained by means of the usual dimensional estimates:

$$c_{44} \frac{a_0^2}{L_z^2} \sim c_{11} \frac{a_0^2}{R_\parallel^2} \sim c_{66} \frac{a_0^2}{R_\perp^2} \sim \frac{1}{c} J B a_0 . \tag{4.40}$$

This estimate represents the balance between tilt, compression, shear, and Lorentz forces per unit volume of the moving bundle. The lengths L_z, $R_\parallel$, and $R_\perp$ are the sizes of the bundle along the z axis, in the direction of bundle motion, and in the transverse direction, respectively. The criterion for the bundle creep is $R_\perp > a_0$. The length scales $R_\perp$, $R_\parallel$, and L_z are related according to

$$L_z \cong \left[\frac{c_{44}}{c_{66}} \right]^{1/2} R_\perp , \quad R_\parallel \cong \left[\frac{c_{11}}{c_{66}} \right]^{1/2} R_\perp . \tag{4.41}$$

The elastic moduli of the vortex lattice, c_{44} and c_{11}, show nontrivial dispersive behavior which complicates the creep picture and changes the values of creep exponents.[2,5] For the case $\mathbf{H} \| \hat{\mathbf{c}}$, the tilt and compression moduli take the form[2,61]

$$c_{44}(k) = \frac{B^2}{4\pi} \frac{1}{1 + (\lambda_{ab}^2/\gamma^2) K^2 + \lambda_{ab}^2 k_z^2} ,$$
$$c_{11}(k) = \alpha(k) c_{44}(k) , \tag{4.42}$$
$$\alpha(k) = \frac{1 + (\lambda_{ab}^2/\gamma^2) k^2}{1 + \lambda_{ab}^2 k^2} ,$$

where $\gamma = \sqrt{M_z/M_\perp}$ and $\mathbf{k} = (\mathbf{K}, k_z)$. Since the characteristic wave vectors are $k_z \sim 1/L_z$ and $K \sim 1/R_\perp$, we find that, in the dispersive region,

$$c_{44} \cong \frac{B^2}{4\pi} \frac{\gamma^2 R_\perp^2}{\lambda_{ab}^2} , \quad R < \lambda_{ab} \gamma ,$$
$$\alpha \cong \begin{cases} 1, & R_\perp < \lambda_{ab} , \\ \dfrac{\lambda_{ab}^2 \gamma^2}{R_\perp^2} , & \lambda_{ab} < R_\perp < \lambda_{ab} \gamma , \\ \gamma^2 , & a_0 < R_\perp < \lambda_{ab} , \end{cases} \tag{4.43}$$

for large fields, where $a_0 < \lambda_{ab}/\gamma$. Combining Eqs. (4.40)–(4.43), we find, for the creep activation energy,

$$U(J) \cong \frac{B^2}{4\pi\gamma^2} \frac{1}{\lambda_{ab}^2} \sqrt{\alpha} R_\perp^5 , \tag{4.44}$$

$$R_\perp \cong d (J_c^{pl}/J)^{1/2} , \quad J < J_c^{pl} , \tag{4.45}$$

$$U(J) \cong \frac{B^2 d^5 \gamma^2}{4\pi \lambda_{ab}^2 \gamma^2} \left[\frac{J_{pl}}{J} \right]^{5/2} \begin{cases} 1, & R_\perp > \lambda_{ab} , \\ \dfrac{\gamma \lambda_{ab}}{R_\perp} , & \lambda_{ab} < R_\perp < \lambda_{ab} \gamma , \\ \gamma , & a_0 < R_\perp < \lambda_{ab} . \end{cases}$$

Since $J_c^{pl} \propto B^{-1/2}$, we have $U(J) \propto B^{3/4}$ in the nondispersive region and in the region of small $R_\perp$, and $U(J) \propto B$ in the intermediate region.

3. Collective creep

Now we consider the regime of collective creep, i.e., $d < R_\perp$, where $R_\perp$ is the transverse dimension of the moving flux bundle. The dynamics of the flux bundles at small currents $J \ll J_c$ is viewed as the sequence of the thermally activated jumps of vortex bundles between static metastable states generated by disorder. The spatial distribution of the metastable states and connection between the metastable states with spacing u and the characteristic size of the vortex bundle R are governed by the scaling relation $u \sim R^\zeta$, where ζ is the wandering exponent depending on the dimensionalities involved (i.e., dimensionalities of the disorder, the driven elastic object, and the space.[2,5] The applied currents select the most favorable hopping distance and the optimal size of vortex bundles, and, therefore, determine the creep activation barriers.

Using once again the quantum-mechanical analogy, one can reduce the problem of *classical* collective creep through columnar disorder to the problem of *quantum* tunneling of a two-dimensional pancake vortex lattice between metastable states generated by time-independent point disorder. We first write the free energy of the vortex lattice as

$$F=\int dz\, d\mathbf{R}\left\{\frac{1}{2}c_{44}\left[\frac{\partial \mathbf{u}}{\partial z}\right]^2+\frac{1}{2}(c_{11})(\mathrm{div}\mathbf{u})^2 +\frac{1}{2}c_{66}(\nabla_\perp \mathbf{u})^2+V_D[\mathbf{R}-\mathbf{u}(z,\mathbf{R})] -\frac{1}{c}JBu_\perp\right\}, \tag{4.46}$$

where $u_\perp$ is the component of $\mathbf{u}$ parallel to the Lorentz force. Note that the tilt modulus c_{44} plays the role of the fictitious particle "mass" and the tilt deformation term represents a fictitious "kinetic energy" in Eq. (4.46). We can consider Eq. (4.46) as the Euclidean action governing the process of quantum tunneling.[2] The creep rate as usual is controlled by the saddle-point trajectory, and in order to find it we have to minimize (4.46) with respect to the size of the bundle, the hopping distance (in the xy plane), and the "duration" of tunneling process in imaginary time. This kind of 2D quantum collective creep has been discussed briefly in Ref. 2 in the strongly dissipative limit. The Euclidean action (4.46) describes a different *nondissipative* limit of quantum tunneling with a strongly dispersive mass c_{44}.

The scaling of the optimal jump for 2D creep is given by $u\sim R^{\zeta_{2,2}}$, $\zeta_{2,2}=\frac{2}{5}$, as long as $u<a_0$ and the structure of the vortex lattice is irrelevant.[2] When $u>a_0$, $u\cong a_0\ln(R_\perp/R_{\mathrm{CDW}})$, where R_{CDW} is the size of the bundle corresponding to $u=a_0$ and can be found from the scaling formula for u:

$$u\cong r_0(R_\perp/R_0)^{2/5}. \tag{4.47}$$

Here r_0 and R_0 are the characteristic scales depending on the particular scenario of the development of the creep process. If we start in the region $B>B^*$, $r_0=u_T$ (the root-mean-square thermal fluctuation of a line) and $R_0=R_c$. If initial conditions correspond to the half-loop creep or VRH processes considered above, the characteristic lengths r_0 and R_0 are to be found by setting $Z=a_0$, $u\cong r^*$, where Z is the size of the vortex bundle along the z axis.

Upon replacing a_0 by u in (4.40) and combining now Eqs. (4.40)–(4.43) and (4.47), we find, for the "static" two-dimensional part of the free energy,

$$E_{2\mathrm{D}}=\sqrt{c_{66}c_{11}(R_\perp)}\,u^2(R_\perp), \tag{4.48}$$

and for the "quantum" action, i.e., creep energy

$$U(J)=c_{44}(R_\perp)\sqrt{\alpha}R_\perp u^2(R_\perp). \tag{4.49}$$

Because in a dispersive region where the transverse size $R_\perp<\lambda_{ab}$, the optimal hopping jump u scales as $u\sim\ln R_\perp$ and one finds, for different ranges of magnetic field,

$$U(J)\cong U_b\left[\frac{R_\perp}{R_0}\right]^{19/5} =U_b\left[\frac{J_b}{J}\right]^{19/8}, \quad a_0<R_\perp<\lambda_{ab}, \tag{4.50a}$$

where $U_b=(B^2/4\pi)(r_0^2/a_0^2\gamma)R_c^3$ and J_b is the characteristic current at which $R_\perp(J)=R_0$ and

$$U(J)\cong U_b\frac{\lambda_{ab}}{R_0}\left[\frac{R_\perp}{R_0}\right]^{14/5} \cong U_b\frac{\lambda_{ab}}{R_0}\left[\frac{J_b}{J}\right]^{14/8}, \quad \lambda_{ab}<R_\perp<\lambda_{ab}\gamma, \tag{4.50b}$$

$$U(J)\cong U_b\frac{\lambda_{ab}^2}{R_0^2}\left[\frac{R_\perp}{R_0}\right]^{9/5}, \quad \gamma\lambda_{ab}<R_\perp, =U_b\left[\frac{\gamma\lambda_{ab}^2}{R_0^2}\right]\left[\frac{J_b}{J}\right]^{9/8}. \tag{4.50c}$$

Note that the obtained results show that the wandering exponent ζ for a vortex lattice subject to columnar disorder coincides with that for the 2D vortex lattice, $\zeta=\frac{2}{5}$.

When the hopping distance u exceeds the vortex spacing a_0, creep is governed by the CDW-like pinning and the corresponding pinning energies read

$$U_{\mathrm{CDW}}(J)\cong U_b\left[\frac{a}{r_0}\right]^2\begin{cases}(J_b/J)^{15/8}\ln^2(J_b/J)^{5/8}, & a_0<R_\perp<\lambda_{ab},\\ \dfrac{\lambda_{ab}}{R_0}\left[\dfrac{J_b}{J}\right]^{5/4}\ln^2\left[\dfrac{J_b}{J}\right]^{5/8}, & \lambda_{ab}<R_\perp<\lambda_{ab}\gamma,\\ \left[\dfrac{a}{R_0}\right]^2\left[\dfrac{J_b}{J}\right]^{5/8}\ln^2\left[\dfrac{J_b}{J}\right]^{5/8}, & \lambda_{ab}\gamma<R_\perp.\end{cases} \tag{4.51}$$

The last result enables us to consider the competition between columnar and point disorder at large scales. At $R_\perp\gg\lambda_{ab}\gamma$, creep energy (4.51) scales as $(R_\perp)\sim R_\perp\ln^2 R_\perp$. Let us superimpose weak point disorder and consider the effect of point disorder on the vortex creep perturbatively. After each elementary jump over $u\cong a_0$, the bundle acquires an additional energy $\delta E\sim\sqrt{a_0R_\perp^2}\sim R_\perp$ due to point disorder (the pinning force due to point disorder is proportional to the square root of the volume δV swept by the bundle during the jump, and $\delta V\propto a_0R_\perp^2$). Thus, since the energy barrier provided by columnary pins scales as $R_\perp\ln^2 R_\perp$ at very large distances $R_\perp$, the Bose-glass dynamics is *stable* with respect to point disorder in this regime.

We now discuss briefly the results describing collective creep at high enough fields $B > B^*$ and high enough temperatures $T > T'$ where the characteristic scale of the pinning potential is controlled by the mean thermal displacements of the vortex lines in the vortex lattice: $u_T^2 \cong \langle u^2 \rangle_{\rm th} \cong T a_0 / \tilde{\epsilon}_1 \epsilon_0$. In this region $R_0 = R_c$, where R_c is given by Eq. (3.59), $r_0 = u_T$, and $J_b = J_c^{\rm col}$ from Eq. (4.38). We find, in this regime,

$$U(J) \cong U_p \begin{cases} [J_c^{\rm col}(T)/J]^{19/8}, & a_0 < R_\perp < \lambda_{ab}, \\ (\lambda_{ab}/R_c)[J_c^{\rm col}(T)/J]^{14/8}, & \lambda_{ab} < R_\perp < \lambda_{ab}\gamma, \\ (\lambda_{ab}^2 \gamma / R_c^2)[J_c^{\rm col}(T)/J]^{9/8}, & \lambda_{ab}\gamma < R_\perp , \end{cases} \tag{4.52}$$

where $U_p = U_b(R_0 = R_c)$.

Another creep scenario, when creep starts in the region of single vortex creep (via half-loop formation or VRH process) and then evolves into a collective creep of vortex bundles as current decreases, can be considered in a similar fashion.

To conclude this section, we discuss briefly the temperature dependence of physical quantities. Taking into account that $R_c \sim (1-t)^{-3/2}$, $T^* \sim (1-t)$, $J_c^{\rm col}(T) \sim (1-t)^{7/2}$, and $U_p \sim (1-t)^{-11/2}$, where $t = T/T_c$, we find, from Eq. (4.52),

$$U(J) \sim \begin{cases} (1-t)^{45/16}, & a_0 < R_\perp < \lambda_{ab}, \\ (1-t)^{19/16}, & \lambda_{ab} < R_\perp < \lambda_{ab}\gamma, \\ (1-t)^{7/16}, & \lambda_{ab}\gamma < R_\perp . \end{cases} \tag{4.53}$$

H. Dynamics of the Mott-insulator phase

Excitations in the Mott insulator differ from those in the Bose glass due to the gap in the excitation spectrum.[31] Because the Mott insulator has both an infinite tilt modulus and is incompressible, (small) currents will flow only within a penetration depth of the sample surface, as they would in a conventional Meissner phase. Low-energy thermal excitations are similar to the half loops discussed in Sec. IV A. The characteristic energy of an excitation of size z^* is of order $U_0 z^* = \sqrt{U_0 \tilde{\epsilon}_1 r^*}$, as we find from optimizing Eq. (4.6) with $f_L = 0$. Variable-range hopping of vortices to distant, nearly degenerate states is impossible because of the gap. Nonlinear current-voltage characteristics will arise because of vortex half loops generated near the sample surface. The physics should be similar to the discussion of transport in a conventional Meissner phase in Ref. 4. Point disorder *never* destabilizes the Mott insulator even in the limit $J \to 0$.

Like variable-range hopping, "variable-range tilting" is also impossible in the Mott insulator. As a result, the Mott insulator should be stable to tilt until the rather large tipping angle θ_a in Eq. (4.31b) is reached. Because the Mott insulator may occur only well below $T_{\rm BG}$, which plays the role of an irreversibility line in this problem, it may be difficult to access experimentally for dynamical reasons.

V. SCALING THEORY OF THE BOSE-GLASS TRANSITION

A quantitative theory of the Bose-glass transition itself is unavailable at present. Our ignorance about the exact dynamics near $T_{\rm BG}$, however, can be packaged into just two critical exponents, as discussed in the Introduction. These exponents can be extracted from computer simulations of simplified models designed to focus on the "universal" asymptotic behavior when the correlation lengths $l_\perp$ and $l_\parallel$ are large.[35] We apply here ideas applied previously to isotropic vortex glasses[4] to transport with $\mathbf{J} \perp \mathbf{B}$.[70] Although the two theories are similar when $\mathbf{H}_\perp = \mathbf{0}$, striking differences arise when we consider the response to tilting the external field. We invoked a similar static scaling assumption [Eq. (3.25)] earlier in our treatment of vortex density fluctuations near $T_{\rm BG}$.

A. Scaling for $\mathbf{H}_\perp = \mathbf{0}$

The scaling behavior of the current and the electric field for $\mathbf{H}_\perp = \mathbf{0}$ is related to the critical properties of the vector potential in the underlying Ginzburg-Landau description of the physics.[4] The in-plane vector potential $\mathbf{A}_\perp$, in particular, gives the current $\mathbf{J}$ and the electric field $\mathcal{E}$ via

$$\mathbf{J} = c \frac{\partial f}{\partial \mathbf{A}_\perp} \tag{5.1a}$$

and

$$\mathcal{E} = -\frac{1}{c} \frac{\partial \mathbf{A}}{\partial t} , \tag{5.1b}$$

where f is the free-energy density. Because the vector potential appears in the anisotropic Ginzburg-Landau theory in the combination

$$\frac{\hbar^2}{2M_\perp} \left| \left(\nabla_\perp - \frac{2ei}{\hbar c} \mathbf{A}_\perp \right) \Psi_{\rm BCS} \right|^2 , \tag{5.2}$$

where $\Psi_{\rm BCS}$ is the BCS order parameter, we expect that the behavior of $\mathbf{A}_\perp$ near the transition is $\mathbf{A}_\perp \sim 1/l_\perp(T)$, where $l_\perp(T)$ is given by Eq. (3.3). Since the free-energy density $f \sim 1/l_\perp^2 l_\parallel$ [with $l_\parallel$ given by (3.6)], we find from (5.1a) that $J \sim 1/l_\perp l_\parallel$. If the relaxation time for a critical fluctuation scales according to Eq. (1.3), Eq. (5.1b) implies that $\mathcal{E} \sim 1/l_\perp \tau \sim 1/l_\perp^{1+z'}$. These expectations are embodied in the scaling hypothesis

$$\mathcal{E} l_\perp^{1+z'} = F_\pm(l_\perp l_\parallel J \phi_0 / cT) , \tag{5.3}$$

where the $\pm$ subscripts allow different scaling functions above and below $T_{\rm BG}$. Note that the scaling combination $l_\perp l_\parallel J \phi_0 / c$ is just the work done by the Lorentz force to move a critical fluctuation (extending a distance $l_\parallel$ along the z axis) a distance $l_\perp$.

Henceforth, we set $\nu_\parallel = 2\nu_\perp \equiv 2\nu'$, in accordance with the exponent relation[31] (3.19), which has been checked with simulations.[35] The primes on the exponents ν' and z' are intended to distinguish these exponents from their counterparts ν and z in the vortex-glass phenomenology.[4] Data at different current levels near $T_{\rm BG}$ should be col-

lapsible into two scaling functions, according to (5.3). Above T_{BG}, the expected linear resistivity at small currents requires that $F_+(x) \sim x$ as $x \to 0$, which leads to Eq. (1.4). Precisely at T_{BG}, we require $F_\pm(x) \sim x^{(1+z')/3}$ as $x \to \infty$ (so that $\mathcal{E}$ remains finite for finite J), which leads to Eq. (1.5). The variable-range hopping prediction (4.18) requires that

$$F_-(x) \sim \exp\left[\frac{-\text{const}}{x^{1/3}}\right] \tag{5.4}$$

as $x \to 0$.

B. Scaling with a perpendicular field

Except for the anisotropically diverging correlation lengths, Bose-glass scaling when $\mathbf{H}_\perp = \mathbf{0}$ is very similar to the vortex-glass scaling hypothesis. In fact, point-disorder-dominated vortex glasses could in principle *also* have correlation lengths which diverged differently parallel and perpendicular to the average field direction.[4] In this case, however, tilting the external field would immediately cause a rotation of the direction of the most strongly diverging length. The response to $\mathbf{H}_\perp \neq \mathbf{0}$ at the Bose-glass transition is very different, because tilting $\mathbf{H}$ attempts to pull vortex trajectories away from the privileged direction singled out by the correlated disorder.

To extend the scaling description, note that $\mathbf{H}_\perp = \partial \mathbf{A}_\perp / \partial z$, and so the ideas of the previous subsection lead to $\mathbf{H}_\perp \sim 1/l_\perp l_\parallel$. Hence we generalize Eq. (5.3) to read

$$\mathcal{E} l_\perp^{1+z'} = \mathcal{F}_\pm(l_\perp l_\parallel J\phi_0/c, H_\perp l_\parallel l_\perp/\phi_0) \ . \tag{5.5}$$

The most interesting consequences of (5.5) arise in the flux liquid regime of Fig. 4, where there is a linear resistivity. Upon linearizing (5.5) for small J, setting $\nu_\parallel = 2\nu_\perp = 2\nu'$, and changing variables to $\theta \approx H_\perp/H_z$ and $t = (T - T_{BG})/T_{BG}$, we recover the scaling form in Eq. (1.8),

$$\rho(t,\theta) \approx |t|^{\nu'(z'-2)} f(\theta |t|^{-3\nu'}) \ . \tag{1.8'}$$

An enlarged view of the cusped region in Fig. 4 together with the expected behavior of the scaling functions $f_\pm(x)$ is shown in Fig. 17. We have argued in Sec. IV D that a finite tilt $H_\perp^c(T)$ is required to destroy the Bose-glass phase. This transition, discussed in Ref. 37, requires a singularity in $f_-(x)$ at $x = \pm x_c$, so that the critical tilt angle θ_c vanishes as $T \to T_{BG}^-$,

$$\theta_c(t) = \pm x_c |t|^{3\nu'} \ , \tag{5.6}$$

which is equivalent to Eq. (1.6). Consistency with Eq. (4.31) requires that

$$f_-(x) \sim (x \pm x_c)^{3/2} \tag{5.7}$$

near these singularities. In very thin samples, this cusp will be rounded off for small reduced temperatures t such that $l_\parallel(T) \approx \tilde{\varepsilon}_1 l_\perp^2(T)/T \geq L$.

The function $f_+(x)$ should be an analytic even function of x at $x = 0$, reflecting the finite tilt modulus in the flux-liquid phase. The angular dependence of the resistivity just above T_{BG} is thus

$$\rho(t,\theta) \approx \rho_0 t^{\nu'(z'-2)}[1 + A t^{-6\nu'}\theta^2] \ , \tag{5.8}$$

where A is a positive constant. The dashed lines in Fig. 17 denote the locus of points where $\rho(t,\theta)$ has increased by a fixed fraction of its value at $\theta = 0$. Note that the coefficient of θ^2 is proportional to $t^{-\nu'(8-z')}$, which diverges as $T \to T_{BG}^+$ provided $z' < 8$. A very sharp rise of the resistivity with tipping angle away from alignment with twin boundaries has, in fact, been observed experimentally.[15,18] We predict a similar strong angular dependence in samples with columnar pins, since $z' \approx 6$.[35] We note finally that Eq. (1.8) is only consistent with a finite resistivity when $t = 0$ and $\theta \neq 0$ provided

$$\rho(0,\theta) \sim \theta^{(z'-2)/3} \ , \tag{5.9}$$

which is equivalent to Eq. (1.7).

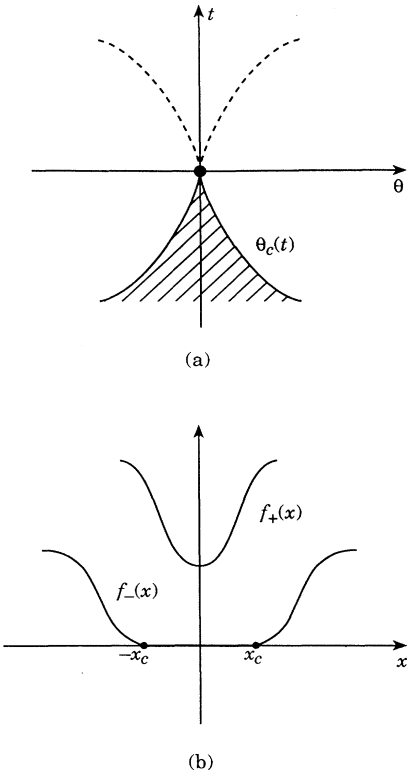

FIG. 17. Scaling description of the response to tilt near the Bose-glass transition. (a) Phase diagram near $T_{BG}(H_\perp = 0)$ as a function of reduced temperature $t = (T - T_{BG})/T_{BG}$ and angle $\theta = H_\perp/H_z$. The dashed lines mark the onset of a sharp drop in the resistivity as a function of angle in the flux liquid. The shaded region is the Bose glass. (b) Scaling functions $f_+(x)$ for $T > T_{BG}(0)$ and $f_\pm(x)$ for $T < T_{BG}(0)$.

C. Irrelevance of point disorder at the transition

It is easy to show that weak disorder has no influence on Bose-glass scaling near T_{BG} itself, at least insofar as it

shifts the local transition temperature. We adapt the Harris criterion[71] for random spin systems to this problem.[72] Our conclusion agrees with explicit computations for a soluble (1+1)-dimensional system.[37] We assume that the point-disorder potential in Eq. (4.32) produces a linear shift in the local Bose-glass transition temperature $T_{\rm BG}(\mathbf{r},z)=T^0_{\rm BG}+\delta T_{\rm BG}(\mathbf{r},z)$, where

$$\delta T_{\rm BG}(\mathbf{r},z)=\text{const}\times\delta V'_D(\mathbf{r},z)\ . \tag{5.10}$$

Point disorder will be irrelevant if the correlation volume near $T_{\rm BG}$ diverges fast enough to efficiently average out the random potential $\delta V'_D(\mathbf{r},z)$. The root-mean-square fluctuation in $\delta T_{\rm BG}$ averaged over a volume $l_\perp^2 l_\parallel$ [see Eq. (4.33)] is

$$(\delta T_{\rm BG})_{\rm rms}\propto(\Delta_0/l_\perp^2 l_\parallel)^{1/2}\sim|t|^{2\nu'}\ . \tag{5.11}$$

This quantity will be much less than distance t to the transition as $|t|\to 0$ (and point disorder will be irrelevant) provided

$$\nu'>\tfrac{1}{2}\ , \tag{5.12}$$

which is guaranteed by the rigorous inequality[31] $\nu'\geq 1$.

VI. PINNING BY TWIN BOUNDARIES

Twin boundaries can be an important source of correlated disorder even if columnar defects produced by irradiation (or embodied in screw dislocations[14]) are absent. Twins are ubiquitous in superconducting $YBa_2Cu_3O_{7-x}$ and La_2CuO_4, where they are needed to accommodate strains produced a crystallographic tetragonal-to-orthorhombic transition. Twins occur in two orthogonal families of lamella called "colonies," whose characteristic dimension (mosaic size) scales as the square of the twin spacing d within the colony.[73] See Fig. 1(c). Our theory should be directly applicable to twinned materials on scales large compared to this mosaic size. Indeed, boson localization rather than vortex-glass physics may well be responsible for the phase transitions observed in Refs. 12 and 13. As discussed in the Introduction, this question can be easily decided experimentally by rotating the magnetic field away from the direction of alignment with the correlated disorder.[15,18]

It is also possible to prepare samples which contain a *single* family of parallel twin planes.[15,18] For $\mathbf{H}\|\hat{\mathbf{c}}$, localization of flux lines by correlated pinning will occur at low temperatures, in the direction orthogonal to the planes. A Bose-glass delocalization transition should occur with increasing temperatures. The tilt modulus will again become infinite below $T_{\rm BG}$, at least for tipping vortices out of alignment with the twins. A scaling theory, such as that presented in Sec. V, should become applicable near the transition, but with different critical exponents and *three* distinct length scales. Equation (5.5), for example, generalizes to

$$\mathcal{E}l_\perp^{1+z'}=\mathcal{F}_+(l_\perp l_\parallel J\phi_0/c, H_\perp l_\parallel\tilde{l}_\perp/\phi_0)\ , \tag{5.5'}$$

where $l_\perp$ and $l_\parallel$ have the same meaning as for columnar pins, and $\tilde{l}_\perp(T)\sim 1/|T-T_{\rm BG}|^{\tilde{\nu}_\perp}$ is a new diverging length describing correlations perpendicular to the field direction but *parallel* to the twin planes. Standard variable-range hopping arguments[32] suggest a current-voltage characteristic $V\sim\exp[-(\tilde{J}/J)^{1/2}]$ in the Bose glass. Rare events, such as exceptionally large gaps between thin spaces, should dominate transport at very low currents, however. A more complete treatment of this fascinating problem will be presented in a future publication.[74]

We conclude this brief discussion with a derivation of the critical-current formula (1.11b) for parallel twin boundaries quoted in the Introduction. Consider the regime of low fields where every vortex is localized on a twin, with well depth U_0 and effective width $2b_0$. The temperature renormalization of the pinning energy and the localization length for $T>T^*$ are given in Eqs. (2.25) and (2.26). This estimate holds, however, only when $l_\perp(T)<d$, i.e., $T<T_{dp}$, where

$$T_{dp}\approx T^*\left[\frac{d}{b_0}\right]^{1/2}\ . \tag{6.1}$$

When $T\gg T_{dp}$, vortices are localized collectively by *many* twin planes in the perpendicular direction. In the absence of strong interaction effects, these lines are presumably *delocalized* in the direction parallel to the planes. To determine $l_\perp(T)$, we carry out a one-dimensional variational calculation analogous to that following Eq. (3.30a). Straightforward estimates of the ground-state energy now lead to

$$E_0\approx\frac{T^2}{\tilde{\varepsilon}_1 l_\perp^2}-\frac{U_0 b_0}{(l_\perp d)^{1/2}} \tag{6.2}$$

in analogy to Eq. (3.32a). Upon minimizing with respect to $l_\perp$, we find

$$l_\perp(T)\approx d\left[\frac{b_0}{d}\right]^{2/3}\left[\frac{T}{T^*}\right]^{4/3}\quad(T>T_{dp}) \tag{6.3}$$

and ground-state energy

$$U(T)=U_0\left[\frac{b_0}{d}\right]^{2/3}\left[\frac{T^*}{T}\right]^{2/3}\quad(T>T_{dp})\ . \tag{6.4}$$

Note that the localization length now grows less slowly with temperature than in Eq. (2.26). When these results are inserted to estimate (2.24a) for the critical current, we recover Eq. (1.11b).

ACKNOWLEDGMENTS

This work was supported by the National Science Foundation, through Grant No. DMR 91-15491 and through the Harvard Materials Research Laboratory. V.M.V. acknowledges support from the Materials Science Division of Argonne National Laboratory via the Department of Energy, BES-Material Sciences, under Contract No. W-31-109-ENG-38. We acknowledge stimulating discussions with D. Bishop, R. Budhani, L. Civale, G. Crabtree, M. Feigel'man, D. S. Fisher, P. L. Gammel, V. Geshkenbein, S. Girvin, T. Hwa, W. Kwok,

P. Le Doussal, M. C. Marchetti, T. Mitchell, L. Radzihovski, and B. Shklovskii.

APPENDIX A: FIRST- AND SECOND-ORDER FREEZING OF ABRIKOSOV FLUX LINES

In this appendix we briefly review theoretical arguments predicting first-order freezing from a flux liquid into a triangular vortex lattice. We also show that this transition can be continuous for the smecticlike crystal which appears in Fig. 4 when columnar pins provide the correlated disorder. From mean-field theory, one expects that the Abrikosov flux lattice appears exactly at H_{c2} via a continuous phase transition.[75] A renormalization-group analysis in $6-\varepsilon$ dimensions,[21] however, shows that thermal fluctuations reduce the ordering temperature and force this transition to become first order below six dimensions. Although this effect is probably unobservable in most conventional superconductors, it should become more pronounced in the strongly fluctuating high-T_c materials.[3] In the physical dimension $d=3$, we can also appeal directly to the following physical argument:[21] Once fluctuations drive the ordering transition significantly below H_{c2}, the system still acquires a nonzero local condensate density below $H_{c2}(T)$,

$$\rho(\mathbf{r}_\perp,z)=\langle|\Psi_{\rm BCS}(\mathbf{r}_\perp,z)|^2\rangle\ , \tag{A1}$$

where $\Psi_{\rm BCS}(\mathbf{r}_\perp,z)$ is the BCS order parameter and the field is assumed to be along z. In a flux liquid, the zeros of $\Psi_{\rm BCS}(\mathbf{r}_\perp,z)$ (i.e., embryonic vortices wandering along the z axis) are disordered, and so the thermal average in Eq. (A1) is independent of position. This quantity becomes modulated, however, once these zeros crystallize. We can then follow the classic analysis of Landau[76] and expand ρ in the Fourier components of the triangular flux lattice:

$$\rho(\mathbf{r}_\perp)=\rho_0+\sum_{\mathbf{G}\neq 0}\rho_{\mathbf{G}}e^{i\mathbf{G}\cdot\mathbf{r}_\perp}\ , \tag{A2}$$

where the $\{\mathbf{G}\}$ are reciprocal-lattice vectors lying in a plane perpendicular to $\hat{\mathbf{z}}$. The free-energy density difference $\delta\mathcal{F}$ between the liquid and crystalline phases can then be expressed as a Taylor series in the $\{\rho_{\mathbf{G}}\}$, which are order parameters for the freezing transition,

$$\delta\mathcal{F}=\frac{1}{2}r\sum_{j=1}^{6}|\rho_{\mathbf{G}_j}|^2+w\sum_{\mathbf{G}_i+\mathbf{G}_j+\mathbf{G}_k=0}\rho_{\mathbf{G}_i}\rho_{\mathbf{G}_j}\rho_{\mathbf{G}_k}+\cdots\ . \tag{A3}$$

The $\mathbf{G}$ vectors included here come from the first ring of six around the origin. The crucial element is the third-order term allowed by the symmetry of a triangular lattice, which leads to a first-order phase transition when $r=r(T)$ decreases with decreasing temperature. Toner has discussed how to incorporate hexatic bond orientational order and quenched random point disorder into this picture.[77]

A recent computer simulation of a lattice-gauge glass model by Hetzel, Sudbo, and Huse does indeed find a first-order transition.[78] The flux array studied in Ref. 78 is somewhat artificial, because it is exactly commensurate with the underlying mesh of points which defines the model. In addition, the star of reciprocal-lattice vectors which defines the order parameter points in a discrete rather than continuous set of directions. This should not alter the basic prediction of a first-order freezing transition, however.[79] The Landau argument correctly predicts a first-order freezing transition for liquids of point particles in three dimensions and is likely to be correct for three-dimensional line liquids as well.

When columnar pins are present, the Landau theory of freezing may be applied to the low-temperature crystal phase shown in Fig. 4. Consider first a magnetic field oriented in the *ab* plane exactly perpendicular to columnar pins aligned with the c axis. We neglect point disorder, which is assumed to affect the physics only at length scales much larger than the vortex-lattice spacing. Vortex lines then run at right angles through the defect "forest" on predominantly "horizontal" trajectories. Although fluxons may deviate to the right or left to pass through particularly favorable "thickets" of columnar pins, their vertical deflections are unconstrained. A low-temperature crystalline phase periodic in two directions is impossible because of the disorder.[9] The vortices can order, however, in smecticlike sheets which are periodic in z, along the c axis. This crystal should freeze from a flux liquid in a way somewhat reminiscent of the nematic–to–smectic-A transition in liquid crystals.[80]

The condensate density (A1) is now modulated in the z direction below the freezing transition, and the order parameter expansion (A2) becomes

$$\rho(z)\approx\rho_0[1+{\rm Re}\{\Phi_{q_0}e^{iq_0z}\}]\ , \tag{A4}$$

where Φ_{q_0} is a complex order parameter describing the amplitude and phase of a density wave with wave vector $\mathbf{q}_0=q_0\hat{\mathbf{z}}\approx(2\pi/a_0)\hat{\mathbf{z}}$. Although integer multiples of $\mathbf{q}_0$ could also appear in the expansion, wave vectors with components perpendicular to $\hat{\mathbf{z}}$ are excluded by the disorder. As in the de Gennes theory of the nematic–to–smectic-A transition,[80] we expand the free-energy density difference between the liquid and crystal phases to quartic order in Φ_{q_0},

$$\delta\mathcal{F}=\tfrac{1}{2}r|\Phi_{q_0}|^2+u|\Phi_{q_0}|^2\ , \tag{A5}$$

with $r\propto(T-T_m)$. Unlike Eq. (A3), a third-order term is not permitted by symmetry, and so the transition can be continuous. Of course, a first-order transition caused by a negative value of u cannot be ruled out, however. To treat thermal fluctuations more accurately, we should allow Φ_{q_0} to have spatial dependence and include gradient terms such as $|\nabla\Phi_{q_0}(\mathbf{r}_\perp,z)|^2$. The continuous phase transition which results should be in the universality class of the three-dimensional XY model, with $\nu_\parallel=\nu_\perp\approx\frac{2}{3}$.

Suppose the field is tilted at some angle away from the *ab* plane, but not so close to the c axis as to produce a lock-in to a Bose-glass phase (see Fig. 4). Fluxon trajectories will now consist of approximately horizontal vortex segments (kinks) which connect vertical portions running along the columnar pins. The low-temperature

phase will now consist of vortex sheets tilted on average which will remain periodic along the c axis. Because the periodicity is still only possible in one direction, the analysis of freezing sketched above for perpendicular field orientations should remain valid.

APPENDIX B: NONLOCAL VORTEX INTERACTIONS

The interaction in Eq. (2.1a) can be of arbitrary range in the plane perpendicular to **B**, but is local in z. We show here that locality in z is an excellent approximation provided Eq. (2.2) is satisfied. Interactions are clearly local in all directions when $a_0 \gtrsim \lambda_{ab}$ (i.e., $B \lesssim \phi_0/\lambda_{ab}^2$), and so we restrict our attention to the high-field regime $B \gg \phi_0/\lambda_{ab}^2$. We assume $\mathbf{B}\|\hat{\mathbf{c}}$ and use the method of Blatter, Geshkenbein, and Larkin[33] to rescale the underlying Ginzburg-Landau free energy onto an isotropic problem. After rescaling, the nonlocal interaction between two flux lines with trajectories $\mathbf{r}_1(z_1)$ and $\mathbf{r}_2(z_2)$ in the limit $L \to \infty$ reads[2]

$$V'_{12}=\varepsilon_0\int_{-\infty}^{\infty}dz'_1\int_{-\infty}^{\infty}dz'_2\left[1+\frac{d\mathbf{r}_1(z'_1)}{dz'_1}\cdot\frac{d\mathbf{r}_2(z'_2)}{dz'_2}\right]\frac{\exp[-\sqrt{|\mathbf{r}_1(z'_1)-\mathbf{r}_2(z'_2)|^2+(z'_1-z'_2)^2}/\lambda_{ab}]}{\sqrt{|\mathbf{r}_1(z'_1)-\mathbf{r}_2(z'_2)|^2+(z'_1-z'_2)^2}} . \tag{B1}$$

The rescaled energy V'_{12} and coordinates z' are related to the parameters in the original problem by[33]

$$V'_{12}=\left[\frac{M_z}{M_\perp}\right]^{1/2}V_{12} , \tag{B2a}$$

$$z'=\left[\frac{M_z}{M_\perp}\right]^{1/2}z . \tag{B2b}$$

This screened "Biot-Sovart" law allows every element of the flux line to interact with every element on the neighboring line. Note that the interaction vanishes when the three-dimensional line elements

$$d\mathbf{R}_i\equiv\left[\frac{d\mathbf{r}_i(z'_i)}{dz'_i},1\right]dz'_i,\quad i=1,2 ,$$

are at right angles. We shall be interested in the limit of nearly straight lines so that $\langle t_i^2(z')\rangle \ll 1$, where

$$\mathbf{t}_i(z')=\frac{d\mathbf{r}_i(z')}{dz'} . \tag{B3}$$

The condition $\langle t_i^2(z')\rangle \ll 1$ is equivalent to Eq. (2.2).

We now set

$$z'=\tfrac{1}{2}(z'_1+z'_2) , \tag{B4a}$$

$$\Delta z=z'_1-z'_2 , \tag{B4b}$$

and expand in Δz with $\mathbf{r}_{12}(z')\equiv\mathbf{r}_1(z')-\mathbf{r}_2(z')$,

$$\mathbf{r}_1(z'_1)-\mathbf{r}_2(z'_2)=\mathbf{r}_{12}(z')+\frac{1}{2}\Delta z[\mathbf{t}_1(z')+\mathbf{t}_2(z')]+\frac{1}{8}(\Delta z)^2\frac{d^2\mathbf{r}_{12}(z')}{d\bar{z}'^2}+\cdots , \tag{B5}$$

to obtain

$$V'_{12}=\varepsilon_0\int_{-\infty}^{\infty}dz'\int_{-\infty}^{\infty}d(\Delta z)\frac{\exp[-\sqrt{r_{12}^2(z')+(\Delta z)^2}/\lambda_{ab}]}{\sqrt{r_{12}^2(z')+(\Delta z)^2}}[1+\mathcal{O}(t_1^2,t_2^2,\mathbf{t}_1\cdot\mathbf{t}_2)] . \tag{B6}$$

Upon neglecting the corrections, which are quadratic in the tangents, and restricting z' to a slab of thickness L, the Δz integral gives

$$V'_{12}\approx 2\varepsilon_0\int_0^L dz'\,K_0[r_{12}(z')/\lambda_{ab}] . \tag{B7}$$

Upon returning to the original coordinates and energies via Eq. (B2), we recover the interaction used in Eq. (2.1a). The contributions from the correction terms in Eq. (B6) are readily estimated. For vortex separations such that $\xi_{ab} \ll r_{12} \ll \lambda_{ab}$, the correction to the logarithmic interaction embodied in $K_0(r_{12}/\lambda_{ab})$ is always $\mathcal{O}(t_1^2,t_2^2,t_1,t_2)$ over this entire range of distances. When $r_{12} > \lambda_{ab}$ the exponential tail in $K_0(r_{12}/\lambda_{ab})$ acquires corrections whenever $r_{12} > r^*$, with

$$r^*=\lambda_{ab}/\langle t_i^2(z')\rangle . \tag{B8}$$

This contribution, induced by nonlocality in z, is similar to the asymptotic retarded $1/r^7$ interaction (instead of a $1/r^6$ van der Waals attraction) between neutral atoms at very large distances induced by the finite speed of light. The interaction strength, however, is only of order $\varepsilon_0\exp(-r^*/\lambda_{ab}) \ll \varepsilon_0$ in this regime for flux lines and hence should have a negligible effect on the statistical mechanics of melting or localization.

Finally, we estimate directly the size of

$$\langle(d\mathbf{r}_i/dz)^2\rangle=\frac{M_z}{M_\perp}\langle t_i^2(z')\rangle .$$

In the flux-liquid phase, the first term to Eq. (2.1a) leads to

$$\left\langle \left[\frac{d\mathbf{r}_i}{dz} \right]^2 \right\rangle \approx \frac{T}{\tilde{\epsilon}_1 \xi_z} \approx \frac{T}{\epsilon_0 \xi_z} \frac{M_z}{M_\perp} , \tag{B9}$$

where we have used the coherence length ξ_z to cut off the path integral over vortex trajectories at short distances. The right-hand side is of order $0.02 M_z/M_\perp$ at $T=77$ K, and so Eq. (2.2) is very well satisfied; vortices are tipped away from normal at a root-mean-square angle of order 7° in YBCO by thermal fluctuations. Interactions will reduce this angle to even smaller values. Even a small tipping angle is sufficient to produce considerable entanglement in macroscopic flux liquids, however.[3] Large tipping angles only arise close to $H_{c2}(T)$, where the condensation energy vanishes.

APPENDIX C: VORTEX PROBABILITY DISTRIBUTIONS

We show here that the probability of finding an individual vortex line at height z with position $\mathbf{r}_\perp$ in an arbitrary binding potential $V_1(\mathbf{r}_\perp)$ is related to the ground-state wave function of the corresponding Schrödinger equation. See Fig. 6(a). The probability distribution at a free surface is proportional to the wave function itself, while the probability far from the surface is proportional to the wave function squared.

Consider first a fluxon which starts at the origin **0** and wanders across a sample of thickness L to position $\mathbf{r}_\perp$. The partition function associated with this constrained path integral may be written as a quantum-mechanical matrix element,[47]

$$\mathcal{Z}(\mathbf{r}_\perp,\mathbf{0};L) = \int_{\mathbf{r}(0)=\mathbf{0}}^{\mathbf{r}(L)=\mathbf{r}_\perp} \mathcal{D}r(z) \exp\left[-\frac{\tilde{\epsilon}_1}{2T} \int_0^L \left| \frac{d\mathbf{r}}{dz} \right|^2 dz - \frac{1}{T} \int_0^L V_1[\mathbf{r}(z)] dz \right] \equiv \langle \mathbf{r}_\perp | e^{-L\mathcal{H}/T} | \mathbf{0} \rangle , \tag{C1}$$

where $|\mathbf{0}\rangle$ is an initial state localized at **0**, while $\langle \mathbf{r}_\perp|$ is a final state localized at $\mathbf{r}_\perp$. The "Hamiltonian" $\mathcal{H}$ appearing in (C1) is

$$\mathcal{H} = -\frac{T^2}{2\tilde{\epsilon}_1} \nabla_\perp^2 + V_1(\mathbf{r}) . \tag{C2}$$

The probability distribution $P(\mathbf{r}_\perp)$ for the vortex tip position at the upper surface is then

$$P(\mathbf{r}_\perp) = \mathcal{Z}(\mathbf{r}_\perp,\mathbf{0};L) \Big/ \int d^2 r_\perp \mathcal{Z}(\mathbf{r}_\perp,\mathbf{0};L) . \tag{C3}$$

Upon inserting a complete set of (real) energy eigenstates $|n\rangle$ with eigenvalues E_n into Eq. (C1), we have

$$\mathcal{P}(\mathbf{r}_\perp) = \frac{\sum_n \psi_n(\mathbf{0}) \psi_n(\mathbf{r}_\perp) e^{-E_n L/T}}{\sum_n \psi_n(\mathbf{0}) \int d^2 r_\perp \psi_n(\mathbf{r}_\perp) e^{-E_n L/T}} . \tag{C4}$$

In the limit $L \to \infty$, the ground state dominates; the probability $P(\mathbf{r}_\perp)$ becomes

$$\mathcal{P}(\mathbf{r}_\perp) \approx \frac{\psi_0(\mathbf{r}_\perp)}{\int d^2 r_\perp \psi_0(\mathbf{r}_\perp)} [1 + \mathcal{O}(e^{-(E_1 - E_0)L/T})] , \tag{C5}$$

where E_1 is the energy of the first excited states. Because the ground wave function is nodeless,[48] $P(r_\perp)$ is always positive and well defined.

Consider now a more general problem of a vortex which enters the sample at $\mathbf{r}_i$, exits at $\mathbf{r}_f$, and passes through $\mathbf{r}_\perp$ at a height z which is far from the boundaries. The normalized probability distribution is now

$$\tilde{\mathcal{P}}(\mathbf{r}_\perp;L) = \tilde{\mathcal{Z}}(\mathbf{r}_\perp;L) \Big/ \int d^2 r_\perp \tilde{\mathcal{Z}}(\mathbf{r}_\perp;L) , \tag{C6}$$

where

$$\tilde{\mathcal{Z}}(\mathbf{r}_\perp;L) = \int d^2 r_i \int d^2 r_f \mathcal{Z}(\mathbf{r}_f,\mathbf{r}_\perp;L-z) \mathcal{Z}(\mathbf{r}_\perp,\mathbf{r}_i;z) \tag{C7}$$

and $\mathcal{Z}(\mathbf{r}_2,\mathbf{r}_1;L)$ is given by Eq. (C1). Upon inserting complete sets of states as before, we find that

$$\tilde{\mathcal{P}}(\mathbf{r}_\perp;L) = \frac{\psi_0^2(r_\perp)}{\int d^2 r_\perp \psi_0^2(r_\perp)} [1 + \mathcal{O}(e^{-L(E_1 - E_0)/T})] . \tag{C8}$$

For large $\mathbf{r}_\perp$, $\psi_0(r_\perp) \propto \exp(-\kappa r)$, where $\kappa^{-1} \equiv l_\perp(T)$ is the localization length induced by the potential $V_1(r)$. Upon comparing Eqs. (C5) and (C8), we see that the probability distribution is more spread out at the surface ($\psi_0 \sim e^{-\kappa r}$) than in the bulk ($\psi_0^2 \sim e^{-2\kappa r}$), because the free-boundary conditions are less constraining. This surface spreading of the probability distribution persists for a distance of order

$$l_x \approx T/(E_1 - E_0) \tag{C9}$$

into the bulk.

APPENDIX D: ESTIMATES OF PHYSICAL QUANTITIES

In this appendix we estimate the characteristic energies, fields, and crossover temperatures for columnar pins using parameters typical of the cuprate high-temperature superconductors. These estimates are necessarily approximate, because we often neglect factors of order unity and because a number of results depends sensitively on the parameter choices.

The first and most straightforward quantity is the

crossover temperature T_0 such that the microscopic pin radius $c_0=\sqrt{2}\xi_{ab}(T_0)$, which determines the formula for the pinning energy U_0 in Eq. (1.9a) and the *effective* defect rod radius b_0 in Eq. (2.3). Upon using a mean-field parametrization of $\xi_{ab}(T)$,

$$\xi_{ab}(T)=\xi_0\left[1-\frac{T}{T_c}\right]^{-1/2}, \tag{D1}$$

where T_c is the zero-field superconducting transition temperature, we readily obtain

$$\frac{T_0}{T}=1-\frac{2\xi_0^2}{c_0^2}. \tag{D2}$$

Upon taking, for example, a rod radius $c_0=35$ Å and zero-temperature coherence length in the ab plane $\xi_0=12$ Å, we find $T_0/T_c=0.76$.

Consider now the temperature dependence of the single column pinning energy $T^*(T)=\sqrt{U_0\tilde{\epsilon}_1 b_0}$. If $T>T_0$, then we find using Eqs. (1.9a) and (2.3) that

$$T^*=\frac{1}{\sqrt{2}}\epsilon_0 c_0\left[\frac{M_\perp}{M_z}\ln\kappa\right]^{1/2}, \tag{D3}$$

where we have used $\tilde{\epsilon}_1\approx(M_\perp/M_z)\epsilon_0\ln\kappa$. Except for a change in prefactor of order unity, the same result holds for $T<T_0$. For numerical estimates it is convenient to eliminate $\epsilon_0=[\phi_0/4\pi\lambda_{ab}(T)]^2$ in favor of the "Ginzburg number,"[2]

$$\mathrm{Gi}=\frac{1}{2}\frac{M_z}{M_\perp}\left[\frac{T_c}{H_c^2\xi_0^3}\right]^2, \tag{D4}$$

where $H_c=\sqrt{2}\phi_0/4\pi\lambda_{ab}(0)\xi_0$ is the thermodynamic critical field at $T=0$. The Ginzburg number is the reduced temperature $(T_c-T)/T_c$ at which fluctuations in the BCS order parameter $\delta\psi_{\mathrm{BCS}}$ become comparable to $\langle\psi_{\mathrm{BCS}}\rangle$. Although small even in high-T_c materials (Gi$\sim$0.01), the Ginzburg number is many orders of magnitude larger than in conventional superconductors. We can then use Eq. (D1) and the relation

$$\frac{M_\perp}{M_z}\epsilon_0^2=\frac{T_c^2\xi_0^2}{8\mathrm{Gi}\xi_{ab}^4} \tag{D5}$$

to find

$$T^*(T)=\frac{c_0}{4\xi_0}\left[\frac{\ln\kappa}{\mathrm{Gi}}\right]^{1/2}(T_c-T). \tag{D6}$$

We next estimate the temperature T_1 at which the entropy of flux-line wandering plays a significant role in determining the localization length and binding free energy of a fluxon interacting with a single columnar pin. The self-consistency relation $T^*(T_1)=T_1$ leads immediately via Eq. (D6) to

$$\frac{T_1}{T_c}=\frac{(c_0/4\xi_0)\sqrt{\ln\kappa/\mathrm{Gi}}}{1+(c_0/4\xi_0)\sqrt{\ln\kappa/\mathrm{Gi}}}. \tag{D7}$$

Upon taking $c_0=35$ Å, $\xi_0=12$ Å, $\kappa=10^2$, and Gi$=10^{-2}$, typical parameters for YBCO, we find that $T_1/T_c=0.94$. As a rough model of a highly anisotropic material such as $Bi_2Sr_2CaCu_2O_8$ (BSCCO), we substitute instead Gi$=10^{-1}$ and find $T_1/T_c=0.83$.

The temperature dependence of the localization length $l_\perp(T)$ for $T>T_1$ is given by Eq. (2.23a). Since $T_1>T_0$, we set $b_0=\sqrt{2}\xi_{ab}(T)$ and use (D6) to find

$$l_\perp(T)\approx\sqrt{2}\xi_0\left[1-\frac{T}{T_c}\right]^{-1/2}\times\exp\left[\left[\frac{4\xi_0}{c_0}\right]^2\frac{\mathrm{Gi}}{\ln\kappa}\frac{T^2}{(T_c-T)^2}\right]. \tag{D8}$$

The depinning temperature T_{dp} is defined by the condition $l_\perp(T)=d$, where d is the average spacing between columnar pins. This leads to a self-consistent equation for $x=T_{dp}/T_c$, namely,

$$\left[\frac{4\xi_0}{c_0}\right]^2\frac{\mathrm{Gi}}{\ln\kappa}\frac{x^2}{(1-x)^2}=\ln\left[\frac{d}{\sqrt{2}\xi_0}(1-x)^{1/2}\right]. \tag{D9}$$

Upon replacing T_{dp} by $T_1\lesssim T_{dp}$ inside the logarithm, we find a formula similar to (D7),

$$\frac{T_{dp}}{T_c}=\frac{(c_0/4\xi_0)\sqrt{\ln\kappa/\mathrm{Gi}}\alpha}{1+(c/4\xi_0)\sqrt{\ln\kappa/\mathrm{Gi}}\alpha}, \tag{D10}$$

with

$$\alpha=\ln^{1/2}\left[\frac{d}{\sqrt{2}\xi_0}\left[1-\frac{T_1}{T_c}\right]^{1/2}\right]. \tag{D11}$$

With $d=300$ Å and the parameters used for YBCO above, we find $T_{dp}/T_c=0.95$. For a highly anisotropic BSCCO-like material we take Gi$=10^{-1}$ and keep all other parameters fixed to estimate $T_{dp}/T_c=0.87$.

When $T>T_{dp}$, collective pinning of a single flux line by an ensemble of columnar pins leads to a localization length which grows according to Eq. (3.32b). Equation (D6) then leads immediately to

$$l_\perp(T)=d\left[\frac{4\xi_0}{c_0}\right]^2\frac{\mathrm{Gi}}{\ln\kappa}\frac{T^2}{(T_c-T)^2}. \tag{D12}$$

For very low fields $B\lesssim\phi/\lambda_{ab}^2$, the Bose-glass transition field $B_{\mathrm{BG}}(T)$ occurs when this localization length equals the vortex spacing a_0. Equation (D12) then leads to

$$B_{\mathrm{BG}}(T)\approx B_\phi\left[\frac{c_0}{4\xi_0}\right]^4\left[\frac{\ln\kappa}{\mathrm{Gi}}\right]^2\left[\frac{T_c}{T}\right]^4\left[1-\frac{T}{T_c}\right]^4, \tag{D13}$$

where $B_\phi=\phi_0/d^2$ is the matching field. A different power law should arise for $1-T/T_c\lesssim\mathrm{Gi}$, because of fluctuation effects.[4]

We also present explicit forms for the interaction field $B^*(T)$ above which interactions between vortices modify columnar pinning in an important way. Upon combining Eqs. (3.28a), (3.28b), and (3.33b) with the results in this appendix, we find

$$B^*(T)\approx B_\phi \quad (T<T_0)\,, \tag{D14}$$

$$B^*(T)\approx B_\phi \left[\frac{c_0}{2\xi_0}\right]^2 \left[1-\frac{T}{T_c}\right] \quad (T_0<T<T_1)\,, \tag{D15}$$

$$B^*(T)\approx 4B_\phi \frac{T^2}{T_c(T_c-T)}\frac{\mathrm{Gi}}{\ln\kappa}\exp\left[-2\left[\frac{4\xi_0}{c_0}\right]^2\frac{\mathrm{Gi}}{\ln\kappa}\frac{T^2}{(T_c-T)^2}\right] \quad (T_1<T<T_{dp})\,, \tag{D16}$$

$$B^*(T)\approx 2^{-13}B_\phi \left[\frac{c_0}{\xi_0}\right]^6 \left[\frac{c_0}{d}\right]^2 \left[\frac{\ln\kappa}{\mathrm{Gi}}\right]^3 \frac{(T_c-T)^6}{T^6} \quad (T_{dp}<T<T_c)\,, \tag{D17}$$

where, again, a different power law obtains for $1-T/T_c \lesssim \mathrm{Gi}$.

Estimates for the characteristic energies and temperatures for pinning by families of twin boundaries can be obtained in a similar fashion.

Finally, we write the field corresponding to the melting temperature $T_m = c_L^2\sqrt{\varepsilon_0\tilde{\varepsilon}_1}a_0$ [see Eq. (3.41)] in terms of the parameters defined above:

$$B_m(T)\approx \frac{\pi}{4}c_L^4\ln\kappa\frac{H_{c2}(0)}{\mathrm{Gi}}\left[\frac{T_c-T}{T}\right]^2\,, \tag{D18}$$

where $H_{c2}(0)=\phi_0/2\pi\xi_0^2$ is the upper critical field at $T=0$.

[1]See, e.g., the reviews in *Phenomenology and Applications of High Temperature Superconductors,* edited by K. Bedell, M. Inui, D. Meltzer, J. R. Schrieffer, and S. Doniach (Addison-Wesley, New York, 1991).

[2]G. Blatter, M. V. Feigel'man, V. B. Geshkenbein, A. I. Larkin, and V. M. Vinokur, Rev. Mod. Phys. (to be published).

[3]D. R. Nelson, Phys. Rev. Lett. **60**, 1973 (1988); D. R. Nelson and H. S. Seung, Phys. Rev. B **39**, 9153 (1989).

[4]M. P. A. Fisher, Phys. Rev. Lett. **62**, 1415 (1989); D. S. Fisher, M. P. A. Fisher, and D. A. Huse, Phys. Rev. B **43**, 130 (1991).

[5]M. V. Feigel'man, V. B. Geshkenbein, A. I. Larkin, and V. M. Vinokur, Phys. Rev. Lett. **63**, 2303 (1989).

[6]D. R. Nelson and P. Le Doussal, Phys. Rev. B **42**, 10 112 (1990).

[7]V. M. Vinokur, M. V. Feigel'man, V. B. Geshkenbein, and A. I. Larkin, Phys. Rev. Lett. **65**, 259 (1990).

[8]M. C. Marchetti and D. R. Nelson, Phys. Rev. B **42**, 9938 (1990); Physica C **174**, 40 (1991).

[9]A. I. Larkin and Y. M. Ovchinnikov, J. Low Temp. Phys. **34**, 409 (1979).

[10]D. A. Huse and S. Seung, Phys. Rev. B **42**, 1059 (1990); J. D. Reger, T. A. Tokayasu, A. P. Young, and M. P. A. Fisher, *ibid.* **44**, 7147 (1991).

[11]D. Huse (private communication).

[12]R. H. Koch, V. Foglietti, W. J. Gallagher, G. Koren, A. Gupta, and M. P. A. Fisher, Phys. Rev. Lett. **63**, 1151 (1989).

[13]P. L. Gammel, L. F. Schneemeyer, and D. J. Bishop, Phys. Rev. Lett. **66**, 953 (1991).

[14]M. Hawley, I. D. Raistrick, J. G. Beery, and R. J. Houlton, Science **251**, 1587 (1991); C. Gerber, D. Anselmetti, J. G. Bednorz, J. Manhort, and D. G. Schlom, Nature (London) **350**, 279 (1991).

[15]G. W. Crabtree, W. K. Kwok, U. Welp, J. Downey, S. Fleshler, K. G. Vandervoort, and J. Z. Lin, Physica C **185-189**, 282 (1991); W. K. Kwok, S. Fleshler, U. Welp, V. M. Vinokur, J. Downey, and G. W. Crabtree, in *Advances in Superconductivity IV,* Proceedings of the 4th International Symposium on Superconductivity, edited by H. Hayakaswa and N. Koshizuka (Springer, New York, 1992), pp. 317–322.

[16]E. M. Forgan *et al.*, Physica C **185-189**, 247 (1991); M. Yehiraj *et al.*, Phys. Rev. Lett. **70**, 857 (1993).

[17]M. Charalambous *et al.*, Phys. Rev. B **45**, 45 (1992).

[18]W. K. Kwok, S. Fleshler, U. Welp, V. M. Vinokur, J. Downey, G. W. Crabtree, and M. M. Miller, Phys. Rev. Lett. **69**, 3370 (1992); S. Fleshler, W. K. Kwok, U. Welp, V. M. Vinokur, M. K. Smith, J. Downey, and G. W. Crabtree, Phys. Rev. B **47**, 14 448 (1993).

[19]D. E. Farrell, J. P. Rice, and D. M. Ginsberg, Phys. Rev. Lett. **67**, 1165 (1991); R. G. Beck, D. E. Farrell, J. P. Rice, D. M. Ginsberg, and V. G. Kogan, *ibid.* **68**, 1594 (1992).

[20]H. Safar, P. L. Gammel, D. A. Huse, D. J. Bishop, J. P. Rice, and D. M. Ginsberg, Phys. Rev. Lett. **69**, 824 (1992).

[21]E. Brezin, D. R. Nelson, and A. Thiaville, Phys. Rev. B **31**, 7124 (1985).

[22]T. K. Worthington, M. P. A. Fisher, D. A. Huse, J. Toner, A. D. Marwick, T. Zabel, C. A. Feild, and F. Holtzberg, Phys. Rev. B **46**, 11 854 (1992).

[23]H. Safar, P. L. Gammel, D. A. Huse, D. J. Bishop, W. C. Lee, J. Giapintzakis, and D. M. Ginsberg, Phys. Rev. Lett. **70**, 3800 (1993).

[24]An alternative explanation is that the flux liquid simply becomes more entangled and viscous as its density increases with increasing field. Flux-line entanglement will prevent crystallization and produce instead a nonequilibrium but continuous "polymer"-glass transition if the barriers to line crossing are sufficiently high. See Refs. 3 and 8. The hysterisis loops associated with first-order freezing would slowly go away as crystallization became more difficult for a fixed cooling rate. The low-temperature dynamics of this polymer glass in the presence of point disorder should be similar to that predicted by the collective pinning theory (Ref. 7), with a *polymeric* shear modulus replacing the usual elastic constant c_{66}.

[25]M. Konczykowski *et al.*, Phys. Rev. B **44**, 7167 (1991).

[26]L. Civale, A. D. Marwick, T. K. Worthington, M. A. Kirk, J. R. Thompson, L. Krusin-Elbaum, Y. Sun, J. R. Clem, and F. Holtzberg, Phys. Rev. Lett. **67**, 648 (1991); a striking enhancement of the irreversibility line (with critical currents

increasing by a factor 10^3 at $T=77$ K) has also been observed quite recently in *thallium*-based compounds by R. C. Budhani, M. Suenaga, and S. H. Liou, *ibid.* **69**, 3816 (1992).

[27]W. Gerhauser *et al.*, Phys. Rev. Lett. **68**, 879 (1992).

[28]V. Hardy *et al.*, Nucl. Instrum. Methods B **54**, 472 (1991).

[29]A preliminary account of this work appeared in D. R. Nelson and V. M. Vinokur, Phys. Rev. Lett. **68**, 2398 (1992).

[30]A similar approach has been proposed by I. F. Lyuksyutov, Europhys. Lett. **20**, 273 (1992). See also remarks by M. P. A. Fisher and D. H. Lee, Phys. Rev. B **39**, 2756 (1989), Fisher, Fisher, and Huse (Ref. 4, Sec. IX), and Nelson (Ref. 1).

[31]M. P. A. Fisher, P. B. Weichman, G. Grinstein, and D. S. Fisher, Phys. Rev. B **40**, 546 (1989), and references therein.

[32]B. I. Shklovskii and A. L. Efros, *Electronic Properties of Doped Semiconductors* (Springer, New York, 1984).

[33]G. Blatter, V. B. Geshkenbein, and A. I. Larkin, Phys. Rev. Lett. **68**, 875 (1992).

[34]T. K. Worthington *et al.*, Physica (Amsterdam) C **153**, 32 (1988).

[35]M. Wallin and S. M. Girvin, Phys. Rev. B **47**, 14 642 (1993); for related calculations directed at real bosons, see W. Krauth, T. Trivedi, and D. Ceperley, Phys. Rev. Lett. **67**, 2307 (1991); E. S. Sorensen, M. Wallin, S. M. Girvin, and A. P. Young, *ibid.* **69**, 828 (1992). Early simulations of Josephson arrays stressing the importance of correlated pinning of vortices were carried out by J. Choi and J. Jose, *ibid.* **62**, 320 (1989).

[36]For related issues arising from pinning by CuO_2 planes, see D. Feinberg, and C. Villard, Phys. Rev. Lett. **65**, 919 (1990).

[37]T. Hwa, D. R. Nelson, and V. Vinokur, Phys. Rev. B **48**, 1167 (1993).

[38]D. S. Fisher (private communication).

[39]D. S. Fisher, in *Phenomenology and Applications of High Temperature Superconductors,* edited by K. Bedell, M. Inui, D. Meltzner, J. R. Schrieffer, and S. Doniach (Addison-Wesley, New York, 1991).

[40]G. S. Mkrtchyan and V. V. Shmidt, Zh. Eksp. Teor. Fiz. **61**, 367 (1971) [Sov. Phys. JETP **34**, 195 (1972)].

[41]D. R. Nelson, in *Phenomenology and Applications of High Temperature Superconductors,* edited by K. Bedell, M. Inui, D. Meltzer, J. R. Schrieffer, and S. Doniach (Addison-Wesley, New York, 1991).

[42]M. B. Feigel'man and V. M. Vinokur, Phys. Rev. B **41**, 8986 (1990).

[43]J. Clem, Phys. Rev. Lett. **38**, 1425 (1977); Phys. Rev. B **26**, 2463 (1982).

[44]E. H. Brandt, J. Low. Temp Phys. **42**, 557 (1981); **44**, 33 (1981); **44**, 59 (1981).

[45]See, e.g., E. H. Brandt, Phys. Rev. Lett. **69**, 1105 (1992).

[46]M. Tinkham, *Introduction to Superconductivity* (McGraw-Hill, New York, 1975).

[47]R. P. Feynman and A. R. Hibbs, *Path Integrals and Quantum Mechanics* (McGraw-Hill, New York, 1965); R. P. Feynman, *Statistical Mechanics* (Benjamin, Reading, MA, 1972).

[48]L. D. Landau and E. M. Lifshitz, *Quantum Mechanics,* 2nd ed. (Pergamon, New York, 1965).

[49]See, e.g., D. R. Nelson, J. Stat. Phys. **57**, 511 (1989).

[50]A. I. Baz', Ya.B. Zel'dovich, and A. M. Perelomov, *Scattering, Reactions and Decay in Nonrelativistic Quantum Mechanics* (Israel Program for Scientific Translations, Jerusalem, 1969).

[51]S. Obukhov and M. Rubinstein, Phys. Rev. Lett. **65**, 1279 (1990).

[52]A more complete treatment should lead to nonlocality in z. See, e.g., E. H. Brandt, Phys. Rev. B **34**, 6514 (1986); Phys. Rev. Lett. **63**, 1106 (1989).

[53]In the flux liquid, "thick" means sample dimensions large compared to an entanglement length so that boson statistics are applicable (Ref. 3). Deep in the Bose glass, statistics are irrelevant because the fictitious quantum "particles" are localized. The thickness dependence of the resistivity in this regime is discussed in Sec. IV.

[54]We assume line-crossing barriers are finite. Two distinct vortex lines may merge to within a coherence length of each other as z varies and then separate again in two distinct trajectories. The thermal average in (3.1) automatically includes a sum over both the "direct" and "exchange" vortex reconnection possibilities.

[55]N. V. Popov, *Functional Integrals and Collective Excitations* (Cambridge University Press, New York, 1981).

[56]J. W. Negele and J. Orland, *Quantum Many-Particle Systems* (Addison-Wesley, New York, 1981), Chaps. 1 and 2.

[57]A more complete treatment shows that a z-independent disorder potential *increases* c_{44}; T. Hwa, P. Le Doussal, D. R. Nelson, and V. M. Vinokur (unpublished).

[58]P. C. Hohenberg, A. Aharony, B. I. Halperin, and E. D. Siggia, Phys. Rev. B **13**, 2986 (1976).

[59]D. B. Josephson, Phys. Rev. Lett. **21**, 608 (1966).

[60]M. C. Marchetti, Phys. Rev. B **43**, 8012 (1991).

[61]See, e.g., M. V. Feigel'man, V. B. Geshkenbein, and A. I. Larkin, Physica C **167**, 177 (1990). The original computation of the anisotropic nonlocal elastic constants needed to describe high-T_c superconductors is due to A. Houghton, R. A. Pelcovits, and A. Sudbo, Phys. Rev. B **40**, 6763 (1989).

[62]Similar modifications arise for atomic wave functions in a strong magnetic field. See Chap. X of Ref. 32.

[63]See, e.g., A. L. Fetter, P. C. Hohenberg, and P. Pincus, Phys. Rev. **147**, 140 (1966).

[64]We ignore the small but interesting Hall voltage which arises perpendicular to J. See, e.g., S. J. Hagen, C. J. Lobb, K. L. Greene, and M. Eddy, Phys. Rev. B **43**, 6246 (1991).

[65]The same analogy was applied to vortex transport in helium films by Ambegaokar *et al.*, Phys. Rev. B **21**, 1806 (1980).

[66]P. H. Kes, J. Aarts, J. van den Berg, and J. A. Mydosh, Supercond. Sci. Technol. **1**, 241 (1989).

[67]J. Hirth and J. Lothe, *Theory of Dislocations,* 2nd ed. (Wiley, New York, 1982).

[68]The corresponding result for the *conductivity* of semiconductors at $T=0$ was first derived by B. I. Shklovskii, Fiz. Tekh. Poluprovodn. **6**, 2335 (1972) [Sov. Phys. Semicond. **6**, 1964 (1973)].

[69]N. L. Lien and B. I. Shklovskii, Solid State Commun. **38**, 99 (1980).

[70]The scaling ideas are very similar to those developed to treatment static and dynamic critical phenomena in the 1960s. See, e.g., H. E. Stanley, *Introduction to Phase Transitions and Critical Phenomena* (Oxford University Press, New York, 1971).

[71]A. B. Harris, J. Phys. C **7**, 1671 (1974).

[72]An identical argument has been made by D. S. Fisher and M. P. A. Fisher (private communication).

[73]T. Roy and T. E. Mitchell, Philos. Mag. A **63**, 225 (1991); T. E. Mitchell and J. P. Hirth, Acta Metall. Mater. **39**, 1711 (1991).

[74]M. C. Marchetti and V. Vinokur (unpublished).

[75]A. A. Abrikosov, Zh. Eksp. Teor. Fiz. **32**, 1442 (1957) [Sov. Phys. JETP **5**, 1174 (1957)]; S. Fetter and P. C. Hohenberg, in *Superconductivity,* edited by R. D. Parks (Dekker, New York, 1969), Vol. II.

[76]L. D. Landau, Phys. Z **11**, 26 (1937); in *The Collected Papers of L. D. Landau,* edited by D. ter Haar (Gordon and Breach–Pergamon, New York, 1965).
[77]J. Toner, Phys. Rev. Lett. **66**, 2523 (1991).
[78]R. E. Hetzel, A. Sudbo, and D. A. Huse, Phys. Rev. Lett. **69**, 518 (1992).
[79]If one lets the interplanar Josephson coupling in Ref. 78 tend to zero, the lattice superconductor reduces to a stack of decoupled planes. The discreteness of the underlying model then *does* have important consequences. It can be shown that only for fillings $f < \frac{1}{12}$ will discreteness not affect the continuous nature of the melting transition. See D. R. Nelson and B. I. Halperin, Phys. Rev. B **19**, 2457 (1979). Since $f = \frac{1}{6}$ in Ref. 78, results for this model in the strongly anisotropic limit are not directly applicable to the cuprate superconductors.
[80]P. G. de Gennes, Solid State Commun. **10**, 753 (1972).